

PREDICTIONS ON ABSORPTION AND SCATTERING
CHARACTERISTIC OF ACOUSTIC SCATTERERS
MODIFIED WITH MICRO-PERFORATED PANELS

A THESIS SUBMITTED TO
THE GRADUATE SCHOOL OF NATURAL AND APPLIED SCIENCES
OF
MIDDLE EAST TECHNICAL UNIVERSITY

BY

ERİNÇ ODABAŞ

IN PARTIAL FULFILLMENT OF THE REQUIREMENTS
FOR
THE DEGREE OF MASTER OF SCIENCE
IN
MECHANICAL ENGINEERING

SEPTEMBER 2012

Approval of the thesis:

**PREDICTIONS ON ABSORPTION AND SCATTERING
CHARACTERISTICS OF ACOUSTIC SCATTERERS MODIFIED WITH
MICRO-PERFORATED PANELS**

Submitted by **ERİNÇ ODABAŞ** in partial fulfillment of the requirements for the degree of **Master of Science in Mechanical Engineering Department, Middle East Technical University** by,

Prof. Dr. Canan Özgen
Dean, Graduate School of **Natural and Applied Sciences**

Prof. Dr. Suha Oral
Head of Department, **Mechanical Engineering**

Prof. Dr. Mehmet Çalışkan
Supervisor, **Mechanical Engineering Dept., METU**

Examining Committee Members:

Asst. Prof. Dr. Yiğit Yazıcıoğlu
Mechanical Engineering Dept., METU

Prof. Dr. Mehmet Çalışkan
Mechanical Engineering Dept., METU

Prof. Dr. Yusuf Özyörük
Aerospace Engineering Dept., METU

Asst. Prof. Dr. Ender Cigeroğlu
Mechanical Engineering Dept., METU

Asst. Prof. Dr. Banu Günel
Graduate School of Informatics, METU

Date:

I hereby declare that all information in this document has been obtained and presented in accordance with academic rules and ethical conduct. I also declare that, as required by these rules and conduct, I have fully cited and referenced all material and results that are not original to this work.

Name, Last Name :

Signature :

ABSTRACT

PREDICTIONS ON ABSORPTION AND SCATTERING CHARACTERISTICS OF ACOUSTIC SCATTERERS MODIFIED WITH MICRO-PERFORATED PANELS

Odabaş, Erinç

M.S., Mechanical Engineering Department

Supervisor: Prof. Dr. Mehmet Çalışkan

September 2012, 103 pages

In this study, the basic absorption and scattering characteristics of acoustic scatterers, specifically Schroeder Diffusers, are investigated. Schroeder Diffusers are one of the most widely used acoustic scatterers in which the scattering phenomenon is predictable due to the geometry of the diffuser, based on a particular mathematical sequence. It is shown that it is possible to increase the amount of absorption by modifying the diffuser structure by means of adding perforated panels into the wells or narrowing diffuser wells. In room acoustics applications, diffusers are conventionally mounted to a wall or ceiling assumed to be rigid enough such that sound wave cannot penetrate through. This thesis proposes a new modification on these diffusers where the diffuser is not backed by a rigid surface; it is hung over a space instead. To construct such a configuration, diffuser wells are terminated with micro-perforated panels (MPP). Inclusion of MPP introduces additional losses; hence, higher absorption can be achieved. However, the most significant absorption

in this configuration is achieved below the first resonance frequency of the panel-air space system due to the existence of non-rigid backing. This thesis aims to model the absorption and scattering mechanisms enabled with the non-rigid backing by improving a previously introduced mathematical model.

Keywords: Schroeder diffusers, micro-perforated panels, low frequency sound absorption

ÖZ

MİKRO-PERFORE PANELLER İLE GELİŞTİRİLEN AKUSTİK SAÇICILARIN SES YUTMA VE SAÇICILIK KARAKTERİSTİKLERİNİN BELİRLENMESİ

Odabaş, Erinç

Yüksek Lisans, Makina Mühendisliği Bölümü

Tez Yöneticisi: Prof. Dr. Mehmet Çalışkan

Eylül 2012, 103 sayfa

Bu çalışmada, akustik saçıcıların, özellikle Schroeder saçıcılarının, ses yutma ve saçıcılık özellikleri araştırılmıştır. Schroeder saçıcıları oda akustiği uygulamalarında sıkça kullanılan saçıcılardan bir tanesidir. Ses saçıcılık özelliği, geometrisinde kullanılan matematiksel seriler sayesinde belirlenebilir. Bu tür saçıcıların ses saçıcılık özelliğinin yanı sıra, belli bir miktar ses yutma özelliği de vardır. Ses yutma miktarının, perfore panel eklenmesi veya saçıcı kuyularının daraltılması yoluyla artırılması mümkündür. Bu tür saçıcılar, oda akustiği uygulamalarında genellikle ses dalgalarının ilerleyemediği, yapı olarak rijit olduğu öngörülen duvarlara veya tavanlara asılarak kullanılırlar. Bu tezde, Schroeder saçıcılarının kullanımı ile ilgili, saçıcının rijit bir yüzey yerine havada asılı kullanıldığı yeni bir uygulama önerilmektedir. Bu şekilde bir uygulamayı gerçekleştirebilmek için saçıcının üzerinde ve arkasında mikro-perfore paneller kullanılmıştır. Saçıcı üzerinde panellerin kullanılması ek enerji kayıpları yaratılarak,

saçıcının ses yutma özelliğinin arttırılmasında etkili olmaktadır. Fakat rijit olmayan arka yüzeyin kullanımı, panel sisteminin getirmiş olduđu ilk rezonans frekansından daha düşük frekanslarda etkili ses yutma özelliği sağlamaktadır. Bu tez, daha önceki çalışmalarda tanımlanan matematiksel modellerin deđiştirilmesi ve geliştirilmesi ile saçıcı üzerinde gerçekleştirilen yeni kullanım şeklinin sağladığı ses yutma ve saçıcılık özelliklerinin belirlenmesi için matematiksel bir model geliştirilmesi üzerinedir.

Anahtar Kelimeler: Schroeder saçıcıları, mikro-perfore paneller, düşük frekanslarda ses yutma özelliği

To My Parents

ACKNOWLEDGMENTS

The author would like to express his respect and gratitude to his thesis supervisor, Dr. Mehmet Çalışkan, professor of the Mechanical Engineering Department, METU, for his continuous guidance, understanding and criticism throughout this study.

The author also extends his sincere thanks to Zühre Sü-Gül and Mezzo Stüdyo for giving him a great opportunity to study and work on practical application areas of room acoustics which deeply integrated him into the area of this thesis work.

Finally, thanks are also to his family and always be loved Dilara Hacıhasanoğlu for their continuous support and patience.

TABLE OF CONTENTS

ABSTRACT.....	iv
ÖZ	vi
ACKNOWLEDGMENTS	ix
TABLE OF CONTENTS	x
LIST OF TABLES	xii
LIST OF FIGURES	xiii
CHAPTERS	
1. INTRODUCTION.....	1
2. PREVIOUS WORKS	5
2.1. Introduction.....	5
2.2. Analytical and Experimental Solutions on Sound Absorption Characteristics of Schroeder Diffusers	6
2.3. Analytical Solutions on Sound Absorption Characteristics of Micro-perforated Panels.....	10
3. FUNDAMENTALS AND GOVERNING EQUATIONS.....	13
3.1. Acoustic Wave Equation	13
3.1.1. Definition of Linear Acoustic Wave Equation.....	13
3.1.2. Harmonic Plane Waves	14
3.1.3. Energy Density and Acoustic Intensity.....	16
3.1.4. Specific Acoustic Impedance and Admittance	18
3.2. Reflection, Transmission and Absorption of Sound Energy	18
3.3. Acoustic Absorbers.....	21
3.3.1. Porous Absorbers	22
3.3.2. Panel (Resonant) Absorbers.....	24
3.4. Acoustic Diffusers (Scatterers).....	26

4. ABSORPTION CHARACTERISTICS OF SCHROEDER DIFFUSERS	31
4.1. Fundamentals of Schroeder Diffusers.....	32
4.2. Absorption Theory for Schroeder Diffusers	36
4.2.1. Micro-perforated Panel Theory.....	36
4.3. Prediction of Absorption for Schroeder Diffusers.....	40
4.3.1. Detached Mathematical Model	42
4.3.2. Combined Mathematical Model.....	57
4.4. Effect of Narrower Wells.....	63
4.5. Scattering Characteristics of the Modified Diffuser	65
5. SAMPLE CASE STUDIES AND RESULTS.....	68
5.1. Sample Scenario Results.....	68
5.2. Comparative Evaluation Scenarios	79
5.2.1. Effect of Narrower Wells.....	80
5.2.2. Effect of Number of Wells and Incidence Angle.....	81
5.2.3. Effect of Panel Impedances.....	84
6. CONCLUSIONS	86
6.1. Introduction.....	86
6.2. Comparative Evaluations and Conclusions	88
REFERENCES	96
APPENDICIES	
A. Derivation of Equation (4.34) from Equation (4.32).....	99
B. Sample Case-2 Design Parameters and Software Results.....	100

LIST OF TABLES

TABLES

Table 5.1 Design Parameters for the Sample Scenario-1.....	69
Table 5.2 Sequenced Well Depths for the Sample Scenario-1	69
Table 5.3 Micro-Perforated Panel Parameters for the Sample Scenario-1	69
Table 5.4 Design Parameters for the Sample Scenario-1.....	79
Table 5.5 Sequenced Well Depths for the Sample Scenario-1	79
Table 5.6 Micro-Perforated Panel Parameters for the Sample Scenario-1	80
Table B.1 Design Parameters for the Sample Case-2	100
Table B.2 Sequenced Well Depths for the Sample Case-2.....	100
Table B.3 Micro-Perforated Panel Parameters for the Sample Case-2.....	100

LIST OF FIGURES

FIGURES

Figure 2.1 A one-dimensional Schroeder Diffuser	6
Figure 3.1 Reflected and transmitted sound field on a boundary	20
Figure 3.2 Porous absorber examples	23
Figure 3.3 Resonant absorber examples	24
Figure 3.4 Micro-perforated panel absorber examples	26
Figure 3.5 Various acoustic diffuser examples	28
Figure 3.6 One and two dimensional Schroeder Diffusers	30
Figure 4.1 Visualization of the dispersed sound field in front of a Schroeder Diffuser, FDTD model [1].....	34
Figure 4.2 Electric circuit representation of a micro-perforated panel impedance....	37
Figure 4.3 Top and side views of a micro-perforated panels showing design parameters	39
Figure 4.4 A figurative representation of a one dimensional Schroeder Diffuser	41
Figure 4.5 Sound fields inside the well of the diffuser	44
Figure 4.6 Sound field inside the well of the diffuser.....	51
Figure 4.7 Sound field inside the well of the diffuser.....	58
Figure 5.1 Absorption Coefficient (1 st Scenario).....	70
Figure 5.2 Specular reflection coefficient in front of the diffuser (1 st Scenario)	71
Figure 5.3 Scattered reflection coefficient in front of the diffuser (<i>red curve</i>), Coefficient of redistribution (<i>blue curve</i>) (1 st Scenario)	72
Figure 5.4 Specular transmission coefficient behind the diffuser (1 st Scenario)	73
Figure 5.5 Scattered transmission coefficient behşnd the diffuser (<i>red curve</i>), Coefficient of redistribution (<i>blue curve</i>) (1 st Scenario).....	74

Figure 5.6 Directivity diagram of the intensity ratios for first (<i>blue vectors</i>) and second (<i>red vectors</i>) spatial harmonics with varying frequency in the reflected field.	75
Figure 5.7 Directivity diagram of the intensity ratios for first (<i>blue vectors</i>) and second (<i>red vectors</i>) spatial harmonics with varying frequency in the transmitted field	76
Figure 5.8 Directivity diagram of the intensity ratios considering whole spatial harmonics with varying frequency for $w = 0.06m$	77
Figure 5.9 Directivity diagram of the intensity ratios considering whole spatial harmonics with varying frequency for $w = 0.12m$	78
Figure 5.10 Directivity diagram of the intensity ratios considering whole spatial harmonics with varying frequency for $w = 0.18m$	78
Figure 5.11 Absorption Coefficient for varying well width, $w = 0.005m$ (<i>blue curve</i>), $w = 0.01m$ (<i>red curve</i>), $w = 0.05m$ (<i>magenta curve</i>), $w = 0.1m$ (<i>black curve</i>)	80
Figure 5.12 Absorption Coefficient for varying sequence modifier, $N = 3$ (<i>blue curve</i>), $N = 5$ (<i>red curve</i>), $N = 7$ (<i>magenta curve</i>), $N = 11$ (<i>black curve</i>).....	82
Figure 5.13 Absorption Coefficient for varying incident angle, $\theta = 0^0$ (<i>blue curve</i>), $\theta = 15^0$ (<i>red curve</i>), $\theta = 30^0$ (<i>magenta curve</i>), $\theta = 45^0$ (<i>black curve</i>).....	83
Figure 5.14 Absorption Coefficient for varying surface mass density and panel thickness, $m = 0.1kg/m^2$ (<i>blue curve</i>), $m = 0.3kg/m^2$ (<i>red curve</i>).....	84
Figure 5.15 Absorption Coefficient for varying surface mass density and panel thickness, $m = 0.5kg/m^2$ (<i>blue curve</i>), $m = 0.7kg/m^2$ (<i>red curve</i>).....	85
Figure 6.1 Normal incidence absorption coefficient of Double-leaf micro-perforated panel absorber (<i>blue curve</i>) and Modified Schroeder Diffuser (<i>red curve</i>).....	89
Figure 6.2 Absorption Coefficient, Space Diffuser (<i>red curve</i>), Regular Schroeder Diffuser (<i>blue curve</i>).....	90

Figure 6.3 Absorption coefficient, space diffuser (<i>red curve</i>), regular Schroeder diffuser with single-leaf micro-perforated panel and with rigid backing (<i>blue curve</i>)	91
Figure 6.4 Absorption coefficient, space diffuser (<i>red curve</i>), regular Schroeder diffuser with double-leaf micro-perforated panels and with rigid backing (<i>blue curve</i>)	92
Figure 6.5 Normal incidence absorption coefficient with respect to varying front panel surface mass density, $m = 0.1 \text{ kg/m}^3$ (red curve), $m = 1 \text{ kg/m}^3$ (blue curve), $m = 1000 \text{ kg/m}^3$ (magenta curve), $m = \infty \text{ kg/m}^3$ (black curve)	93
Figure 6.6 Normal incidence absorption coefficient with respect to varying rear panel surface mass density, $m = 0.1 \text{ kg/m}^3$ (red curve), $m = 1 \text{ kg/m}^3$ (blue curve), $m = 1000 \text{ kg/m}^3$ (magenta curve), $m = \infty \text{ kg/m}^3$ (black curve)	93
Figure B.1 Absorption Coefficient (2 nd Scenario)	101
Figure B.2 Specular reflection coefficient (2 nd Scenario)	101
Figure B.3 Scattered reflection coefficient (<i>red curve</i>), Coefficient of redistribution (<i>blue curve</i>) (2 nd Scenario)	102
Figure B.4 Specular transmission coefficient (2 nd Scenario)	102
Figure B.5 Scattered transmission coefficient (<i>red curve</i>), Coefficient of redistribution (<i>blue curve</i>) (2 nd Scenario)	103

CHAPTER 1

INTRODUCTION

Acoustic scatterers are widely used in room acoustics applications to achieve various functions that the enclosed space such as an auditorium or a concert hall should have in order to function properly regarding sound quality and acoustical comfort. The sound quality and acoustical comfort are determined with respect to various acoustical parameters which generally depend on the distribution of the sound energy within the enclosed space at a certain time frame. The amount of the sound energy within the space should be comparably less when the interested space is a recording studio or a lecture room; however, the amount of sound energy should be kept at a certain level such that the space can function properly regarding the activity performed inside. Concert halls, opera houses are examples of such spaces. When the amount of sound energy is in concern, sound absorbers are generally sufficient to accomplish this quest. However; when the distribution of the energy is in concern, absorbers are insufficient alone in most cases. The enclosing boundaries of the space should have the feature to reflect incoming sound waves in a manner that the reflected sound waves are dispersed rather than being directed to a certain location.

Acoustic diffusers (scatterers) are such surfaces that are geometrically modified to disperse the incoming sound waves.

In this thesis, absorption and scattering behavior of acoustic scatterers, particularly Schroeder Diffuser, is investigated. The study focuses on a specific case where Schroeder Diffusers are modified such a way that the usage of the diffuser can be

extended by eliminating geometrical boundary behind it. In conventional applications of diffusers, scattering surfaces are usually applied to walls and ceilings. This kind of diffusers can be called as conventional diffusers.

Structural boundaries such as walls, ceilings, etc. are generally assumed to be rigid when sound propagation phenomenon is going to be investigated. All previous mathematical models and experimental studies are performed to investigate the scattered sound field in front of conventional diffusers. Once the sound field is determined, some other characteristics such as absorption characteristics of the diffuser can be analyzed afterwards.

When compared with various types of acoustic absorbers, a Schroeder Diffuser can be classified as a combination of quarter wave resonant absorbers with different depths. Regarding quarter wave resonant absorbers as well as panel absorbers, the resonance frequencies where the absorption can be maximized is determined by the depth of the airspace within the absorber. The longer the wave length of the interested frequency to be absorbed, the deeper the resonant absorber should be. Consequently, absorbing sound energy at low frequencies is usually a hard task to achieve due to geometrical constraints regarding high depth values required for the airspace within the absorber. To accomplish this task, several modifications can be applied to Schroeder Diffusers by means of adding perforated panels into the diffuser wells or narrowing the width of the diffuser to introduce additional losses. However, high depth values are again inevitable in these configurations. In Chapter 2, all previous studies on absorption mechanism of Schroeder Diffusers, regarding regular configurations and modified versions to increase absorption are introduced. There are theoretical as well as experimental studies that investigate the absorption behavior.

To obtain adequate absorption at low frequencies without increasing the well depths of the Schroeder Diffuser is the main motivation in this thesis work. To achieve this task; a special use of perforated panels, which are micro-perforated panels (MPP) in

this particular case, is employed. The diffuser is modified with MPP as did similarly in previous studies; however, mentioned modification further removes the geometrical boundary at the back of the diffuser. Eventually, the diffuser should not be applied to a rigid surface such as a wall or a ceiling. It can be hung over the air space such that both the front and rear surfaces are exposed to the fluid medium which is simply air in room acoustic applications. This modification is done by replacing the rigid back surface of the diffuser with MPP. The non-rigid medium at the back of the diffuser enables low frequency absorption at very low frequencies while preserving the well depths at reasonable small values.

This thesis study is about to construct a mathematical model to analyze the absorption mechanism of this particular configuration. In Chapter 3, the fundamental and governing equations of sound propagation and necessary parameters to determine the absorption coefficient are introduced.

In Chapter 4, the mathematical model of the proposed modification is constructed and deeply analyzed. The model is composed of two parts which investigate the absorption coefficient of the diffuser with different assumptions. The first model is based on a comparably rough assumption to determine necessary parameters in a simple manner. The second model is actually a better version of the first model which reflects the analytical behavior of the diffuser more accurate. Furthermore, other improvements to further increase the absorption enabled by the diffuser are introduced. Beside the absorption characteristics, the scattered energy distribution of the modified diffuser is also theoretically constructed both for the sound fields in front and at the back of the diffuser.

In Chapter 5, the results of the mathematical analyses are introduced. The amount of absorption arisen by the defined modification is compared with previous analytical results. The effect of design parameters as well as MPP parameters on absorption and scattering is deeply discussed.

Finally, Chapter 6 introduces the conclusion which simply analyzes mathematical model results and compares the modified diffuser with the ones investigated in previous studies.

CHAPTER 2

PREVIOUS WORKS

2.1. Introduction

This chapter will look through literature in several aspects, namely analytical and experimental solutions on sound absorption characteristics of Schroeder Diffusers and analytical solutions on sound absorption characteristics of micro-perforated panels.

Schroeder diffuser is one of the most significant outcomes in diffuser design, producing optimum diffusion by utilizing small number of simple design equations. A Schroeder Diffuser is a periodic structure which simply consists of a number of adjacent wells having different depths and separated by thin fins. The depth of each well is designated by a mathematical number sequence. Figure 2.1 shows a typical example of a Schroeder Diffuser.

The main principle behind the theory of Schroeder Diffusers is phase grating of the reflected waves. An incident wave coming towards the Schroeder Diffuser penetrates into the wells. Due to the depth difference, the time required for the wave to travel in each well and reach to the diffuser surface is different. The interference of these waves reflected from the bottom with phase difference determines the radiation pattern of the sound field. By adjusting the depth sequence of the wells, radiation pattern can be altered to desired polar pattern. Schroeder showed that by selecting

quadratic residue sequence as the number sequence of the well depths, an even energy distribution in each diffraction lobe is achieved [1].

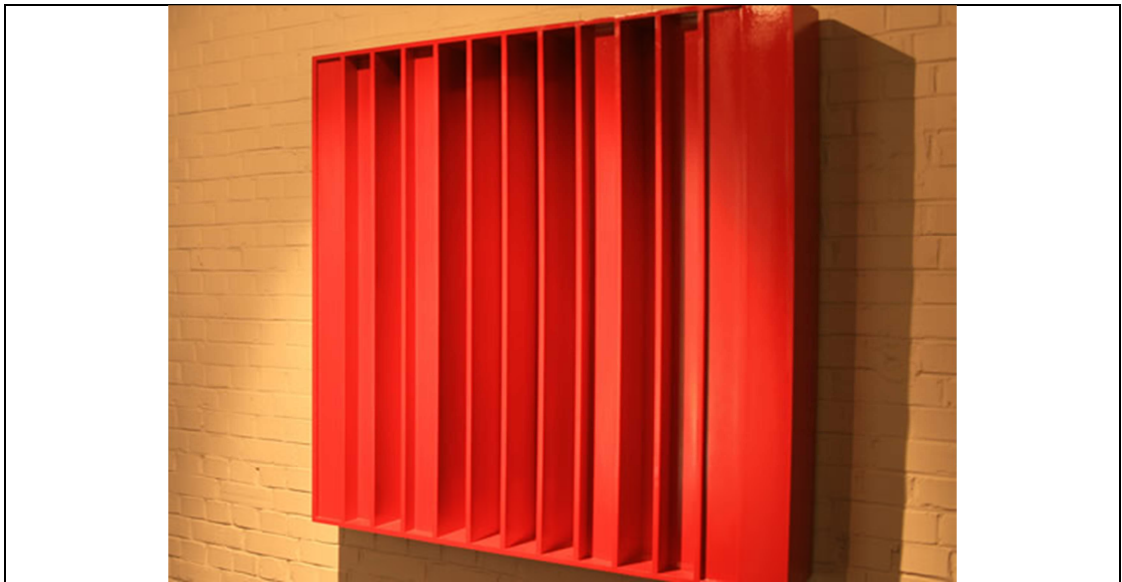


Figure 2.1 A one-dimensional Schroeder Diffuser

2.2. Analytical and Experimental Solutions on Sound Absorption Characteristics of Schroeder Diffusers

After the theory behind Schroeder Diffusers is constructed, many researchers started to investigate it analytically and experimentally. Besides the scattering performance of the diffuser, some researches are done on sound absorption performances. Before reported in the journals in 1991, K. Fujiwara and T. Miyajima conducted experiments on two-dimensional Schroeder Diffusers and showed that high amount of sound energy absorption was observed when a practical diffuser is constructed [2].

Surprisingly, good results were observed at low frequencies. They used three different specimens with different surface finishing understanding that the smoothness of diffuser surfaces could probably played a role in the high absorption coefficient values at low frequencies. They repeated the experiment for several times with a different surface varnish. However, the reasons behind this behavior at low frequencies of the diffuser had still not been clear yet.

After a short while, an analytical approach was developed by H. Kuttruff [3] to explain high amount of absorption which had arisen from the experiments of K. Fujiwara and T. Miyajima. In his study, Kuttruff developed the mathematical model assuming uniform constant pressure field at diffuser surface and computed sound absorption by taking the average surface admittance of the diffuser. He suggested that pressure differences at each well entrance induce additional air flows creating equalizing flows which indeed level out the pressure difference at well entrances. Existence of these equalizing flows reaching high velocities at well entrances is the main reason for the high absorption in the near field. In order to observe the high amount of absorption in near field the width of each well was very small compared to the acoustic wavelength of the interested frequency range. Even more, to reduce scattered reflections in the study, leaving only specular reflection, the period length of the diffuser is also kept small compared to the wavelength of interest.

This model had only explained the absorption behavior in the Fujiwara's experiments when the period length of the diffuser in Kuttruff's model is kept 1/10 compared to Fujiwara's. This was not the real case. However he explained the reason behind the high absorption caused by high velocity equalizing air flows in the near field. This high velocity profile in the near field is also investigated by K. Fujiwara, K. Nakai and H. Torihara experimentally [4]. Measurements are conducted in Kundt tube using fine cork powder to observe the velocity field at diffuser surface. The high velocity air flow is observed at well edges which show resemblances with the numerical results that they carried out to model the velocity profile.

Assuming constant pressure field and computing absorption with average surface admittance at well entrances as Kuttruff did is a rough approximation since the absorption due to oscillating high velocity sound waves at well entrances are not included in average surface admittance model. More accurate mathematical model was introduced by P. F. Mechel who studied scattering and absorption mechanism of Schroeder Diffuser by investigating the mutual interaction of the wells with Fourier analysis [5]. Mechel constructed a Fourier decomposition model to consider the coupling between differently tuned wells more rigorously, which is explained in detail in his book [6]. In the model the results are obtained with and without considering the effect of viscous and thermal losses in the wells. He further investigated how resistive layers placed in front of diffuser surface increases the absorption and turns it to a practical absorber. He also showed that implementing primitive root sequence as the mathematical number sequence of the diffuser could yield to a better absorber compared to quadratic residue sequence.

In order to implement Fourier analysis into the model, diffuser should be periodic. With this approach, the number of wells extends to infinity which excludes the admittance discontinuities at borders caused by finite number of elements. To calculate the absorption coefficient of a Schroeder diffuser with this model, one should consider the interaction between infinite numbers of wells, however; Mechel showed that the index limits in the calculation of infinite number of linear equations can be set to a finite number since Fourier representation converges. This convergent behavior of the analysis eases the computational burden of the mathematical model.

Mechel's study investigates absorption mechanism of Schroeder Diffusers theoretically and more accurately. There are several studies that confirm this mathematical model with experimental data. Absorption mechanism of one – dimensional Schroeder Diffuser is investigated both theoretically and experimentally in T. Wu, T. J. Cox and Y. W. Lam's study [7]. This study mainly focuses on the absorption characteristics of Schroeder Diffuser. Scattering behavior of the diffuser

is not the concern. Since scattering is not the main point, study further investigates the effect of viscous, shear and thermal losses by narrowing well width of the diffuser to millimeter size. Mutual interactions between wells are studied using Mechel's Fourier analysis. Theoretical results are later compared with experimental results of the modeled specimen. Measurements are conducted in an impedance tube with a square cross section for normal incidence sound absorption performance. The results from the experiment show that Mechel's mathematical model represents the physical behavior of the diffuser more accurately. Study further investigates the effect of a resistive layer; a thin mesh wire in the study, in front of diffuser channels that improves the absorption gained by the diffuser. This effect of the resistant layer is both mathematically modeled in theoretical calculations and confirmed with impedance tube experiments.

The amount of absorption and the frequency range where effective absorption occurs depend on the distribution of differently tuned wells of the diffuser. This tuning can be modified and optimized to improve the absorption characteristic of the diffuser and provides an environment where the cut-off frequencies can be altered to desired frequency bands. By achieving even distribution of resonance frequencies of wells, higher absorption can be obtained. This modification is simply done with a numerical optimization. T. Wu, T. J. Cox and Y. W. Lam's study also gives an idea about how this optimization creates a more practical diffuser as an absorber [7]. This numerically optimized mathematical model is also compared with experimental results. The data generally fit with the analytical results.

These studies show that Schroeder diffusers provide good absorption even below the design frequency of the diffuser. A better absorption characteristic can be maintained even at lower frequencies by adding acoustic mass to the structure. Using perforated panels for this purpose is a good choice. Perforated panel absorbers provide high absorption at low frequencies when used with air back cavities. Hence, using these panels in some of the wells introduce lower resonance frequencies and alter the

resonance frequency distribution of the structure. This modification extends the effective absorption range of the Schroeder diffuser which already provides good absorption at mid frequencies. T. Wu, T. J. Cox and Y. W. Lam also investigated this modification in their study [8] both theoretically and experimentally. Fourier analysis is used for mathematical model of the mutual interactions between wells. A numerical optimization procedure is also involved to further improve the absorption characteristic of the diffuser at low frequencies. This is done by changing the locations of added perforated panels in the channels. By optimizing the air back cavity depth of the panel absorber system; resonance frequency distribution is further modified to shift effective absorption range to lower frequencies. In the paper, effect of resistive layer in front of the diffuser surface is also studied when perforated panels are present. Study concludes fascinating results that Schroeder diffusers can provide high absorption at low frequencies as well as at mid frequencies.

2.3. Analytical Solutions on Sound Absorption Characteristics of Micro-perforated Panels

Since late sixties, micro-perforated panels are used in some research and commercial applications for absorption purposes. These panels are generally used with porous materials and they serve as a protective layer [9]. After a while, its necessity increased due to some sound absorption applications in severe conditions where porous materials are not applicable.

Micro-perforated panels are perforated panels where perforation size is reduced to sub millimeter size. Unlike the perforated panel, smaller aperture size provides better acoustic resistance with low acoustic reactance to enhance low frequency absorption when used with an air back cavity [10]. Its acoustic resistance capacity provided

application areas where porous absorbers cannot be used or perforated panels are insufficient.

An MPP is constructed with a lattice network of short tubes which are in sub millimeter size. Specific acoustic impedance of the short tube over a cross section area can be found by investigating the sound propagation in narrow tube [11]. Total acoustic impedance of the panel can be obtained by using an electric-circuit model where both acoustic resistance and reactance of the panel itself and the short tube lattice are included. This electrical circuit analogy for the prediction of sound absorption of micro-perforated panels is used in several studies [12, 13 and 14]. However equivalent circuit theory includes approximations specifically to model the boundary conditions. A better and more sophisticated model is studied in K. Sakagami, T. Nakamori, M. Morimoto and M. Yairi's work [14]. In the model Helmholtz integral equation is employed to model the absorptivity of micro-perforated panels. The prediction and the results are more rigorous and strict when explaining the low frequency response of the absorber. Low frequency absorption is not so exaggerated as is observed in equivalent circuit analogy, and revised theory in this study gives lower resonant peaks in absorption predictions.

The resonance frequencies of the absorber depend on the depth of the cavity behind as well as the configuration of the panel absorber. An MPP can be constructed by using a single panel with an air back cavity or using two MPPs separated with a channel with or without an air back cavity. The absorption prediction of each configuration is investigated in several papers both theoretically [13] and experimentally [15]. MPP provide effective absorption at the resonance frequency of the air back cavity in a sense of Helmholtz resonators. Using double-leaf micro-perforated panels (DLMPP) with a cavity between shifts the resonance frequency of the absorber to lower frequencies. Hence, by changing the configuration of the system while keeping the depth of the air back cavity, an effective absorber at lower frequencies can be produced. Maa's work [16] shows that using two panels

overlapping each other produces two resonance frequency regions, yielding a broader effective absorption range. However this type of configuration is still effective at the resonance frequency region of the absorber.

On the other hand, using DLMPP with a cavity between but without a rigid backing significantly increases the absorption even in lower frequencies other than the resonance frequency region. In this type of panel system the rear panel acts as a non-rigid backing and this configuration can be used as a space absorber. In K. Sagakami, M. Morimoto and W. Koike's work, the absorption mechanism of this double-leaf panel system is studied [14]. In Maa's work, however; this type of behavior at low frequencies is not observed. Hence there is another mechanism, which is still dominant at these low frequencies. This mechanism is due to the amount of acoustic resistance provided by micro-perforation. The acoustic reactance of the panel system tends to go to zero with decreasing frequency. Hence, only the acoustic resistance of the panel can produce such absorption below the resonance frequency region.

CHAPTER 3

FUNDAMENTALS AND GOVERNING EQUATIONS

3.1. Acoustic Wave Equation

3.1.1. Definition of Linear Acoustic Wave Equation

In fluids, acoustic waves are transmitted as longitudinal waves, namely compression waves. Compression waves are transmitted via successive compression and expansion of fluid particles in contact resulting in a pressure variation compared to the absolute pressure of the fluid medium. The amplitude of this pressure fluctuation is very small when compared to the amplitude of absolute pressure of the medium. Regarding perfect gases; thermodynamically, this compression and expansion action can be considered as isentropic. Since the variation in fluid pressure is small, energy transfer between any adjacent fluid particles is not at an appreciable amount. No entropy change occurs under these conditions. Excluding the effect of viscosity in real fluids, high energy transfers and nonlinear effects of high pressure variations, the acoustic wave propagation is simply considered as an adiabat (adiabatic and reversible) [17].

Under these circumstances, in order to express the acoustic wave propagation in fluids, a functional relationship should be determined between the instantaneous density ρ and the particle velocity u . This relationship can be expressed by the continuity equation on a differential fluid element as given in Equation (3.1).

$$\frac{\partial \rho}{\partial t} + \nabla \cdot (\rho \vec{u}) = 0 \quad (3.1)$$

The other fundamental equation to express the fluid motion is the force balance equation. Since viscosity effects and high pressure variations are neglected, this force equation can be expressed as;

$$\rho_0 \frac{\partial \vec{u}}{\partial t} = -\nabla p \quad (3.2)$$

This is the linear Euler's equation which is applicable for acoustic wave propagation with small amplitudes.

By taking the time derivative of the Equation (3.1) and the divergence of Equation (3.2), the well-known linear acoustic wave equation is determined by combining modified continuity and force equations:

$$\nabla^2 p = \frac{1}{c^2} \frac{\partial^2 p}{\partial t^2} \quad (3.3)$$

where p is the variation in fluid pressure as a consequence of successive compression and expansions within the propagation of acoustic wave and c is the speed of sound.

3.1.2. Harmonic Plane Waves

Harmonic plane waves are a particular solution set of acoustic wave equation where the fluid medium is homogenous and isotropic. The restriction on homogeneity and isotropy eventually concludes to constant speed of sound where the propagation of sound wave is non-dispersive. The main property of a harmonic plane wave is that

the magnitude and phase of each acoustic particle has a constant value on any plane which is perpendicular to the direction of propagation. This characteristic property of harmonic plane waves applies to any diverging acoustic wave far away from the source at large distances. If the direction of propagation is set to be on x axis; the general representation of a harmonic plane wave in Cartesian coordinates is;

$$p(x, t) = Ae^{j(\omega t - kx)} + Be^{j(\omega t + kx)} \quad (3.4)$$

Sign of the wave number k determines the propagation direction of the harmonic plane wave. $+kx$ indicates that the wave is propagating on negative $-x$ direction while $-kx$ indicates that the direction of propagation is on positive $+x$ direction. The general solution is composed of two terms which are propagating on opposite directions. Regarding the magnitudes of the coefficients of each term, the solution can be either a propagating wave on a particular direction or a standing wave which does not propagate at all. These coefficients are complex valued and determined by the boundary conditions in which the acoustic medium is restricted with.

Furthermore; the particle velocity associated with the acoustic pressure is determined by the Euler's equation as;

$$\vec{u}_x = \vec{u} \hat{x} = \left[\frac{A}{\rho_0 c} e^{j(\omega t - kx)} - \frac{B}{\rho_0 c} e^{j(\omega t + kx)} \right] \hat{x} \quad (3.5)$$

The relation between acoustic pressure and particle velocity is determined by a significant parameter which is known as the acoustic impedance. For harmonic plane waves, the acoustic impedance is simply $\pm \rho_0 c$, where $\rho_0 c$ is the ambient density of the homogenous medium.

Equation (3.4) represents the acoustic wave motion in 1D Cartesian coordinates where both solutions of propagating waves in either directions are available.

Considering only propagating waves, the harmonic plane wave solution can be written in 3D Cartesian coordinates for any arbitrary direction as;

$$p(x, t) = Ae^{j(\omega t - k_x x - k_y y - k_z z)} \quad (3.6)$$

The frequency in time domain, ω , is related to the spatial frequency k , namely the wave number, with dispersion relation. In 3D Cartesian coordinates the dispersion relation is written as;

$$\left(\frac{\omega}{c}\right)^2 = k^2 = k_x^2 + k_y^2 + k_z^2 \quad (3.7)$$

The expression between the frequencies in both time and spatial domains is only related with the speed of sound. This type of propagation phenomena is called as non-dispersive which applies to propagation of sound in fluids since only the compression waves travel through the medium. The other type of propagation phenomenon is dispersive in which the speed of sound is not constant and depends on frequency of the harmonic motion in time. Dispersive propagation of sound generally exists in solids where transverse waves also originates and propagates in the medium.

3.1.3. Energy Density and Acoustic Intensity

The energy transmitted with an acoustic wave can be divided into two components: the kinetic energy of a fluid particle due to the particle velocity arisen from the wave motion and the other is the potential energy that is stored in the compressed fluid particles during wave motion. At a particular time frame; the amount of energy stored within a unit volume of fluid medium can be expressed as the sum of both instantaneous kinetic and potential energy densities, joules per cubic volume (J/m^3);

$$\varepsilon_i = \frac{1}{2} \rho_0 \left[u^2 + (p/\rho_0 c)^2 \right] \quad (3.8)$$

Equation (3.8) describes the amount of energy density at an instantaneous time frame. Since sound energy is transmitted with acoustic waves, the energy density of the medium varies with respect to the particular time frame. The total average energy carried with the acoustic wave is evaluated by integrating the energy density of the fluid over the period of the acoustic wave and taking the time average. Eventually; the energy density for an acoustic wave of single frequency is described as;

$$\varepsilon = \langle \varepsilon \rangle_T = \frac{1}{T} \int_0^T \varepsilon_i dt = \frac{p^2}{2\rho_0 c^2} \quad (3.9)$$

On the other hand, the instantaneous acoustic intensity is the instant rate of work done by a fluid element onto the adjacent element per unit area during the propagation of acoustic wave. Instantaneous acoustic intensity in watts per square meter (W/m^2) for a mono frequency acoustic wave is defined as;

$$I(t) = pu \quad (3.10)$$

Similar with energy density; by integrating instantaneous intensity over the whole period of the mono frequency acoustic wave and taking time average; acoustic intensity of a sound wave can be obtained as;

$$I = \langle I(t) \rangle_T = \frac{1}{T} \int_0^T I(t) dt = \pm \frac{p^2}{2\rho_0 c} \quad (3.11)$$

Since the acoustic intensity is the average rate of energy transfer through a unit area normal to the direction of propagation, the sign of acoustic intensity might differ with respect to the direction of propagation.

3.1.4. Specific Acoustic Impedance and Admittance

Specific acoustic impedance is defined as the ratio of the acoustic pressure to the particle velocity associated with that acoustic pressure in a medium. Since the particle velocity is a directional field regarding the direction of propagation, the specific acoustic impedance is also direction dependent. For harmonic plane waves, it is defined as;

$$Z = \frac{p}{u} = \pm \rho_0 c \quad (3.12)$$

The acoustic impedance is a real valued parameter for harmonic plane waves propagating in a medium; however, it takes complex values for standing and diverging waves. In general, the specific acoustic impedance is composed of two terms. The real term is called as the acoustic resistance and the imaginary term is called as the acoustic reactance.

$$Z = R + iM \quad (3.13)$$

The specific acoustic admittance of a medium is nothing but the inverse of the specific acoustic impedance which is expressed as;

$$G = \frac{1}{Z} \quad (3.14)$$

3.2. Reflection, Transmission and Absorption of Sound Energy

Sound waves generated from a source are transmitted in an unbounded medium as propagating waves. When propagating waves encounter a solid boundary or a fluid medium change, reflected and transmitted sound waves are generated. The dynamics

of reflection and transmission is basically depending on the boundary conditions and the incidence angle of the incoming acoustic wave.

In general, a portion of incident wave incoming to a boundary is reflected back to the medium and the other portion of the incident wave is transmitted into the encountered medium. This phenomenon is simply be discussed when harmonic plane waves are involved. Unless one of the medium is solid, it is simple to obtain the general behavior of reflection and transmission of the sound waves with boundary conditions. When a solid boundary is encountered some complications arise due to the coupling of acoustic and mechanical waves at the boundary of contact.

The amount of energy reflected from a boundary is described with the ratio of the reflected sound energy to the incident sound energy. This ratio is known as the reflection coefficient. Reflection coefficient is obtained by the ratio of sound intensities of the reflected and incident acoustic waves. Likewise; the amount of transmitted energy is obtained with the use of transmission coefficient which is simply the ratio of sound intensities of the transmitted and incident acoustic waves.

$$r = I_r / I_i \quad (3.15)$$

$$\tau = I_t / I_i \quad (3.16)$$

The simple case to observe reflection and transmission phenomena is the change of medium on the direction of propagation. The specific acoustic impedances of both medium are labeled as $\rho_1 c_1$ and $\rho_2 c_2$ in Figure 3.1. Since the total energy is presevered; the reflected and transmitted sound energy sum is equal to the energy of the incident acoustic wave. This conservation is all true for the acoustic intensities, reflection and transmission coefficients.

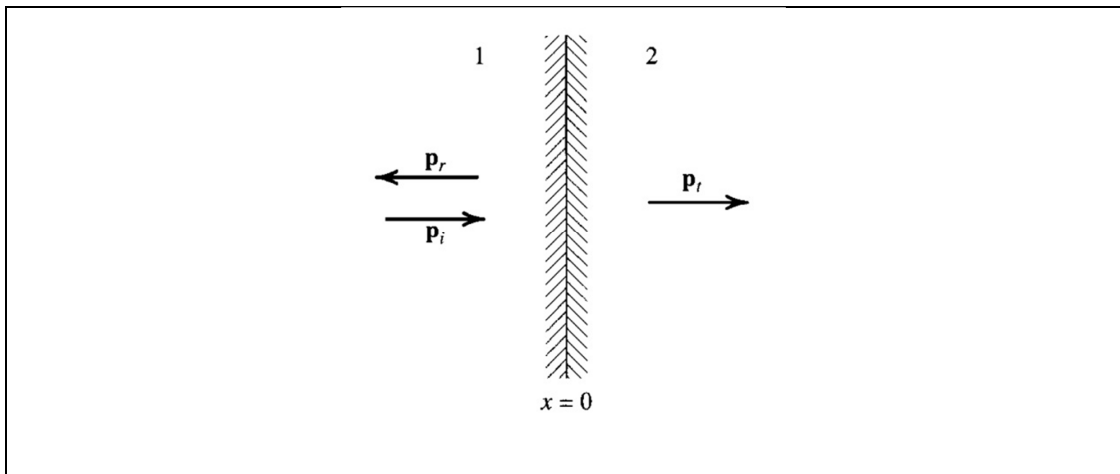


Figure 3.1 Reflected and transmitted sound field on a boundary

Absorption of sound is a mechanism in which the energy carried with the acoustic wave is dissipated and transformed to another form of energy. The form this energy can be thermal or mechanical with respect to the boundary or medium that the acoustic wave encounters while travelling in a medium. Dissipation of sound energy always exists when the sound waves propagate in a medium. This dissipation is generally due to the thermal relaxation of fluid molecules when excited with a wave form. Dependent to the specific acoustic impedance and the porosity of the medium the amplitude of this dissipation is variable. However; when a solid boundary is encountered, a portion of the transmitted energy through the solid boundary might be transformed to mechanical energy, mostly by means of mechanical vibrations. Then, this mechanical energy is dissipated due to damping characteristics of the solid.

$$I_r + I_t = I_i \quad (3.17)$$

$$r + \tau = 1 \quad (3.18)$$

The amount of absorbed energy is simply determined with the absorption coefficient, which is nothing but the ratio of absorbed energy density to the incident sound energy density. However, rather than evaluating the amount of absorbed energy density which is quite impossible, it is easier to determine the absorption coefficient by satisfying the energy conservation. Since the reflection and transmission coefficients can be evaluated using boundary conditions, the absorption coefficient can be determined by;

$$\alpha = 1 - (r + \tau) \quad (3.19)$$

Solid media support two types of elastic waves, which are longitudinal and transverse waves. If the transverse dimension of the solid is larger than the wavelength of the incoming acoustic wave, the phase speed of the propagating wave in the solid medium is not the bar speed, rather the bulk speed. If the wavelength of the acoustic wave is comparable or smaller than the transverse dimension of the solid, then the appropriate phase speed of propagation is the bar speed. Bar speed as the appropriate propagation speed is observed generally in plates or membranes. If this is the case, the direction of the elastic transverse wave propagating on a plate or a membrane is perpendicular to the normal of the plate's surface. This type of media is called *locally reacting* where no wave propagation exists parallel to the surface of the plate or membrane. Otherwise the medium is called *bulk reacting*, where longitudinal waves can propagate through the solid with the bulk speed of the elastic wave.

3.3. Acoustic Absorbers

Acoustic absorbers are devices to absorb sound energy and transform it to various types of energy forms described previously. The need of acoustic absorbers has

arisen in room acoustic to treat reverberation characteristic of an enclosed space. Reverberation characteristic of a room is the basic feature that defines the behavior of energy decay. It is simply related with the amount of sound energy that cumulates within the room after a sound source is off. This cumulated energy then, decays due to various types of energy dissipation. The acoustic parameter that defines this behavior of the enclosed space is reverberation time. The reverberation time is loosely the time required to observe the decay of sound energy level after a sound source is off in an enclosed space. The reverberation time is high in spaces with hard surfaces or large volumes such as cathedrals where sound echoes successively added up and start ringing in the space. On the other hand small spaces with soft and acoustically absorbent materials have less reverberation time where sound energy decay occurs quickly. Acoustic absorbers are basic devices to control reverberation characteristics of a room via dissipating incoming sound energy.

There are various types of acoustic absorbers; however they are generally classified into two major groups with respect to the type of energy dissipation within the absorber:

1. Porous Absorbers
2. Panel (Resonant) Absorbers

3.3.1. Porous Absorbers

Materials such as carpets, cushions, curtains, acoustic tiles and foams, cotton and mineral wools are called porous absorbers given in Figure 3.2. Sound absorption in such materials occurs via viscous and thermal dissipation of the acoustic wave that penetrates into those materials. Since air is a viscous medium, the air perturbation

with an acoustic wave is viscously dissipated within the pores of porous absorbers. There are also losses due to thermal dissipation especially in low frequencies [11].

To absorb sound energy, an absorber should be placed somewhere where the particle velocity is high. The particle velocity is usually zero at room boundaries. Due to low velocity profile at boundaries, it is not possible to obtain adequate absorption when an absorber mounted on a room boundary. Hence the thickness of the porous absorber should be enough to cover the maximum velocity range of an acoustic wave travelling at particular frequency. The wavelength of the low frequency sound is long; the thickness of the porous absorber should be also long to obtain significant absorption at low frequencies. This is a great disadvantage for porous absorbers regarding the effectiveness at low frequencies.

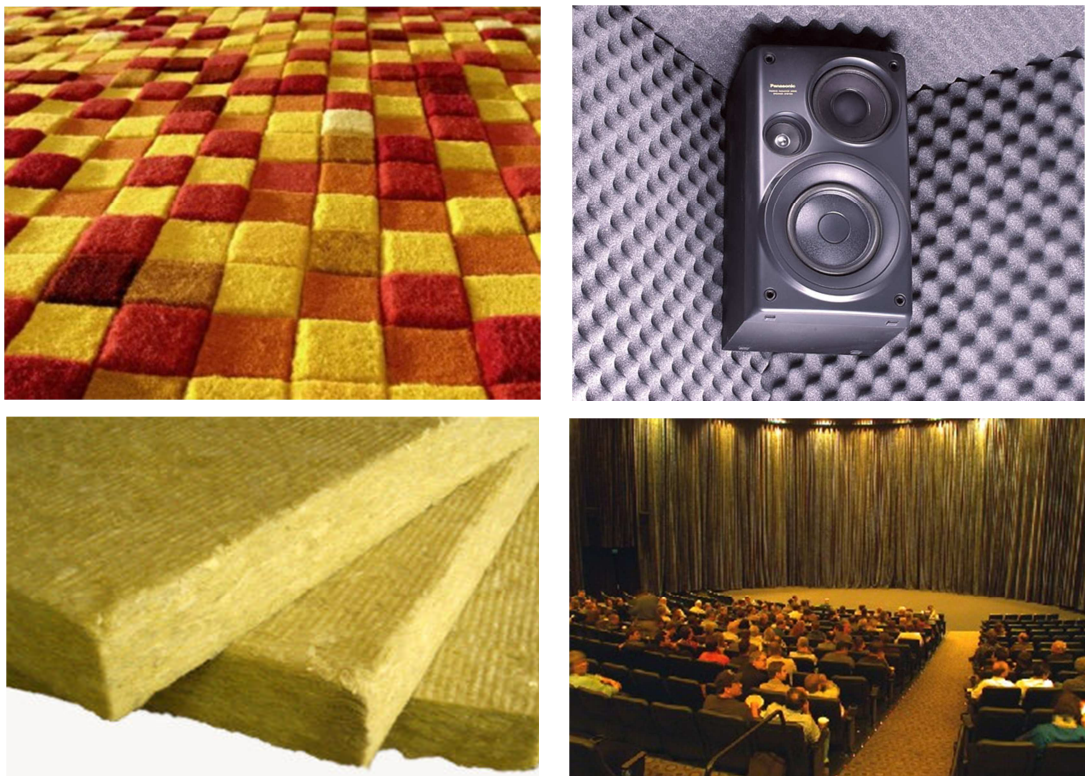


Figure 3.2 Porous absorber examples

3.3.2. Panel (Resonant) Absorbers

Panel absorbers are devices, unlike porous absorbers, granting absorption via converting acoustic energy to mechanical energy by means of mechanical vibration. Various examples of resonant absorbers are given in Figure 3.3. By introducing resonance frequencies, it is possible to obtain significant absorption at particular bandwidths including low frequencies. Moreover, absorption treatments are generally applied to room boundaries where porous absorbers are inefficient since the particle velocity is low at room boundaries. Most of the resonant absorbers are efficient at absorption when placed to room boundaries.

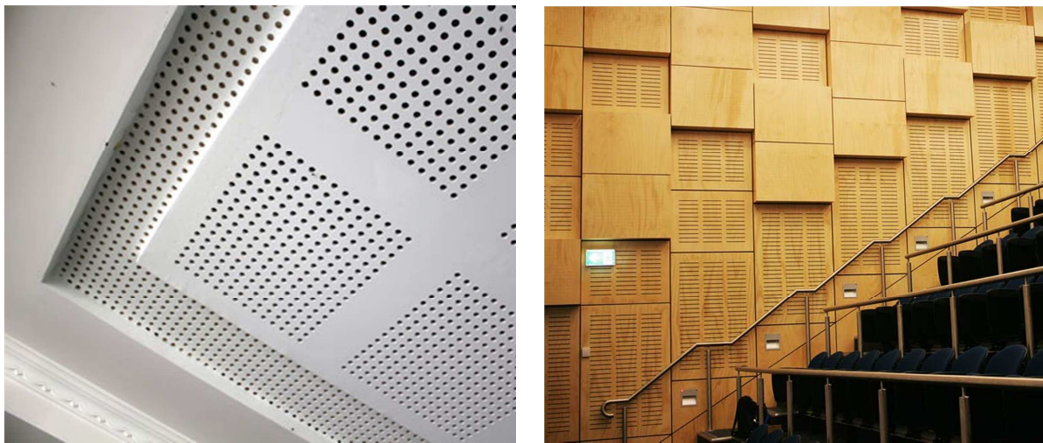


Figure 3.3 Resonant absorber examples

Resonant absorbers are mechanically analogous with a mass vibrating with a spring. Hence, these devices introduce resonance frequencies with respect to mass and spring characteristics of the system [18]. It is possible to change the range of resonance frequencies by changing the vibrating mass and the stiffness of air spring behind the mass. The most common resonant absorber type is the Helmholtz

resonator. Helmholtz resonators are panel absorbers with a neck on the panel of the device.

A large portion of acoustic energy transmitted with the incoming acoustical wave is transformed to mechanical energy by resonant absorbers. The amount of this energy conversion is higher at the resonant frequencies of the absorber. However, transformed mechanical energy should be dissipated in order to absorb the sound energy. This mechanism can be provided by mounting porous materials into the neck of the resonant absorbers or just behind the panel where the particle velocity is high. In the second case, the porous material should not be so close to the membrane in order not to prevent the movement of the vibrating panel. Another way to gain more absorption without using porous materials is to decrease the aperture size of the neck on the panel. Smaller opening introduces viscous losses in which adequate amount of resistance is provided to enhance absorption.

The use of smaller openings in resonant absorbers is a breakthrough since the necessity of using porous materials to dissipate mechanical energy is avoided. These devices are generally called as perforated panel absorbers in which the perforation size can be modified to determine the amount of energy dissipation. The most effective version of perforated panels is micro perforated panels where the apertures are in sub millimeter size as shown in Figure 3.4. The effective diameter is just a bit larger than the boundary layer thickness, hence appreciable amount of viscous losses are achieved as the air passes through small holes. There is no need to use porous materials behind the perforated panel. By changing the depth of the air back cavity, the resonance frequency can be altered to low frequencies and with high amount of viscous dissipation, appreciable absorption is achieved at low frequencies. Maa [16], the pioneer of the micro perforated panels in the early 1960s, showed that the amount of absorption is maximized when the aperture size and the panel thickness are close to each other. So, using thinner panels increases the potential of the absorber with sub millimeter size apertures.



Figure 3.4 Micro-perforated panel absorber examples

The major challenge regarding resonant absorbers is the limited bandwidth where the effective absorption is obtained. Although the vibrating mass and air spring system provide single frequency resonances, the bandwidth can be extended by using porous materials within the panel absorber or decreasing the aperture size of the perforations in order to increase viscous losses. On the other hand, using double layer micro perforated panels with an air cavity in between introduces additional resonance frequencies. Arranging cavity depths and the mass reactance of the panels, the resonance frequencies can be manipulated so that a wide effective bandwidth with significant absorption can be achieved with evenly distributed resonance frequencies.

3.4. Acoustic Diffusers (Scatterers)

Acoustic diffusers (scatterers) are devices, like acoustic absorbers, to control the acoustic behavior of an enclosed space. Unlike absorbers, acoustic diffusers are not energy dissipating units; rather they function to control the reflection patterns of the incoming acoustic waves, thereby reducing effects of room resonances.

In large auditoria or concert halls, echoes and flutter echoes are the major problems that are worsening the intelligibility and the quality of sound that is perceived by listeners. Echoes are usually generated by the hard reflections from the boundaries of an enclosed space. Unlike reverberation in a room, echoes are late coming reflections from a boundary with a level significantly above the general reverberation in a room. Hence, they are heard as the direct sound coming with a short delay, which results in a local energy adding up in a short time frame. Echoes are generally formed by the reflections from parallel walls yielding to standing waves creating uneven sound energy distribution in an enclosed space.

Similar with reverberation control, unwanted echoes can be also controlled with acoustic absorbers. The uneven energy distribution can be avoided by removing the excess energy within the room. However, in some cases the amount of energy should be preserved. In concert halls, operas or such spaces with unique functions and necessitated acoustical quality; the amount of energy within, in other words the reverberation in the room, should be maintained. Hence, the number of acoustic absorbers employed is limited and acoustic diffusers are preferred to control the distribution of this energy in those places.

The main problem is to control the direction of the reflected wave from hard smooth surfaces. Such surfaces reflect the incoming acoustic wave with an angle identical with the incident angle. Since the surface is smooth or not irregular enough, the reflected sound energy is sent to a particular direction. The most critical example to this case is the reflection of sound from parallel surfaces.

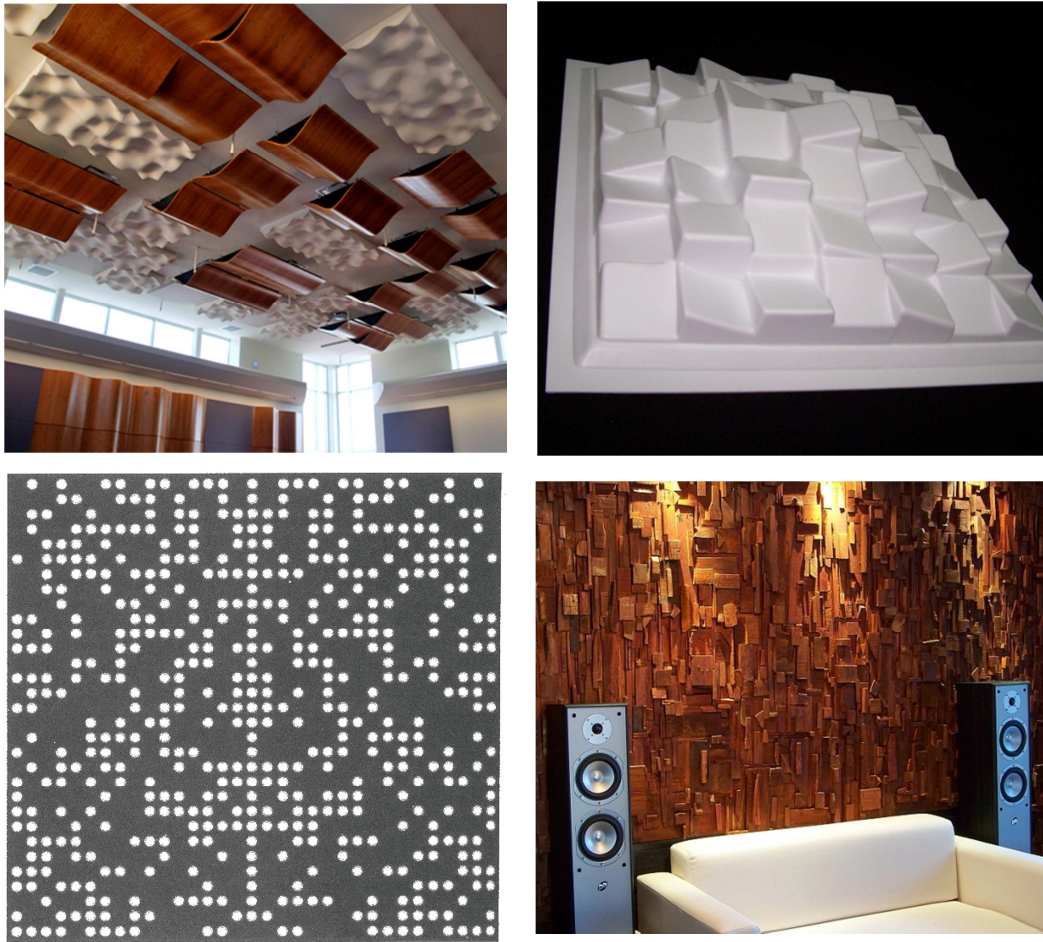


Figure 3.5 Various acoustic diffuser examples

When a parallel wall construction exists in the space, standing waves at particular frequencies are formed with respect to the wavelength of the incoming wave. This phenomenon results in energy peaks and dips at certain locations in the room. Consequently, the perception of sound at that particular frequency is not going to be the same compared to any other location in the room. To control this uneven distribution problem, the hard and smooth surfaces should be treated. The most common use of acoustic diffusers is to cover this reflection problem.

An acoustic diffuser is simply a surface or a group of surfaces that control the direction of the reflected sound waves. There are various examples of acoustic diffusers presented in Figure 3.6. Any irregular surface is assumed to be a diffuser; however, the amount of dispersed energy compared to the directly reflected energy might not be sufficient enough to avoid echoes.

The reflection from a surface can be understood with the definitions of specular and scattered reflections. Specular reflection is the direct reflection from a surface with an angle identical to the incident angle of an incoming sound wave. On the other hand, scattered reflection is a portion of reflected energy which is dispersed to the surrounding due to the roughness or the configuration of a surface. The ratio of scattered energy to the total reflected energy is called as the scattering coefficient. Scattering coefficient is the parameter that gives information about the dispersion of the reflected energy.

The distribution of irregularities or the geometry of a material surface determines the scattering characteristics and the directivity pattern of the reflected sound energy. Since the distribution of irregularities is random, it is hard to predict the scattered reflection and directivity patterns of the surface. However, the geometry of a surface can be arranged so that the direction of the scattered energy can be determined analytically. The most common example of acoustic diffusers with configured surface geometry is Schroeder Diffusers which are demonstrated in Figure 3.6. Apart from every other surface configuration, Schroeder diffusers are constructed on very simple design equations and provide predictable reflection patterns and optimum diffusion. Since recently, Schroeder Diffusers are widely used in room acoustic applications such as in concert halls, recording studios, etc. [19, 20].

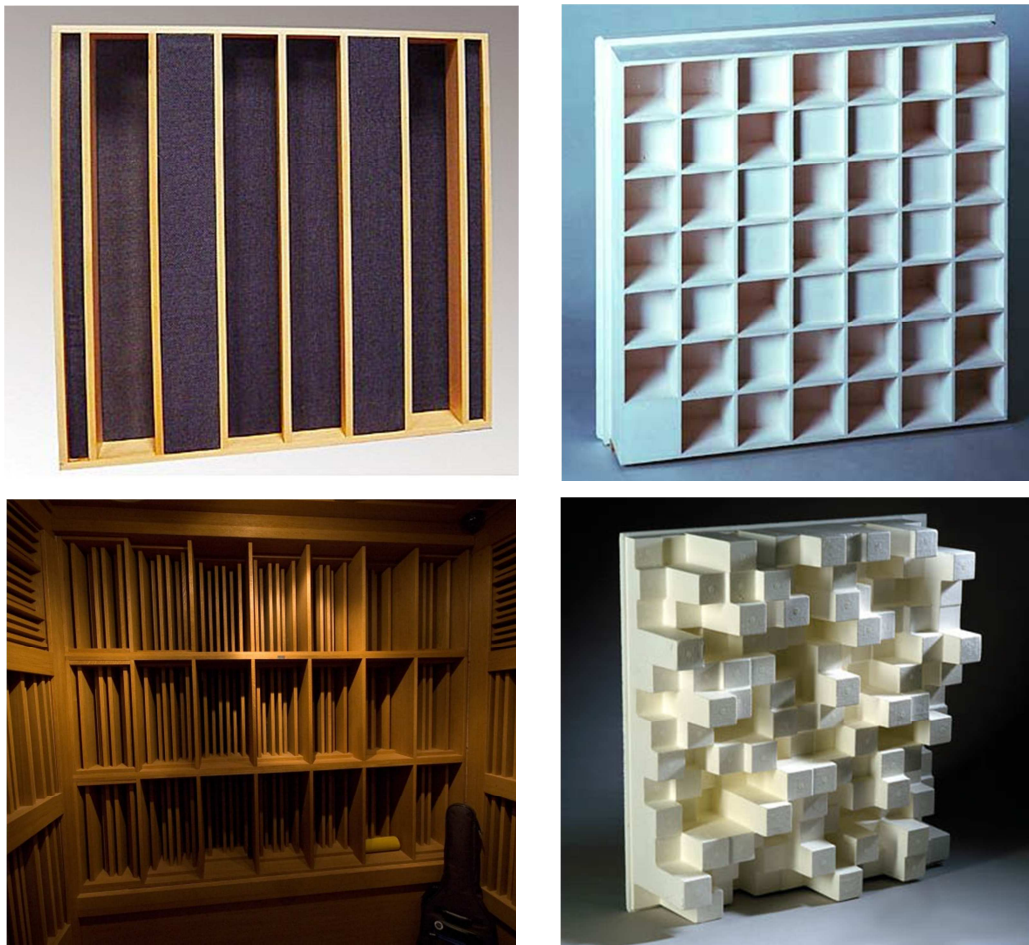


Figure 3.6 One and two dimensional Schroeder Diffusers

The design equations and the qualitative and quantitative perspectives of Schroeder diffusers will be presented and deeply discussed in the following chapter.

CHAPTER 4

ABSORPTION CHARACTERISTICS OF SCHROEDER DIFFUSERS

Schroeder diffusers are mostly used to scatter the incoming sound to create a diffuse field. However, appreciable amount of energy can be absorbed at certain frequencies as well. Preceding studies on the absorption characteristics of Schroeder Diffusers are presented in Chapter 2 in details.

Diffusers or absorbers are generally mounted onto the room boundaries to control the reflection patterns and absorption. The back of the devices are covered with a boundary which are assumed to be rigid. Eventually no sound propagation occurs through the rigid medium, that is the incoming sound energy is either reflected, absorbed or both. Although this is the most conventional way of employing these devices; panel absorbers can also be used as a space absorber, when hung on the airspace. Therefore the rigid backing is replaced with free or reverberant field since there is no boundary at the back of the absorber any more. This particular construction of panel absorbers enabled the significant low frequency absorption. DLMPP with an air gap between and hung over the space is a good example of this particular construction. With respect to the depth of the air gap between two panels a resonance frequency is introduced at some particular frequency. However, the existence of the free or reverberant field behind the rear panel grants low frequency transmission and absorption regardless of the resonance frequency. Due to the wavelength of the acoustic wave, incident energy directly penetrates through the absorber. Some of this energy is absorbed within the absorber by means of viscous

dissipation or mechanical energy conversion, the other portion is transmitted to the non-rigid fluid medium. By arranging the air gap depth and panel properties the amount of absorption can be maximized. This phenomenon is discussed in K. Sagakami, M. Morimoto and M. Yairi's work [14]. In the study, micro perforated panels are used to construct the panel absorber. The results have shown that the absorption coefficient at very low frequencies are maximized at a range between 0.4 – 0.5. This amount of absorption cannot be achieved with a regular construction of an absorber with a rigid backing.

A similar approach can be applied to a Schroeder diffuser by replacing the rigid backing with a non-rigid fluid medium. This particular use of the diffuser can be called as a space diffuser since both surfaces are exposed to a fluid medium, particularly air in architectural acoustics. Hence, the idea of space absorber, which is mentioned above, is inserted to the diffuser concept to observe how much absorption is going to be generated with Schroeder diffusers.

In the next section, the general theory of 1D space diffusers, implementation of micro perforated panels into the diffuser, narrower slits and the theory of absorption within the diffuser is going to be introduced and deeply analyzed. The absorption model is constructed on Mechel's Fourier Decomposition Method. However, this method is for conventional Schroeder diffusers with a rigid backing. In the following chapter this theory is going to be extended for non-rigid backings.

4.1. Fundamentals of Schroeder Diffusers

Schroeder diffusers are the most significant leap in diffuser design introduced by Schroeder [21], enabling diffusion by phase grating. Fundamentals of the diffuser are based on a simple design equation and have predictable directivity patterns with

optimized diffusion. A Schroeder diffuser is a combination of wells with different depths brought together and separated with fins. Yet they are used as a single unit, plenty number of them can be used to form a periodic structure. The basic principle behind diffusion is based on phase grating. When an acoustic wave is incident on a Schroeder diffuser surface, it penetrates into the differently tuned wells. Since the depth of each well is different, the time required for the wave to go into the well, reflect from the bottom and return to the surface is different for each well. This results in a group of waves with different phases when they return to the surface of the diffuser. The interaction of these waves creates a dispersed sound field which propagates to the far field. The wave front of each wave has a spatial phase difference that grants diffusion. The phenomenon can be understood with the following figure. The finite difference time domain (FDTD) model of a cylindrical wave incident on a Schroeder diffuser is shown in Figure 4.1.

The depth sequence of the differently tuned wells can be constructed with a different combination which enables distinct polar reflection patterns. Schroeder showed that the energy reflected to each diffraction lobe direction is going to be the same with a quadratic residue sequence when tuning the well depths. There are other sequences such as primary residue sequence that the tuning can be modified with. Regarding 1D quadratic residue sequence, the depth sequence number of each well can be determined by;

$$s_n = \text{mod}(n^2, N) \quad (4.1)$$

where s_n is the sequence number of the n^{th} well and N is the total number of wells in one period that should be a prime number. For instance; for $N = 7$, $s_n = [0, 1, 4, 2, 2, 4, 1]$.

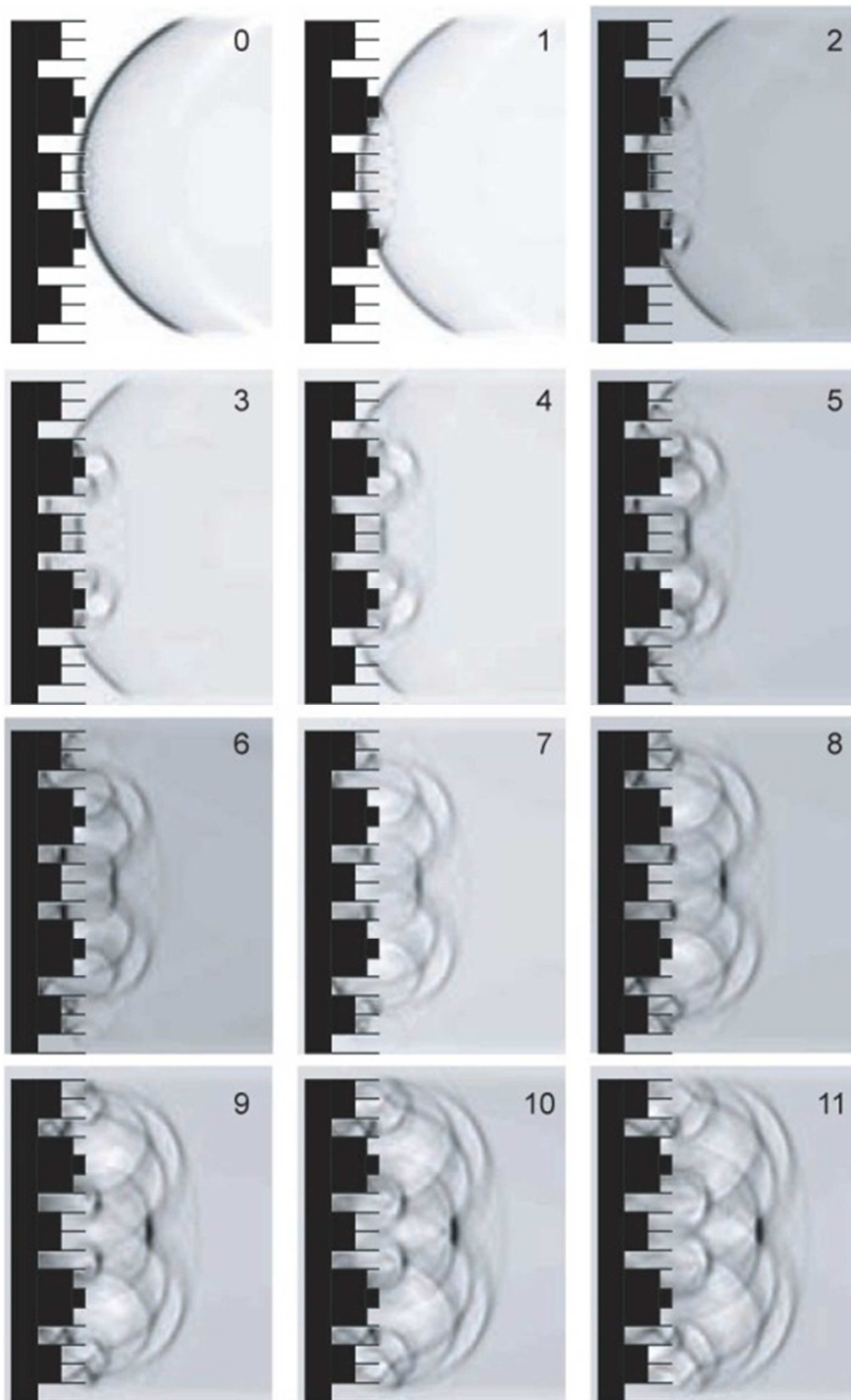


Figure 4.1 Visualization of the dispersed sound field in front of a Schroeder Diffuser, FDTD model [1]

Schroeder diffusers work at integer multiples of the design frequency, f_0 , which is generally set to the lowest frequency limit. Then the depth of a particular well can be obtained from the following equation;

$$l_n = \frac{s_n \lambda_0}{2N} \quad (4.2)$$

λ_0 is the design wavelength corresponding to the design frequency. f_0 is not the lowest frequency that the dispersion begins but it is the frequency where even distribution of scattered energy in diffraction lobes occurs. Below the design frequency scattering also occurs up to one or two octave bands below, when compared to a hard plane surface.

The design equations are basically constructed on plane wave propagation in the wells. Eventually, an upper frequency limit exists where cross modes appear to propagate in the wells. This requirement can be implemented into the theory by arranging the width of the wells presented in the following equation as;

$$w = \frac{\lambda_{\min}}{2} \quad (4.3)$$

where λ_{\min} is the minimum wavelength and w is the width on single well. Width values lower than the determined limit can also be assigned. Dispersion also occurs below this limit for defined well width, since these are complicated structures. However, the manner of dispersion may not be determined with the fundamental theory.

The energy directed to each energy lobe is greatly dependent on the repeat width or the period of the diffuser which is designated as $L = (w + h) \cdot N$, where h is the thickness of the fins. When the width of the wells is kept small, only one major energy lobe can appear at design frequency. A diffuser with narrow wells can only

create significant diffusion above the design frequency. The great amount of energy below this particular frequency is either specularly reflected or absorbed by the diffuser.

4.2. Absorption Theory for Schroeder Diffusers

The absorption theory for a space diffuser configured with DLMPP is going to be explained in two different models: A detached mathematical model and a combined mathematical model. In both models, losses within the viscous and thermal boundary layers in the wells are not included in the first place. This approximation provides a simple calculation since the wave number of the propagating wave in the wells is considered identical to the wave number in free field. However, the model is going to yield to an accurate prediction for large slits since the boundary layer thicknesses are very small when compared to the width of the wells. Otherwise, the effect of the boundary layers should be taken into account for narrow slits since the boundary layer thicknesses are considerable when compared to the width of the wells. This effect of thermal and viscous losses is going to be included for narrow slit predictions later.

4.2.1. Micro-perforated Panel Theory

Micro perforated panels are basically known for their good absorption characteristics even at low frequencies due to high viscous losses through sub millimeter size apertures. The theory behind absorption mechanism of micro perforated panels is introduced by Maa [16]. These absorbers have many advantages since they are light weight, inexpensive and remove the necessity of porous materials which might be

harmful to human health. Micro perforated panel absorbers are basically composed of a panel, which is a sub millimeter aperture lattice with a low aperture ratio and an air gap behind.

The resonance frequencies introduced by both apertures and the panel are at a close range. Due to this fact, their simultaneous effects should be considered together. The acoustic impedance of the panel system can be constructed on a parallel connection of the impedances of the panel and apertures. Since the connection is parallel, the effect of one element greatly depends on its relative impedance to the other. If the impedance of the panel is greater than the apertures, then the effectiveness of the panel absorber significantly depends on the apertures. This is true for the opposite case. Eventually, the impedance of the micro perforated panel can be adjusted by modifying the panel and aperture parameters.

The impedance of the panel can be constructed on electric circuit analogy [15]. The acoustic resistance and reactance of the panel are connected in series. Similarly, the acoustic resistance and reactance of the apertures are connected in series. Resulting acoustic impedances of both the apertures and the panel are connected in parallel as shown in Figure 4.2.

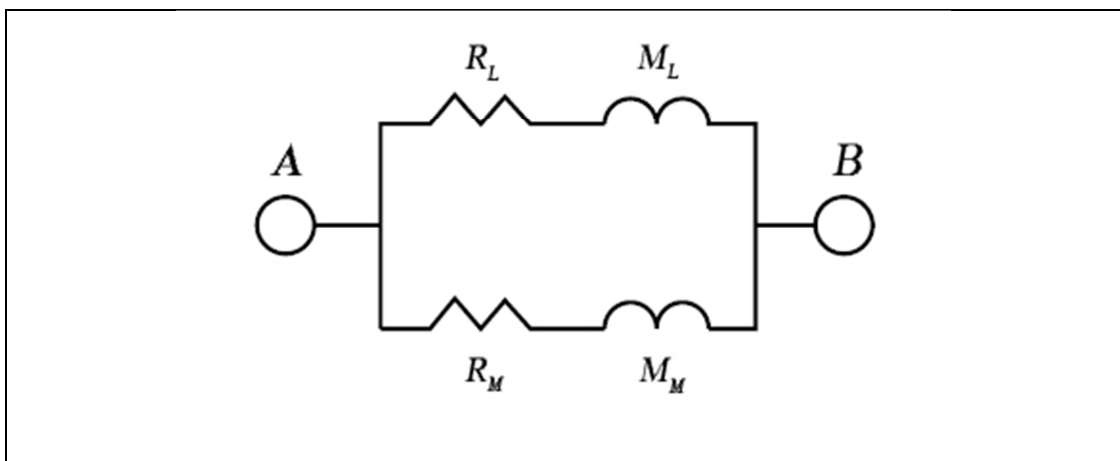


Figure 4.2 Electric circuit representation of a micro-perforated panel impedance

First, acoustic impedance of each element should be determined. For a tension free panel, the normal specific acoustic impedance of the panel is normalized by characteristic acoustic impedance of air and defined as;

$$z_M = \frac{R_M + jM_M}{\rho c} = r' + j\omega m'' \quad (4.4)$$

R_M and M_M stand for acoustic resistance and reactance of the imperforated panel respectively. r' is the normalized acoustic resistance of the panel and depends on the mounting conditions. $m'' = m'/\rho c$, where m' is the surface mass density of the panel (kg/m^2). $\omega = 2\pi f$, where f is the interested frequency (Hz).

Secondly, the effect of apertures should be determined separately. The sub millimeter size apertures can be considered as short tubes. The propagation of sound in short tubes is first introduced by Rayleigh, and then a simple version of it is discussed by Crandall. Since the calculation of the propagation of sound is not simple, Crandall proposed two solutions regarding small and large apertures. To determine the acoustic impedance of the apertures, Maa combined both solutions together and introduced an approximate solution for sub millimeter size apertures. When compared with conventional perforated panels, Maa's approximate solution for the aperture impedance provided a significant feature where acoustic resistance becomes very dominant for sub millimeter size apertures. Eventually, the use of porous materials is not necessitated to provide good absorption.

The normalized specific acoustic impedance of the apertures can be calculated as;

$$z_L = \frac{R_L + jM_L}{\rho c} = r + j\omega m \quad (4.5)$$

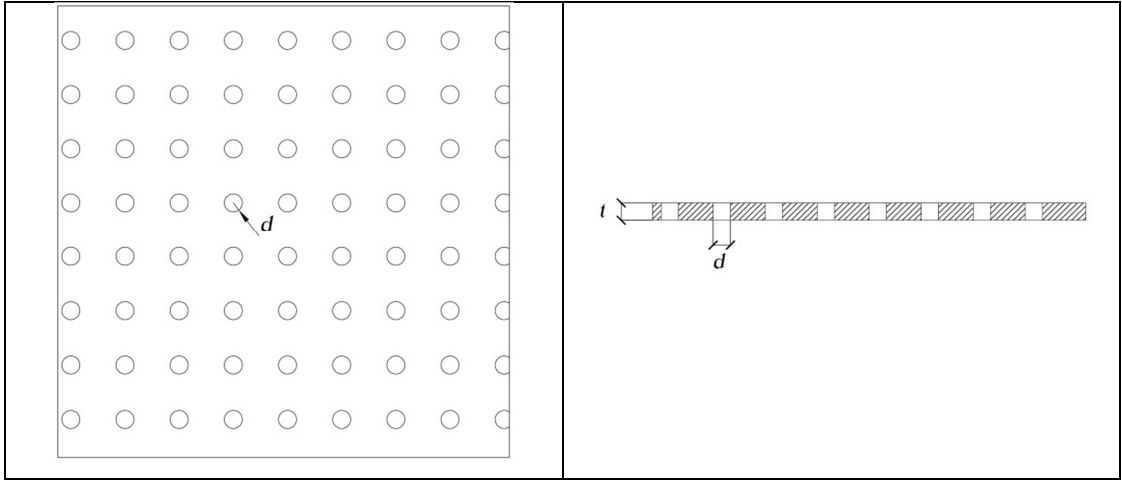


Figure 4.3 Top and side views of a micro-perforated panels showing design parameters

R_L and M_L stand for acoustic resistance and reactance of the apertures respectively. r and m are the normalized acoustic resistance and reactance of apertures and can be defined as;

$$r = \frac{g_1}{d^2} \frac{t}{p} K_r \quad (4.6)$$

$$m = 0.294 \cdot 10^{-3} \frac{t}{p} K_m \quad (4.7)$$

K_r and K_m are defined as;

$$K_r = \sqrt{1 + \frac{x^2}{32} + \frac{x\sqrt{2}}{8} \frac{d}{t}} \quad (4.8)$$

$$K_m = 1 + \frac{1}{\sqrt{9 + \frac{x^2}{2}}} + 0.85 \frac{d}{t} \quad (4.9)$$

and,

$$x = g_2 d \sqrt{f} \quad (4.10)$$

As shown in Figure 4.3, t is the panel thickness (mm), d is the aperture size (mm), p is the aperture ratio which is defined by the ratio of total aperture area to the panel area, g_1 and g_2 are constants. For non-metallic materials; $g_1 = 0.147$ and $g_2 = 0.316$. For metallic materials; $g_1 = 0.335$ and $g_2 = 0.210$. When the normalized acoustic impedance of both apertures and the panel are determined, the normalized specific acoustic impedance of the panel system can be determined as;

$$z_p = \frac{z_M z_L}{z_M + z_L} \quad (4.11)$$

4.3. Prediction of Absorption for Schroeder Diffusers

The main idea in this study is to determine the absorption characteristics of a Schroeder Diffuser where the back of the diffuser is exposed to a free or reverberant field. Since both surfaces are not restricted with a rigid surface it is better to call it as “*Space Diffuser*”. The theory of absorption for conventional type of Schroeder diffusers are deeply analyzed in Mechel’s work. In this chapter, the mathematical model to analyze the absorption characteristics of the Schroeder diffusers is going to be extended for space diffusers. In conventional diffusers the bottom of each well is assumed to be rigid. Hence the pressure gradient at the bottom of each well becomes zero. Unlike conventional types, this rigidity is going to be replaced with DLMPP to enhance low frequency absorption by adding acoustic mass and introducing high viscous losses through sub millimeter size apertures. Figure 4.4 shows a schematic representation of a 1D quadratic residue space diffuser.

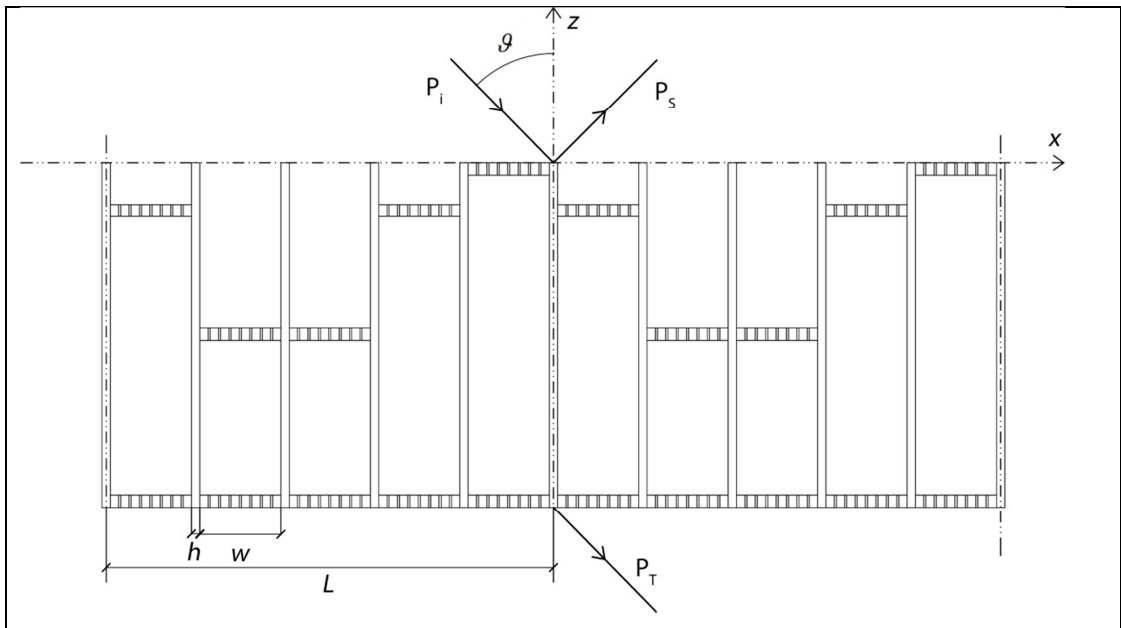


Figure 4.4 A figurative representation of a one dimensional Schroeder Diffuser

To deeply understand the absorption mechanism in space diffusers, just like conventional Schroeder diffusers, the sound propagation in the diffuser wells should be investigated. By this approach, the sound field in front of the diffuser surface, as well as at the back of the diffuser should be determined. After the boundary conditions are set, the governing equation which expresses both scattered and transmitted energy distribution can be obtained.

There are two methods to predict the reflected sound intensity at a point in front of the Schroeder diffuser. One of them is the average admittance method where the surface admittances of differently tuned wells are averaged to end up with a single admittance value. Average surface admittance method assumes a uniform pressure field in front of the diffuser, which is an approximate method and cannot clearly clarify the mutual interactions between the wells. The second method is the Fourier expansion method, introduced by Mechel [5]. This method is capable to rigorously model the mutual interaction and more correctly considers the coupling between the

wells. The restriction in this case is that the diffuser should be periodic. Infinitely many number of Schroeder diffusers should be set to form a periodic structure. With Fourier expansion, the sound field in front of the periodic surface can be expanded with the harmonics of the incident wave at a particular frequency. Later on, the use of infinitely many numbers of diffusers is going to be narrowed down to a finite number since the solution is going to converge to a single value.

4.3.1. Detached Mathematical Model

To construct a reasonable mathematical model while predicting absorption characteristics, pressure functions both scattered and transmitted sound field should be determined. To do that the prediction model closely follows Mechel's method. Since the diffuser structure is periodic, the scattered and transmitted sound fields are also periodic. It is less complicated to analyze each sound field when the other is not periodic in the first place. Hence, a detached model can be constructed on a periodic sound field in front of the diffuser while the field is not periodic at the back. Similarly, the same model can be constructed in which the field is periodic at the back while non-periodic at front. Afterwards, the contribution of spatial harmonics on both sides of the diffuser is going to be included in the theory.

Firstly, the sound field in front of the diffuser surface is going to be assumed as periodic. As shown in Figure 4.4, the field at the front can be decomposed into the incident sound field $p_i(x, z)$ and the scattered field $p_s(x, z)$. For simplicity $e^{j\omega t}$ components will be neglected in the equations.

$$p(x, z) = p_i(x, z) + p_s(x, z) \quad (4.12)$$

$$p_i(x, z) = P_i \cdot e^{j(-k_x x + k_z z)} \quad (4.13)$$

$$p_s(x, z) = \sum_{n=-\infty}^{\infty} A_n \cdot e^{-j(\beta_n x + \gamma_n z)} \quad (4.14)$$

where $k_x = k \cdot \sin \theta$ and $k_z = k \cdot \cos \theta$ from dispersion relation.

Since the sound field in front of the diffuser surface is periodic, the wave numbers in the x and z directions of spatial harmonics are;

$$\beta_n = k_x + n \frac{2\pi}{L} \quad (4.15)$$

$$\gamma_n = \sqrt{k^2 - \beta_n^2} = -jk \sqrt{\left(\sin \theta + n \frac{\lambda}{L}\right)^2 - 1} \quad (4.16)$$

where $\lambda = 2\pi/k$, the wavelength of the interested frequency and L is the period width of the space diffuser. The acoustic wave components within the scattered field which are propagating into far field should not have a complex wave number in z direction. Hence, corresponding propagating harmonics indices n_s can be determined from;

$$\left(\sin \theta + n_s \frac{\lambda}{L}\right)^2 \leq 1 \quad (4.17)$$

Harmonic indices that do not satisfy above requirement cannot propagate into far field. Eventually, the scattered field is composed of both propagating and evanescent waves due to the periodicity in x direction.

The non-periodic sound field at the back of the diffuser can be described as;

$$p_t(x, z) = P_t \cdot e^{j(-k_x x + k_z z)} \quad (4.18)$$

When the sound propagation in a single well is set, it can be expanded into the whole structure. Therefore, sound fields and the boundary conditions on diffuser boundaries

are going to be determined for a single well. The pressure fields inside a single well can be examined in two regions (2nd and 3rd regions) as shown in Figure 4.5. In both regions, there are two wave components; one of them is a transmitted wave and the other is a reflected wave yielding an evanescent wave together. Since the width of the wells is small compared to the wavelength of the incoming sound wave, only the fundamental modes can propagate into the wells, i.e. $w \ll \lambda/2$. Hence, the sound propagation inside the wells is nearly one-dimensional wave propagation on z direction. This condition enables the cancellation of higher modes in the wells which are generated by the reflections from the fin walls of each well.

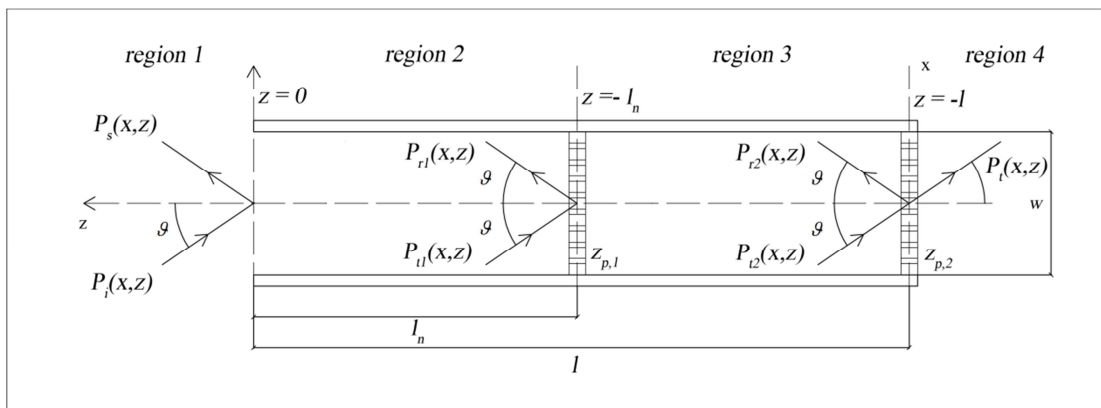


Figure 4.5 Sound fields inside the well of the diffuser

For simplicity the sound propagation inside wells is assumed to be lossless. The effect of viscous and thermal boundary layers inside wells is going to be included later. Since the losses are neglected the wave number of one-dimensional wave propagation inside wells is a real valued number, and identical with the wave number in the free field. As shown in Figure 4.5, the pressure fields in both regions are defined as;

$$\begin{aligned}
p_{t1}(x, z) &= P_{t1} \cdot e^{j(-k_x x + k_z z)} \\
p_{r1}(x, z) &= P_{r1} \cdot e^{-j(k_x x + k_z z)} \\
p_{t2}(x, z) &= P_{t2} \cdot e^{j(-k_x x + k_z z)} \\
p_{r2}(x, z) &= P_{r2} \cdot e^{-j(k_x x + k_z z)}
\end{aligned} \tag{4.19}$$

The corresponding velocity components in z direction for each pressure field are defined as;

$$\begin{aligned}
v_{i,z}(x, z) &= -\left(\frac{\cos \theta}{\rho_0 c}\right) \cdot P_i \cdot e^{j(-k_x x + k_z z)} \\
v_{s,z}(x, z) &= \frac{1}{\rho_0 c} \cdot \sum_{n=-\infty}^{\infty} A_n \frac{\gamma_n}{k} \cdot e^{-j(\beta_n x + \gamma_n z)} \\
v_{t1,z}(x, z) &= -\left(\frac{\cos \theta}{\rho_0 c}\right) \cdot P_{t1} \cdot e^{j(-k_x x + k_z z)} \\
v_{r1,z}(x, z) &= \left(\frac{\cos \theta}{\rho_0 c}\right) \cdot P_{r1} \cdot e^{-j(k_x x + k_z z)} \\
v_{t2,z}(x, z) &= -\left(\frac{\cos \theta}{\rho_0 c}\right) \cdot P_{t2} \cdot e^{j(-k_x x + k_z z)} \\
v_{r2,z}(x, z) &= \left(\frac{\cos \theta}{\rho_0 c}\right) \cdot P_{r2} \cdot e^{-j(k_x x + k_z z)} \\
v_{t,z}(x, z) &= -\left(\frac{\cos \theta}{\rho_0 c}\right) \cdot P_t \cdot e^{j(-k_x x + k_z z)}
\end{aligned} \tag{4.20}$$

Defined pressure field functions and corresponding velocity components in z direction are the general solutions for the wave propagation inside and outside the diffuser. In order to determine the complex pressure amplitudes, the boundary conditions must be set. There are three boundaries where medium changes occur.

At $z=0$, there is neither a solid boundary nor a medium change. However, the sound field in the 1st region is a periodic field while it is not in the 2nd region. This condition is also true for the wave numbers. Since the wave numbers in each sound field is not the same, a boundary can be defined between two regions. The first condition is that the net force on the interference of two regions should be equal to zero in Equation (4.21). The second condition arises due to the fluid contact. Since both regions are fully in contact, the velocity components for both fields in z direction should be identical at the boundary Equation (4.22).

$$p_i(x,0) + p_s(x,0) - [p_{t1}(x,0) + p_{r1}(x,0)] = 0 \quad (4.21)$$

$$P_i + \sum_{n=-\infty}^{\infty} A_n \cdot e^{-jn\frac{2\pi}{L}x} - (P_{t1} + P_{r1}) = 0$$

$$-\cos\theta \cdot P_i + \sum_{n=-\infty}^{\infty} A_n \frac{\gamma_n}{k} \cdot e^{-jn\frac{2\pi}{L}x} + \cos\theta \cdot P_{t1} - \cos\theta \cdot P_{r1} = 0 \quad (4.22)$$

At $z=-l_n$, the propagating acoustic wave inside the well encounters the second boundary. The contact between the air inside wells and the micro perforated panel introduces mechanical and acoustical wave coupling. The MPP thickness is set to be very small, approximately as the size of the apertures to enhance acoustic resistance. Since the solid thickness is comparably small when compared to the wavelength of the incoming acoustic wave, the propagation speed of the mechanical transverse wave on the panel is the bar speed rather than the bulk speed of the panel. Similarly;

a thin panel thickness makes the panel a locally reacting absorber. Eventually, no wave propagation occurs on the panel on z direction. The mechanical wave propagation speed $V(x)$ is defined only on x direction. The first boundary condition at $z = -l_n$ can be defined as introducing the net driving pressure in Equation (4.23).

$$\delta p(x) = p_{t,1}(x, -l_n) + p_{r,1}(x, -l_n) - [p_{t,2}(x, -l_n) + p_{r,2}(x, -l_n)] \quad (4.23)$$

Since the acoustic waves on the 2nd and the 3rd region are coupled with the mechanical wave on the panel, Newton's 2nd law should be satisfied at the boundary contact Equation (4.24). Since the panel thickness is very small compared to the depth of the diffuser, pressure variation over the panel thickness is ignored. The second boundary condition is due to the fluid – solid contact. Since both the micro perforated panel and air media covering the panel is in full contact, the velocity components of the acoustic waves on z direction should be the same as the bar speed $V(x)$ Equation (4.25).

$$\delta p(x) = V(x) \cdot Z_{p,1} \quad (4.24)$$

$$P_{t,1} \cdot e^{jk_z l_n} + P_{r,1} \cdot e^{-jk_z l_n} + P_{t,2} \cdot e^{jk_z l_n} + P_{r,2} \cdot e^{-jk_z l_n} = V(x) \cdot Z_{p,1}$$

$$\begin{aligned} V(x) &= \left(\frac{\cos \theta}{\rho_0 c} \right) \cdot (P_{r,1} \cdot e^{-jk_z l_n} - P_{t,1} \cdot e^{jk_z l_n}) \\ &= \left(\frac{\cos \theta}{\rho_0 c} \right) \cdot (P_{r,2} \cdot e^{-jk_z l_n} - P_{t,2} \cdot e^{jk_z l_n}) \end{aligned} \quad (4.25)$$

where $Z_{p,1}$ is the specific acoustic impedance of the first micro perforated panel which is not normalized with the characteristic impedance of air.

The third boundary which is at $z = -l$ is similar with the boundary at $z = -l_n$. The driving pressure on the second micro perforated panel is now;

$$\delta p(x) = p_{t,2}(x, -l) + p_{r,2}(x, -l) - p_t(x, -l) \quad (4.26)$$

Hence the boundary conditions are also the same and can be defined as;

$$\delta p(x) = V(x) \cdot Z_{p,2} \quad (4.27)$$

$$P_{t,2} \cdot e^{jk_z l} + P_{r,2} \cdot e^{-jk_z l} - P_t \cdot e^{jk_z l} = V(x) \cdot Z_{p,2}$$

$$V(x) = \left(\frac{\cos \theta}{\rho_0 c} \right) \cdot (P_{r,2} \cdot e^{-jk_z l} - P_{t,2} \cdot e^{jk_z l}) = - \left(\frac{\cos \theta}{\rho_0 c} \right) \cdot P_t \cdot e^{jk_z l} \quad (4.28)$$

where $Z_{p,2}$ is the specific acoustic impedance of the second micro perforated panel at $z = -l$.

When the boundary conditions are set, the linear system of equations can be solved. There are 6 boundary conditions, hence 6 linear equations, and 6 unknowns which are the pressure ratios of the reflected and transmitted acoustic waves to the incident wave. Therefore; 6 equations arising from the boundary conditions can be sum up to one single equation as;

$$\begin{aligned} & \left[g^{(8)} g^{(1)} - g^{(4)} g^{(5)} \right] \cdot P_i + \left[g^{(8)} g^{(2)} - g^{(4)} g^{(6)} \right] \cdot \sum_{n=-\infty}^{\infty} A_n e^{-jn \frac{2\pi}{L} x} + \\ & \left[g^{(8)} g^{(3)} - g^{(4)} g^{(7)} \right] \cdot \sum_{n=-\infty}^{\infty} A_n \frac{\gamma_n}{k} e^{-jn \frac{2\pi}{L} x} = 0 \end{aligned} \quad (4.29)$$

The coefficients of the incident pressure amplitude and the Fourier expansion terms can be determined by modifying boundary conditions. They can be expressed as;

$$\begin{aligned}
g^{(1)} &= (1 - z_{p,1} \cos \theta) \cdot e^{-2jk_z l_n} \\
g^{(2)} &= \frac{1}{2} \cdot \left[(1 - z_{p,1} \cos \theta) \cdot e^{-2jk_z l_n} + (1 + z_{p,1} \cos \theta) \right] \\
g^{(3)} &= \frac{1}{2 \cos \theta} \cdot \left[-(1 - z_{p,1} \cos \theta) \cdot e^{-2jk_z l_n} + (1 + z_{p,1} \cos \theta) \right] \\
g^{(4)} &= -\frac{1}{2} \cdot \left[z_{p,2} \cos \theta \cdot e^{-2jk_z l} + (2 + z_{p,2} \cos \theta) \cdot e^{-2jk_z l_n} \right]
\end{aligned} \tag{4.30}$$

$$\begin{aligned}
g^{(5)} &= -e^{-2jk_z l_n} \\
g^{(6)} &= \frac{1}{2} \cdot (1 - e^{-2jk_z l_n}) \\
g^{(7)} &= \frac{1}{2 \cos \theta} \cdot (1 + e^{-2jk_z l_n}) \\
g^{(8)} &= \frac{1}{2} \cdot \left[(2 + z_{p,2} \cos \theta) \cdot e^{-2jk_z l_n} - (z_{p,2} \cos \theta \cdot e^{-2jk_z l}) \right]
\end{aligned} \tag{4.31}$$

$z_{p,1}$ and $z_{p,2}$ are the specific acoustic impedances of the 1st and the 2nd MPP which are normalized with the characteristic impedance of air, $\rho_0 c$.

The Equation (4.30) can be modified such that the driving pressure on the whole diffuser structure and the corresponding velocity field on z direction in front of the diffuser surface are related with the acoustic admittance of the diffuser surface. The relation is simply expressed in Equation (4.32).

$$\cos \theta \cdot P_i - \sum_{n=-\infty}^{\infty} A_n \frac{\gamma_n}{k} e^{-jn \frac{2\pi}{L} x} = G(x) \left[P_i + \sum_{n=-\infty}^{\infty} A_n e^{-jn \frac{2\pi}{L} x} \right] \tag{4.32}$$

The well depths l_n are periodic with the diffuser period width L . Hence the surface acoustic admittance $G(x)$ is also periodic with L . Therefore; $G(x)$ can be expanded with Fourier transform as;

$$G(x) = \sum_{n=-\infty}^{\infty} g_n e^{-jn\frac{2\pi}{L}x}, \quad (4.33)$$

$$g_n = \frac{1}{L} \int_0^L G(x) e^{+jn\frac{2\pi}{L}x} dx.$$

Equation (4.33) is inserted into Equation (4.32) after multiplying by $e^{+jm\frac{2\pi}{L}x}$ and integration over L ;

$$\sum_{n=-\infty}^{\infty} A_n \left[g_{m-n} + \delta_{m,n} \left(\frac{\gamma_n}{k} \right) \right] = P_i (\delta_{m,0} \cos \theta - g_m) \quad (4.34)$$

$$m = -\infty, \dots, +\infty$$

where $\delta_{m,n}$ is the dirac delta function. Derivation of Equation (4.34) can be found in Appendix A.

One can obtain for the spatial spectral components of the admittance of one-dimensional Schroeder Diffuser as;

$$g_n = \frac{b}{T} \sum_{k=0}^{N-1} G(x_k) e^{-jn\pi(2k+1)/N} \cdot \frac{\sin(\pi nb/T)}{\pi nb/T} \quad (4.35)$$

When $n = 0$, the term in the denominator becomes zero which results in a singularity in the linear equations. This can be overcome by taking the limit of the gap function when n approaches to zero. Hence; when $n = 0$ the spectral components can be obtained as;

$$g_n = \frac{b}{T} \sum_{k=0}^{N-1} G(x_k) e^{-jn\pi(2k+1)/N} \quad (4.36)$$

Equation (4.34) is a group of infinitely many numbers of linear equations, where the pressure ratios A_n/P_i can be obtained as the solution of the linear equations. The

infinite number of linear equations can be terminated at where the solution of the linear equation system converges at $n = \pm 2N$. Then the pressure ratios, A_n/P_i of the scattered pressure field $P_s(x, z)$ in front of the diffuser surface can be determined. Eventually, the reflection coefficient of the diffuser can be described as the intensity ratios of the scattered and specularly reflected waves to the incident wave as indicated in Equation (4.37).

$$r(\theta) = \left| \frac{A_0}{P_i} \right|^2 + \frac{1}{\cos \theta} \sum_{n_s \neq 0} \left| \frac{A_{n_s}}{P_i} \right|^2 \sqrt{1 - \left(\cos \theta + n_s \frac{\lambda}{L} \right)^2} \quad (4.37)$$

The first term is due to the reflection of the fundamental mode which is the specular reflection with an angle θ . The second term is the radiating spatial harmonics of the incident wave which is the scattered reflection.

The reflection coefficient of the diffuser is obtained with Fourier decomposition model, where the sound field in front of the diffuser is periodic. The similar approach is now applied to determine the periodic sound field behind the diffuser while it is non-periodic at front. To ease the calculations coordinate axis is transformed as in Figure 4.6.

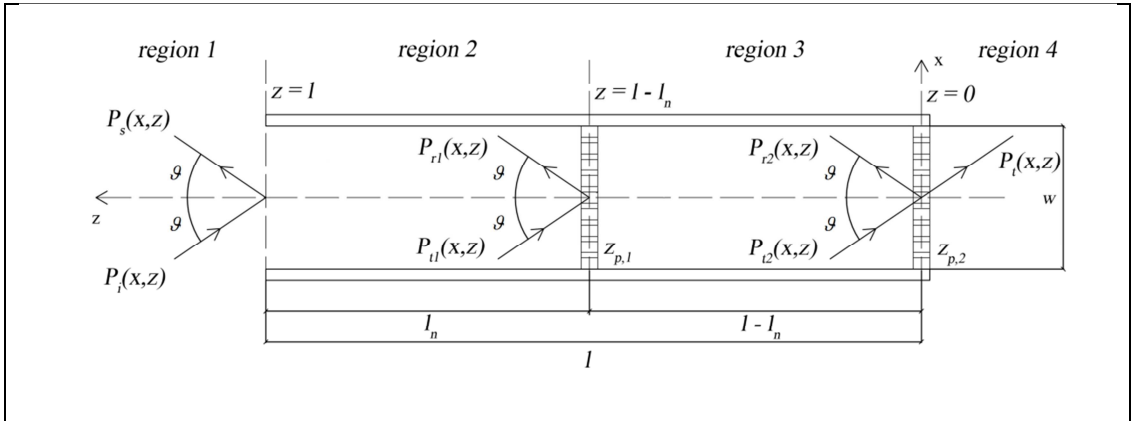


Figure 4.6 Sound field inside the well of the diffuser

Since the sound field in front of the diffuser is assumed to be non-periodic, the incident and the reflected acoustic waves can be represented as;

$$p_i(x, z) = P_i \cdot e^{i(-k_x x + k_z z)} \quad (4.38)$$

$$p_s(x, z) = P_s \cdot e^{-j(k_x x + k_z z)} \quad (4.39)$$

The transmitted acoustic wave behind the diffuser is expressed as a periodic sound field as;

$$p_t(x, z) = \sum_{n=-\infty}^{\infty} B_n \cdot e^{j(-\beta_n x + \gamma_n z)} \quad (4.40)$$

The period of the diffuser in x direction is preserved; therefore, the wave numbers in x and z directions are similar as in the periodic field defined in Equation (4.15) and Equation (4.16).

The formulations of the acoustic pressures within the wells in the 2nd and 3rd regions can be expressed as the same in Equation (4.19). Similarly, the velocity components in z direction are expressed as in Equation (4.20) except the transmitted and the reflected acoustic wave velocities. They should be modified as;

$$v_{s,z}(x, z) = \left(\frac{\cos \theta}{\rho_0 c} \right) \cdot P_s \cdot e^{-j(k_x x + k_z z)} \quad (4.41)$$

$$v_{t,z}(x, z) = \frac{-1}{\rho_0 c} \cdot \sum_{n=-\infty}^{\infty} B_n \frac{\gamma_n}{k} \cdot e^{j(-\beta_n x + \gamma_n z)}$$

To determine the complex pressure amplitudes, boundary conditions should be set. With respect to the new coordinate system, boundaries are defined on $z=0$, $z=l-l_n$ and $z=l$.

At $z = 0$, two boundary conditions are defined. The acoustic pressure acting on both sides of the micro perforated panel introduces the first condition as the force equation on the panel which is expressed in Equation (4.43). The second boundary condition is arisen due to the continuity of the fluid – solid media. Since both media are fully in contact, the velocity components of the acoustic and mechanical waves should match the expression in Equation (4.44).

$$\delta p(x) = p_{t,2}(x,0) + p_{r,2}(x,0) - p_t(x,0) \quad (4.42)$$

$$\delta p(x) = V(x) \cdot Z_{p,2} \quad (4.43)$$

$$P_{t,2} + P_{r,2} - \sum_{n=-\infty}^{\infty} B_n e^{-jn\frac{2\pi}{L}x} = V(x) \cdot Z_{p,2}$$

$$V(x) = \frac{-1}{\rho_0 c} \cdot \sum_{n=-\infty}^{\infty} B_n \frac{\gamma_n}{k} \cdot e^{-jn\frac{2\pi}{L}x} = \cos \theta \cdot (P_{r,2} - P_{t,2}) \quad (4.44)$$

Since the other micro perforated panel is present at $z = l - l_n$, similar boundary conditions can be defined as;

$$\delta p(x) = p_{r,1}(x, l - l_n) + p_{t,1}(x, l - l_n) - [p_{r,2}(x, l - l_n) + p_{t,2}(x, l - l_n)] \quad (4.45)$$

$$\delta p(x) = V(x) \cdot Z_{p,1}$$

$$\begin{aligned} & P_{t,1} \cdot e^{jk_z(l-l_n)} + P_{r,1} \cdot e^{-jk_z(l-l_n)} - \left(P_{t,2} \cdot e^{jk_z(l-l_n)} + P_{r,2} \cdot e^{-jk_z(l-l_n)} \right) \\ & = V(x) \cdot Z_{p,1} \end{aligned} \quad (4.46)$$

$$V(x) = P_{r,1} \cdot e^{-jk_z(l-l_n)} - P_{t,1} \cdot e^{jk_z(l-l_n)} = P_{r,2} \cdot e^{-jk_z(l-l_n)} - P_{t,2} \cdot e^{jk_z(l-l_n)} \quad (4.47)$$

The last boundary is at $z = l$ where there is no solid – fluid contact. Eventually, the boundary conditions at $z = l$ can be expressed as the continuity of the fluid medium. The total acoustic pressures of the sound fields in the 1st and the 2nd regions as well as the velocity components in the z direction should be equal at the boundary.

$$P_i \cdot e^{jk_z l} + P_s \cdot e^{-jk_z l} = P_{t,1} \cdot e^{jk_z l} + P_{r,1} \cdot e^{-jk_z l} \quad (4.48)$$

$$P_s \cdot e^{-jk_z l} - P_i \cdot e^{jk_z l} = P_{r,1} \cdot e^{-jk_z l} - P_{t,1} \cdot e^{jk_z l} \quad (4.49)$$

After the boundary conditions are set, the linear system of equations can be solved. There are 6 boundary conditions, hence 6 linear equations, and 6 unknowns which are the pressure ratios of the reflected and transmitted acoustic waves to the incident wave. Therefore; the 6 equations arising from the boundary conditions can be sum up to one single equation as;

$$\begin{aligned} & \left[g^{(6)} g^{(1)} - g^{(2)} g^{(5)} \right] \cdot P_i + \left[g^{(6)} g^{(3)} - g^{(2)} g^{(7)} \right] \cdot \sum_{n=-\infty}^{\infty} B_n e^{-jn \frac{2\pi}{L} x} + \\ & \left[g^{(6)} g^{(4)} - g^{(2)} g^{(8)} \right] \cdot \sum_{n=-\infty}^{\infty} B_n \frac{\gamma_n}{k} e^{-jn \frac{2\pi}{L} x} = 0 \end{aligned} \quad (4.50)$$

The coefficients of the incident pressure amplitude and the Fourier expansion terms can be determined by modifying boundary conditions. They can be expressed as;

$$\begin{aligned}
g^{(1)} &= 1 - Z_{p,1} \cos \theta \\
g^{(2)} &= e^{-2jk_z(l-l_n)} \cdot (1 + Z_{p,1} \cos \theta) \\
g^{(3)} &= -\frac{1}{2} (1 + e^{-2jk_z(l-l_n)}) \\
g^{(4)} &= \frac{1}{2 \cos \theta} \left[(1 - Z_{p,2} \cos \theta) \cdot e^{-2jk_z(l-l_n)} - (1 - Z_{p,2} \cos \theta) \right]
\end{aligned} \tag{4.51}$$

$$\begin{aligned}
g^{(5)} &= -1 \\
g^{(6)} &= e^{-2jk_z(l-l_n)} \\
g^{(7)} &= \frac{1}{2} [1 - e^{-2jk_z(l-l_n)}] \\
g^{(8)} &= \frac{1}{2 \cos \theta} \left[(1 + Z_{p,2} \cos \theta) + e^{-2jk_z(l-l_n)} \cdot (1 - Z_{p,2} \cos \theta) \right]
\end{aligned} \tag{4.52}$$

Equation (4.50) can be expressed a similar way in which the acoustic admittance is expressed in Equation (4.53).

$$\begin{aligned}
&\frac{\left[g^{(6)} g^{(1)} - g^{(2)} g^{(5)} \right]}{\left[g^{(6)} g^{(4)} - g^{(2)} g^{(8)} \right]} \cdot P_i + \frac{\left[g^{(6)} g^{(3)} - g^{(2)} g^{(7)} \right]}{\left[g^{(6)} g^{(4)} - g^{(2)} g^{(8)} \right]} \cdot \sum_{n=-\infty}^{\infty} B_n e^{-jn \frac{2\pi}{L} x} + \\
&\sum_{n=-\infty}^{\infty} B_n \frac{\gamma_n}{k} e^{-jn \frac{2\pi}{L} x} = 0
\end{aligned} \tag{4.53}$$

$$g_{res}^1 \cdot P_i + g_{res}^2 \cdot \sum_{n=-\infty}^{\infty} B_n e^{-jn \frac{2\pi}{L} x} + \sum_{n=-\infty}^{\infty} B_n \frac{\gamma_n}{k} e^{-jn \frac{2\pi}{L} x} = 0$$

Since each term in g^1_{res} and g^2_{res} are composed of a periodic term which is the depth sequence of the QRD, l_n ; they can be expanded with Fourier decomposition. As did in the former analysis, Equation (4.32) is adapted and implemented into Equation (4.53).

$$\sum_{n=-\infty}^{\infty} B_n \left[(g^2_{res})_{m-n} + \delta_{m,n} \left(\frac{\gamma_n}{k} \right) \right] = P_i \left(-(g^1_{res})_m \right) \quad (4.54)$$

$$m = -\infty, \dots, +\infty$$

One can obtain for the spatial spectral components of g^1_{res} and g^2_{res} as explained in Equation (4.3.24).

Equation (4.54) is a group of infinitely many numbers of linear equations, where the pressure ratios B_n/P_i can be obtained as the solution of the linear equations. The infinite number of linear equations can be terminated at where the solution of the linear equation system converges at $n = \pm 2N$. Then the pressure ratios, B_n/P_i of the scattered pressure field $P_s(x, z)$ in front of the diffuser surface can be determined. Eventually, the reflection coefficient of the diffuser can be described as the intensity ratios of the scattered and specularly reflected waves to the incident wave as indicated in Equation (4.55).

$$\tau(\theta) = \left| \frac{B_0}{P_i} \right|^2 + \frac{1}{\cos \theta} \sum_{n_s \neq 0} \left| \frac{B_{n_s}}{P_i} \right|^2 \sqrt{1 - \left(\sin \theta + n_s \frac{\lambda}{L} \right)^2} \quad (4.55)$$

The first term is due to the transmission of the fundamental mode which is the specular transmission with an angle θ . The second term is the radiating spatial harmonics of the incident wave which is the scattered transmission.

4.3.2. Combined Mathematical Model

The previous work deals with the absorption mechanism that took place in the space diffuser in a simple manner. This simplification is due to the ignorance of radiating spatial harmonics at one side of the diffuser while the periodic spatial harmonics on the other side are being evaluated with Fourier decomposition method. This approach enabled the condition in which the reflected and transmitted sound fields are treated and computed separately. This computation is mainly based on the evaluation of specular and scattered wave amplitudes and intensity ratios both in front and the back of the diffuser. Once the intensity ratios are obtained mathematically, the absorption coefficient can be determined by;

$$\alpha(\theta) = 1 - [r(\theta) + \tau(\theta)] \quad (4.56)$$

The reflection and transmission coefficients are obtained separately as indicated in Equation (4.37) and Equation (4.55). In each computation only one unknown is apparent which is the pressure amplitudes of the radiated spatial harmonics and the mathematical model is called as the detached model. Now, theory is going to be extended such that the contribution of spatial harmonics on both sides of the diffuser is included. The model can be constructed on a similar sketch in Figure 4.7, where sound fields are both periodic in front and at the back of the diffuser.

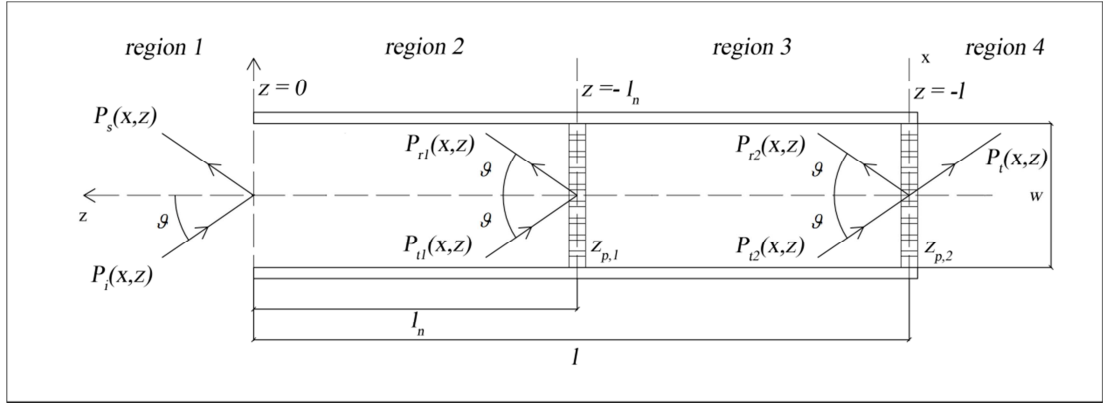


Figure 4.7 Sound field inside the well of the diffuser

The incident, reflected and transmitted sound fields are now all periodic in x direction and expressed as in Equation (4.57).

$$p_i(x, z) = P_i \cdot e^{j(-k_x x + k_z z)}$$

$$p_s(x, z) = \sum_{n=-\infty}^{\infty} A_n \cdot e^{-j(\beta_n x + \gamma_n z)} \quad (4.57)$$

$$p_t(x, z) = \sum_{n=-\infty}^{\infty} B_n \cdot e^{j(-\beta_n x + \gamma_n z)}$$

The propagation of the sound inside the diffuser wells are treated as did in previous method. The wavelength of the interested maximum frequency is large compared to the well width; hence, only plane wave propagation occurs inside the wells. Therefore, the acoustic wave pressures of propagating waves on z direction inside the wells can be defined as in Equation (4.19). The relation between the periodic wave number β_n on x direction and wave number γ_n on z direction is as similar as expressed in Equation (4.15) and Equation (4.16).

A set of linear equations can be defined to construct boundary conditions as did in the previous section. Boundary conditions are all the same; for this time, both reflected and transmitted sound waves are composed of infinitely many spatial harmonics which are periodic on x direction. Eventually, all boundary conditions at $z = 0$, $z = -l_n$ and $z = -l$ are defined as;

$$P_i + \sum_{n=-\infty}^{\infty} A_n \cdot e^{-jn\frac{2\pi}{L}x} - (P_{t1} + P_{r1}) = 0 \quad (4.58)$$

$$-\cos\theta \cdot P_i + \sum_{n=-\infty}^{\infty} A_n \frac{\gamma_n}{k} \cdot e^{-jn\frac{2\pi}{L}x} + \cos\theta \cdot P_{t1} - \cos\theta \cdot P_{r1}$$

$$P_{t,1} \cdot e^{jk_z l_n} + P_{r,1} \cdot e^{-jk_z l_n} + P_{t,2} \cdot e^{jk_z l_n} + P_{r,2} \cdot e^{-jk_z l_n} = V(x) \cdot Z_{p,1}$$

$$V(x) = \left(\frac{\cos\theta}{\rho_0 c} \right) \cdot (P_{r,1} \cdot e^{-jk_z l_n} - P_{t,1} \cdot e^{jk_z l_n}) \quad (4.59)$$

$$= \left(\frac{\cos\theta}{\rho_0 c} \right) \cdot (P_{r,2} \cdot e^{-k_z l_n} - P_{t,2} \cdot e^{k_z l_n})$$

$$P_{t,2} \cdot e^{jk_z l} + P_{r,2} \cdot e^{-jk_z l} + \sum_{n=-\infty}^{\infty} B_n \cdot e^{j\left(-n\frac{2\pi}{L}x + \gamma_n l\right)} = V(x) \cdot Z_{p,2}$$

$$V(x) = \left(\frac{\cos\theta}{\rho_0 c} \right) \cdot (P_{r,2} \cdot e^{-jk_z l} - P_{t,2} \cdot e^{jk_z l}) \quad (4.60)$$

$$= \frac{-1}{\rho_0 c} \cdot \sum_{n=-\infty}^{\infty} B_n \frac{\gamma_n}{k} \cdot e^{j\left(-n\frac{2\pi}{L}x + \gamma_n l\right)}$$

Six linear equations can be reduced to two equations eliminating the complex pressure amplitudes of the acoustic waves propagating inside the QRD wells. Eventually, the relation between two unknown pressure amplitudes of the reflected and the transmitted acoustic waves and the pressure amplitude of the incident wave can be expressed in the following equations;

$$\begin{aligned}
& g^{(1)} P_i + g^{(2)} \sum_{n=-\infty}^{\infty} A_n \cdot e^{-jn \frac{2\pi}{L} x} + g^{(3)} \sum_{n=-\infty}^{\infty} A_n \frac{\gamma_n}{k} \cdot e^{-jn \frac{2\pi}{L} x} \\
& + g^{(4)} \sum_{n=-\infty}^{\infty} B_n \cdot e^{-j \left(n \frac{2\pi}{L} x + \gamma_n l \right)} + g^{(5)} \sum_{n=-\infty}^{\infty} B_n \frac{\gamma_n}{k} \cdot e^{-j \left(n \frac{2\pi}{L} x + \gamma_n l \right)} = 0
\end{aligned} \tag{4.61}$$

$$\begin{aligned}
& g^{(6)} P_i + g^{(7)} \sum_{n=-\infty}^{\infty} A_n \cdot e^{-jn \frac{2\pi}{L} x} + g^{(8)} \sum_{n=-\infty}^{\infty} A_n \frac{\gamma_n}{k} \cdot e^{-jn \frac{2\pi}{L} x} \\
& + g^{(9)} \sum_{n=-\infty}^{\infty} B_n \cdot e^{-j \left(n \frac{2\pi}{L} x + \gamma_n l \right)} + g^{(10)} \sum_{n=-\infty}^{\infty} B_n \frac{\gamma_n}{k} \cdot e^{-j \left(n \frac{2\pi}{L} x + \gamma_n l \right)} = 0
\end{aligned}$$

The coefficients $g^{(k)}$ are determined by modifying the boundary conditions, simply eliminating the terms other than A_n and B_n and can be expressed as;

$$\begin{aligned}
g^{(1)} &= e^{-2jk_z l_n} (1 - Z_{p,1} \cos \theta) \\
g^{(2)} &= \frac{1}{2} \left[e^{-2jk_z l_n} (1 - Z_{p,1} \cos \theta) + (1 + Z_{p,1} \cos \theta) \right] \\
g^{(3)} &= \frac{1}{2 \cos \theta} \left[(1 + Z_{p,1} \cos \theta) - e^{-2jk_z l_n} (1 - Z_{p,1} \cos \theta) \right] \\
g^{(4)} &= -\frac{1}{2} \left[e^{-jk_z l} + e^{jk_z (l-2l_n)} \right] \\
g^{(5)} &= -\frac{1}{2 \cos \theta} \left[e^{jk_z (l-2l_n)} (1 + Z_{p,2} \cos \theta) - e^{-jk_z l} (1 - Z_{p,2} \cos \theta) \right]
\end{aligned} \tag{4.62}$$

$$\begin{aligned}
g^{(6)} &= -e^{-2jk_z l_n} \\
g^{(7)} &= \frac{1}{2}(1 - e^{-2jk_z l_n}) \\
g^{(8)} &= \frac{1}{2\cos\theta}(1 + e^{-2jk_z l_n}) \\
g^{(9)} &= \frac{1}{2}\left[e^{jk_z(l-2l_n)} - e^{-jk_z l}\right] \\
g^{(10)} &= \frac{1}{2\cos\theta}\left[e^{jk_z(l-2l_n)}(1 + Z_{p,2}\cos\theta) + e^{-jk_z l}(1 - Z_{p,2}\cos\theta)\right]
\end{aligned} \tag{4.63}$$

Since coefficients of the spatial harmonic components are also periodic with period L on x axis, they can be expanded with Fourier. Finally, the two modified boundary conditions can be expanded to yield in the following system of linear equations;

$$\begin{aligned}
\sum_{n=-\infty}^{\infty} \left[A_n \left(g_{m-n}^{(2)} + \frac{\gamma_n}{k} g_{m-n}^{(3)} \right) + B_n e^{-j\gamma_n l} \left(g_{m-n}^{(4)} + \frac{\gamma_n}{k} g_{m-n}^{(5)} \right) \right] &= -P_i \cdot g_m^{(1)} \\
\sum_{n=-\infty}^{\infty} \left[A_n \left(g_{m-n}^{(7)} + \frac{\gamma_n}{k} g_{m-n}^{(8)} \right) + B_n e^{-j\gamma_n l} \left(g_{m-n}^{(9)} + \frac{\gamma_n}{k} g_{m-n}^{(10)} \right) \right] &= -P_i \cdot g_m^{(6)}
\end{aligned} \tag{4.64}$$

$$m = -\infty, \dots, +\infty$$

In Equation (4.64) two infinitely large systems of linear equations are formed. These equations can be expressed in matrix form to obtain spatial harmonic components. The matrix form of the above equations is expressed as;

$$\begin{aligned}
[K_1]\{A_n\} + [K_2]\{B_n\} &= -P_i\{U_1\} \\
[K_3]\{A_n\} + [K_4]\{B_n\} &= -P_i\{U_2\}
\end{aligned} \tag{4.65}$$

where the coefficient vectors and matrices U and K are defined as;

$$\{U_1\} = \begin{Bmatrix} \vdots \\ g_m^{(1)} \\ \vdots \end{Bmatrix} \quad (4.66)$$

$$\{U_2\} = \begin{Bmatrix} \vdots \\ g_m^{(6)} \\ \vdots \end{Bmatrix}$$

$$[K_1] = \begin{bmatrix} \ddots & & & \\ & g_{m-n}^{(2)} + \frac{\gamma_n}{k} g_{m-n}^{(3)} & & \\ & & \ddots & \\ & & & \ddots \end{bmatrix}$$

$$[K_2] = \begin{bmatrix} \ddots & & & \\ & e^{-i\gamma_n l} \left(g_{m-n}^{(4)} + \frac{\gamma_n}{k} g_{m-n}^{(5)} \right) & & \\ & & \ddots & \\ & & & \ddots \end{bmatrix}$$

$$[K_3] = \begin{bmatrix} \ddots & & & \\ & g_{m-n}^{(7)} + \frac{\gamma_n}{k} g_{m-n}^{(8)} & & \\ & & \ddots & \\ & & & \ddots \end{bmatrix}$$

$$[K_4] = \begin{bmatrix} \ddots & & & \\ & e^{-i\gamma_n l} \left(g_{m-n}^{(9)} + \frac{\gamma_n}{k} g_{m-n}^{(10)} \right) & & \\ & & \ddots & \\ & & & \ddots \end{bmatrix} \quad (4.67)$$

Once coefficient matrices K and vectors U are obtained, one can simply derive the pressure ratios for reflected and transmitted sound waves by solving Equation (4.65). As described in Equation (4.37) and Equation (4.55), reflection and transmission

coefficients can be obtained. The absorption coefficient is then calculated due to the energy balance introduced in Equation (4.56).

4.4. Effect of Narrower Wells

In the previous chapters, the propagation of the acoustic wave inside wells is assumed to be lossless. This assumption is only true when the width of each well is large compared to the viscous and thermal boundary layer thicknesses. In this section the effect of thermal and viscous losses at boundary layers is going to be included in the absorption theory.

In the real case, when the sound propagation inside a narrow slit is in concern, there are three waves that propagate into the slit: propagating acoustic wave, thermal wave and a shear wave. In practice, attenuation due to the thermal and shear wave only occurs in the boundary layers which are only of a size of a millimeter thick. When the cross-sectional dimensions of the slit are large compared to thermal and viscous boundary layer thicknesses, the attenuation caused by the thermal and shear waves are incorporated with the boundary conditions of the propagating acoustic wave [11]. Otherwise, all propagating waves inside the slit should be defined and solved with respect to their own boundary conditions.

When no energy is absorbed while propagation inside the slit, the wave number $k = c/\omega$ is real and is equal to the wave number in free field in one-dimensional space. On the other hand, if the viscous and thermal-conduction effects are not negligible, the wave number k will have a positive imaginary part, corresponding to wave attenuation nearer to boundaries. Morse and Ingard [11] derived the complex wave number for a cylindrical tube. The same approach can be adapted to the narrow slit [11]. In order to correctly analyze the propagation of the fundamental mode in the

narrow slit a pressure wave P_p , temperature τ_p , the tangential u_{pz} and normal u_{px} velocity components should be defined.

$$\begin{aligned}
 P_p(x, z) &= \cos\left(\frac{\pi qx}{w}\right) e^{-jk_t z} \\
 \tau_p(x, z) &= \frac{\gamma-1}{\alpha\gamma} \cos\left(\frac{\pi qx}{w}\right) e^{-jk_t z} \\
 u_{pz}(x, z) &= \frac{k_t}{\rho ck} \cos\left(\frac{\pi qx}{w}\right) e^{-jk_t z} \\
 u_{px}(x, z) &= \frac{1}{i\omega\rho} \frac{\pi q}{w} \sin\left(\frac{-\pi q|x|}{w}\right) e^{-jk_t z}
 \end{aligned} \tag{4.68}$$

$k_t^2 = k^2 - \left(\frac{\pi q}{w}\right)^2$ is the wave number along tangential direction and $\pi q/w$ is the wave number component along normal direction. The constant q should be adjusted to fit the boundary conditions. Since the walls of the narrow slit are rigid, the temperature fluctuation τ and the particle velocity u on the boundary surface is zero. After a series of calculations, the constant πq can be defined as;

$$(\pi q)^2 = -(1+j)k^2 w [d_v + (\gamma-1)d_h] \tag{4.69}$$

This equation is valid for $w/d_v \gg 1$. d_v and d_h stand for the boundary layer thicknesses of viscous and thermal boundary layers correspondingly [11].

$$d_v = \sqrt{\frac{2\mu}{\rho\omega}} \approx 0.21 \frac{1}{\sqrt{f}} (cm)$$

$$d_h = \sqrt{\frac{2K}{\rho\omega C_p}} \approx 0.25 \frac{1}{\sqrt{f}} (cm)$$
(4.70)

where $\omega = 2\pi f$, μ is coefficient of viscosity, K is the coefficient of thermal conductivity and C_p is the heat capacity per unit mass at constant pressure.

When πq is set the wave number along normal direction inside the slit k_t can be obtained as;

$$k_t \approx k + \frac{k}{2w}(1-j)[d_v + (\gamma-1)d_h]$$
(4.71)

On the other hand the density of the air inside the narrow slit is also a complex number, including a reactive term. The effective density in the slit can be expressed as;

$$\rho_e = \rho[1 + (1-j)d_v/b]$$
(4.72)

4.5. Scattering Characteristics of the Modified Diffuser

The previous sections focus on the mathematical model to predict the absorption characteristic of the space diffuser. The method is simply based on the radiation of the spatial harmonic components of both reflected and transmitted sound waves into far field. In Equation (4.37) the distribution of specular and scattered energy densities in the reflected sound field are explained. Similarly, in Equation (4.55), the distribution of specular and scattered energy densities in the transmitted sound field

are introduced. The latter terms in both equations is the description of scattering coefficient for both reflected and transmitted sound fields. They can be summarized as;

$$r_s(\theta) = \frac{1}{\cos \theta} \sum_{n_s \neq 0} \left| \frac{A_{n_s}}{P_i} \right|^2 \sqrt{1 - \left(\sin \theta + n_s \frac{\lambda}{L} \right)^2} \quad (4.73)$$

$$\tau_s(\theta) = \frac{1}{\cos \theta} \sum_{n_s \neq 0} \left| \frac{A_{n_s}}{P_i} \right|^2 \sqrt{1 - \left(\sin \theta + n_s \frac{\lambda}{L} \right)^2}$$

where $r_s(\theta)$ is referring to the scattering coefficient in the reflected sound field whereas $\tau_s(\theta)$ is referring to the scattering coefficient in the transmitted sound field. Both parameters are defined to identify the ratio of the energy density reflected or transmitted in a scattered manner with respect to the total energy density within the incoming acoustic wave. However, the main purpose of a diffuser is to scatter a portion of the acoustic waves reflected from the surface, and transmitted through the diffuser in this particular case of this thesis. Therefore, a new parameter should be defined to identify the amount of scattered energy within the total reflected or transmitted energy. This new parameter is called as the coefficient of redistribution which is simply the ratio of scattered energy density of the scattered acoustic waves with respect to the total reflected energy density. The same is true for the transmitted sound field which is introduced in this study. Eventually, the coefficient of redistribution for both reflected and transmitted fields can be defined implicitly as;

$$u_r(\theta) = r_s(\theta)/r(\theta) \quad (4.74)$$

$$u_t(\theta) = \tau_s(\theta)/\tau(\theta)$$

The coefficient of redistribution gives information about the amount of energy carried with the spatial harmonic components of the reflected and transmitted sound fields. The angle of scattering or the angular distribution of the spatial harmonics can be obtained from Equation (4.75).

$$\theta_s = \arcsin(\sin(\theta) + n_s \lambda / L) \quad (4.75)$$

CHAPTER 5

SAMPLE CASE STUDIES AND RESULTS

In chapter 4, the mathematical model that represents the sound fields both at front and the back of the diffuser is constructed. Furthermore, the analytical expression for reflection, transmission and absorption coefficients are derived with respect to the built model.

In this chapter, the absorption and scattering characteristics of the diffuser are going to be demonstrated as a solution of the mathematical model. A MATLAB code is developed to evaluate the numerical results. Since there is no computational burden, the frequency resolution of the simulations is kept at high, namely 1 Hz.

5.1. Sample Scenario Results

In this section a sample scenario is evaluated numerically with the developed MATLAB Code. The first scenario is set to observe the amount of absorption at low frequencies with low diffuser depth. The design parameters and depth sequence values of the diffuser wells are given in Table 5.1, 5.2 and 5.3.

Table 5.1 Design Parameters for the Sample Scenario-1

Design Frequency [Hz]	750
Prime Number Sequence	7
Well Width [m]	0.06
Fin Length [m]	0.003
Diffuser Depth [m]	0.227
Incidence Angle [degrees]	45
Interested Frequency Rang [Hz]	1:8000

Table 5.2 Sequenced Well Depths for the Sample Scenario-1

Depth Sequence [m]						
1 st Well	2 nd Well	3 rd Well	4 th Well	5 th Well	6 th Well	7 th Well
0	0.032	0.130	0.065	0.065	0.130	0.032

Table 5.3 Micro-Perforated Panel Parameters for the Sample Scenario-1

	Front MPP	Rear MPP
Aperture Diameter [mm]	0.7	0.7
Aperture Ratio [%]	10	10
Surface Mass Density [kg/m ²]	0.1	0.1
Panel Thickness [mm]	1	1

The absorption coefficient curve as a result of the first scenario is demonstrated in Figure 5.1.

In Figure 5.1, it is obvious to see that the absorption coefficient at low frequencies, especially below 500 Hz, is above 0.5 even if the depth of the diffuser is set to 0.227m. In a regular double-leaf micro-perforated panel absorber construction without a rigid backing, one should notice the existence of peaks on absorption curve at the resonance frequencies of the absorber. These resonances are located at

frequencies where the imaginary part of the surface impedance approaches to zero which is mainly dependent on the air cavity depth between micro-perforated panels. Since a Schroeder Diffuser is composed of a number of wells with different depth values, there are numerous resonance frequencies introduced. Eventually, the absorption curve consists of many resonances where absorption can reach high values.

The absorption provided at even lower frequencies, namely below 500 Hz for this particular configuration, is introduced due to the existence of non-rigid backing. Unlike conventional resonant absorbers, in which the absorption curve starts from zero and increases gradually as the interested frequency reaches to the first resonance frequency, the absorption coefficient starts from a moderate value of 0.5 for this particular modification. This behavior of the structural modification on the QRD directly matches with the absorption behavior of the double-leaf panel absorber in Sagakami and Morimoto's work [14].

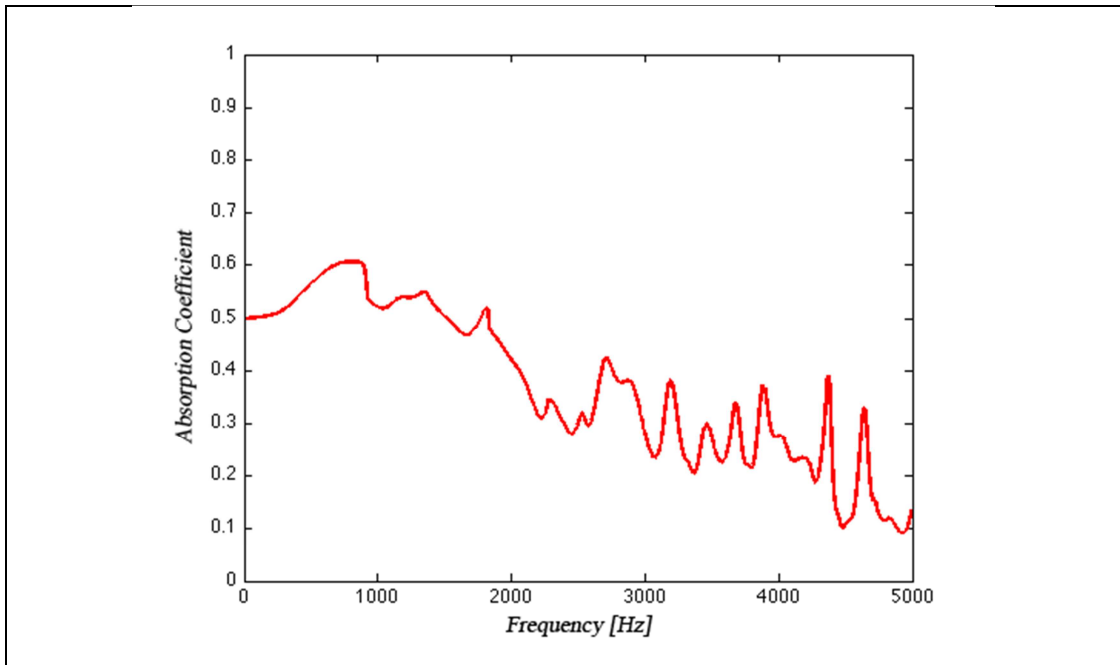


Figure 5.1 Absorption Coefficient (1st Scenario)

The mathematical model evaluates the absorbed energy using the fact that total energy is conserved. The sound energy distribution in the reflected and transmitted fields is also an important feature that should be investigated. In Figure 5.2 and 5.3, the energy distribution in front of the diffuser is demonstrated. It is a fact that the reflection occurs either as a specular reflection where the incidence angle is preserved, or as a scattered reflection.

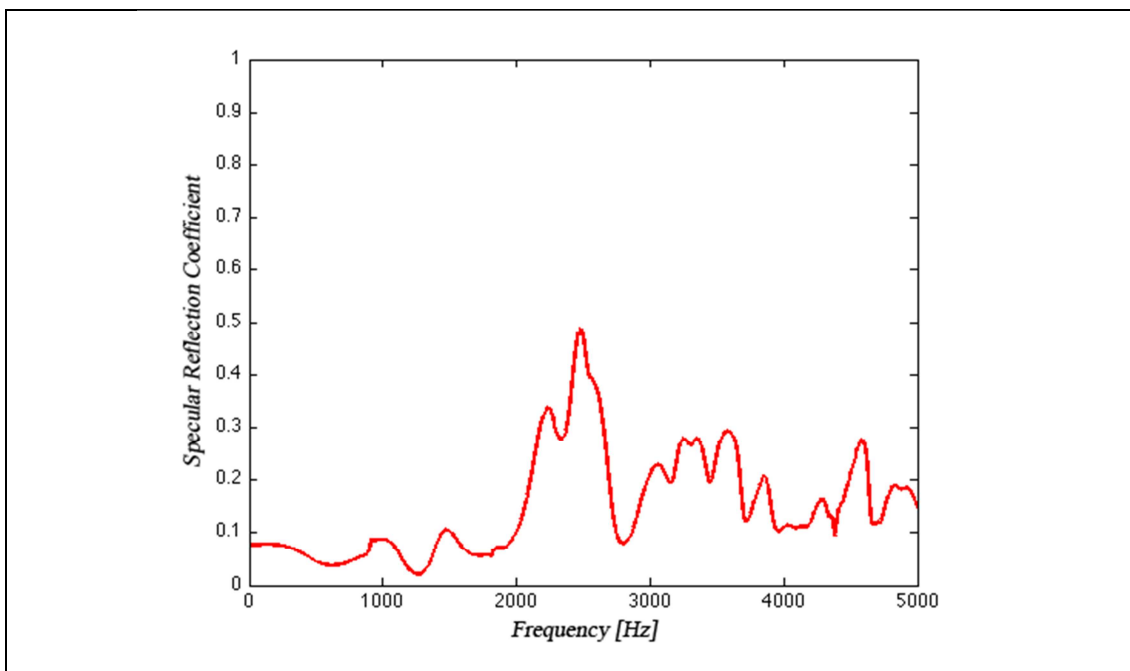


Figure 5.2 Specular reflection coefficient in front of the diffuser (1st Scenario)

Scattered reflection in the mathematical model is defined as the sum of energies carried with the reflected spatial harmonics that can propagate into the far field. The frequency where the scattering starts to occur can be determined from Equation (4.3.5). The wave number γ_n of a propagating wave should not be imaginary.

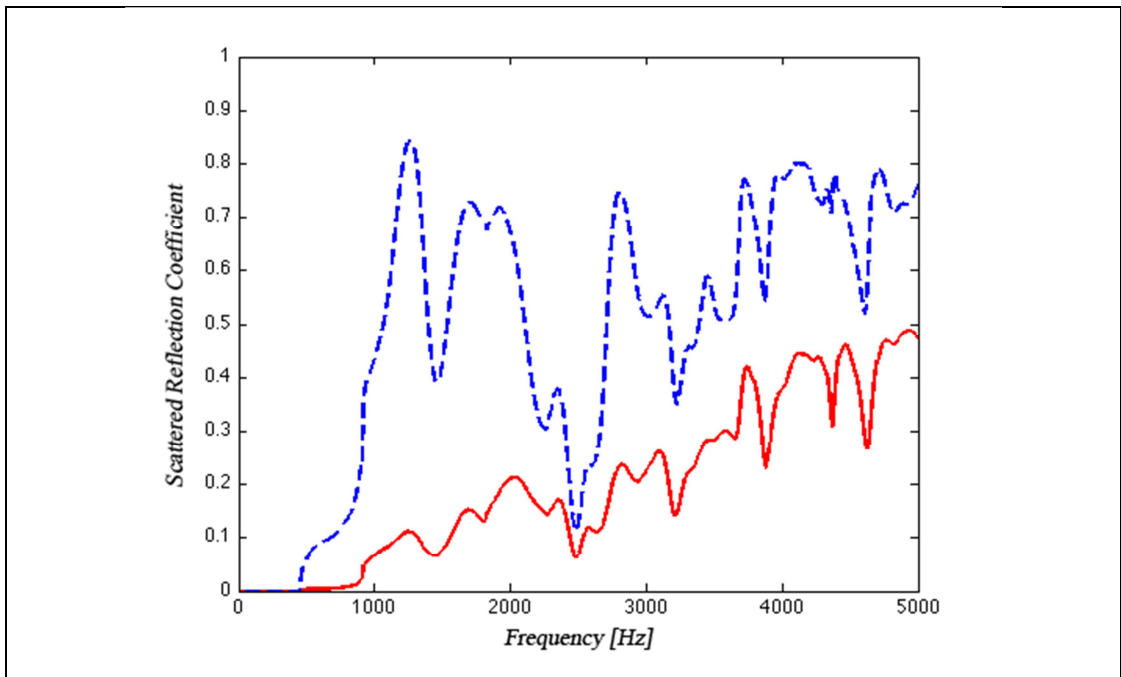


Figure 5.3 Scattered reflection coefficient in front of the diffuser (*red curve*), Coefficient of redistribution (*blue curve*) (1st Scenario)

Therefore the first spatial harmonic for $n = 1$ or $n = -1$ occurs at 492 Hz for this particular sample case as shown in Figure 9. The blue curve represents the scattering coefficient. The curve remains at zero until the first spatial harmonic propagates to far field at 492 Hz. This frequency can be called as a cut-off frequency for the scattering. After cut-off frequency, the number of spatial harmonics increases since the wavelength of the interested frequency decreases when compared to the period of the diffuser. Consequently, it is an inevitable fact that at lower frequencies only specular reflection dominates. This behavior can only be changed by increasing the period of the diffuser.

The red curve in Figure 5.3 indicates the ratio of scattered energy density to the total reflected energy density which is also called as coefficient of redistribution. One should realize that the purpose of the diffuser is not avoiding reflection. This is generally not possible. Its main attribute is to increase the portion of scattered energy

in the total reflected energy. Therefore, the coefficient of redistribution is an important parameter in the design of diffusers.

In this sample case, the coefficient of redistribution is also zero until the cut-off frequency since scattering coefficient is zero. Moreover, it is convenient that the coefficient of redistribution approaches to zero where scattering coefficient also approaches to zero. However the difference between two curves represents the amount of scattering provided by the diffuser. The larger the gap between two curves, the more scattering is observed.

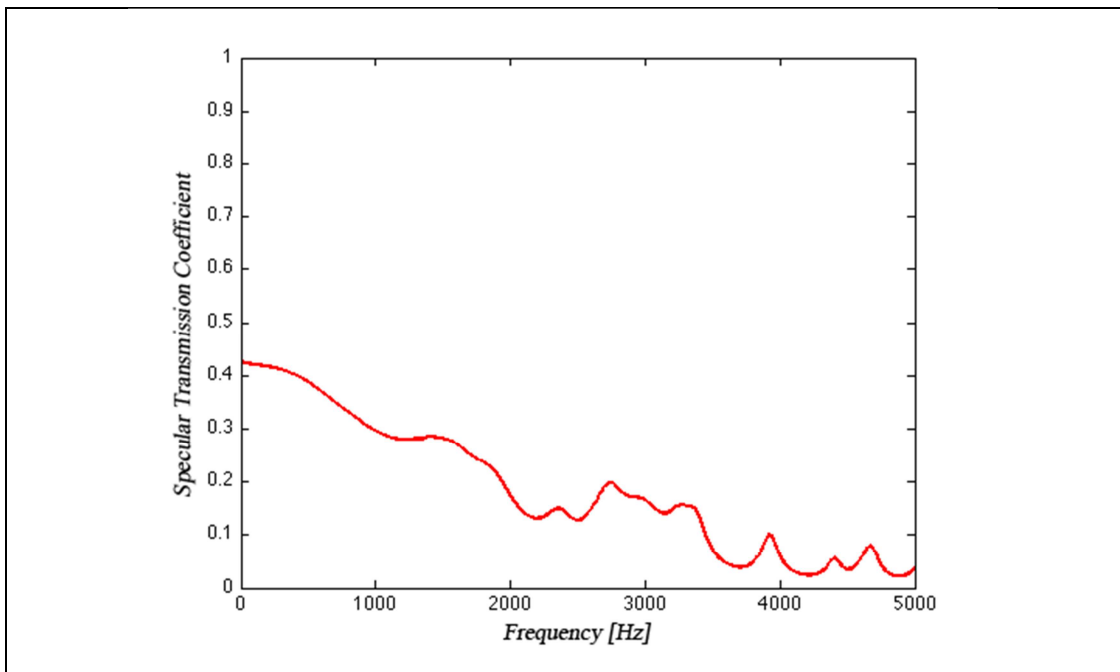


Figure 5.4 Specular transmission coefficient behind the diffuser (1st Scenario)

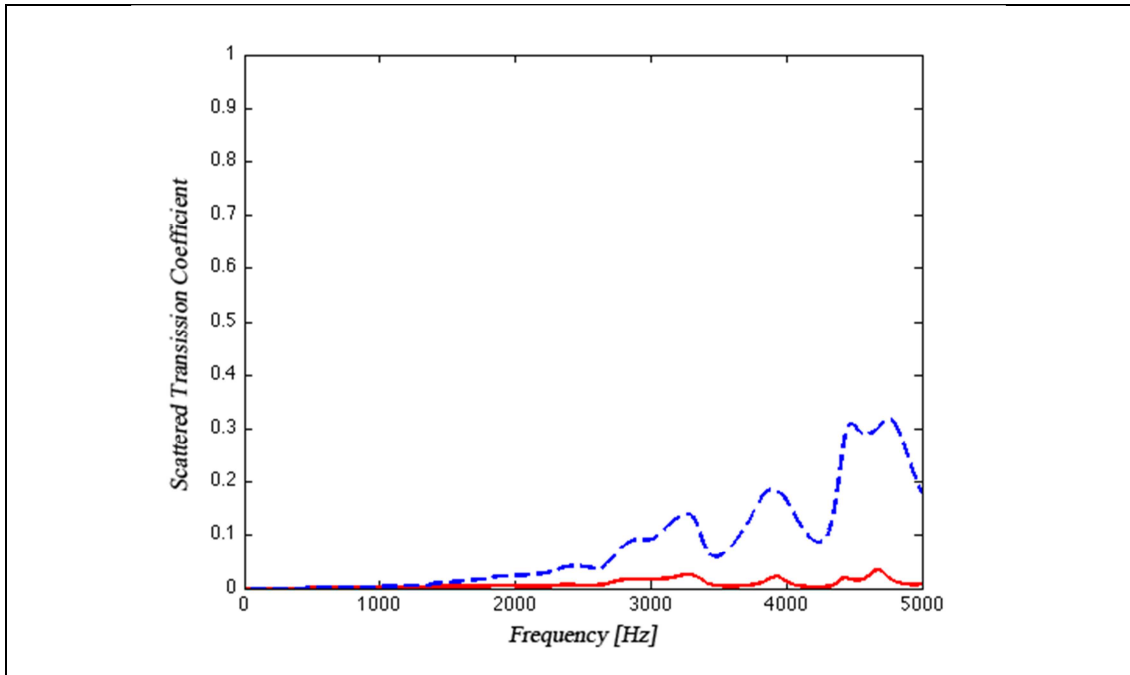


Figure 5.5 Scattered transmission coefficient behind the diffuser (*red curve*), Coefficient of redistribution (*blue curve*) (1st Scenario)

The new feature introduced in this study is that a transmitted sound field exists behind the diffuser. The amount of sound energy transmitted through the diffuser is investigated with the transmission coefficient. The mathematical model is constructed such that the sound fields around the diffuser can be decomposed into its spatial harmonics since periodicity exist. Therefore, the transmitted sound field is also analyzed by introducing specular transmitted energy which is in the direction of the incidence angle and the transmitted energy via scattering.

In Figure 5.4 and 5.5 specular transmission and scattered transmission coefficients are demonstrated. At first glance, the amount of specular transmission is higher compared with the specular reflection in Figure 5.4. This is because, the wavelength at lower frequencies is very large compared to the depth of the diffuser, so the acoustic wave can penetrate through the diffuser and reaches to the transmitted sound field. After a certain frequency limit, both specular and scattered energy decreases

and transmission of sound becomes less significant. However, the coefficient of redistribution gradually increases and maintains its value for a wide frequency range. This behavior shows that the scattering dominates at the transmitted field even if the transmitted acoustic energy is insignificant. Indeed, this frequency range begins after the transition region where specular reflection becomes less dominant due to the decreasing wavelength of the incoming acoustic wave.

The scattering coefficient curves give information only about the amount of energy reflected as scattering. The information on the angular distribution of spatial harmonics which form the scattering sound can be predicted using Equation (4.5.3). Since this is not a conventional polar directivity diagram in a frequency band, it is more convenient to demonstrate the results for a particular spatial harmonic in a defined frequency domain. Figure 5.6 demonstrates the angular distribution of the first and second spatial harmonics between 50 Hz and 1200 Hz. The frequency increment is set to 50 Hz.

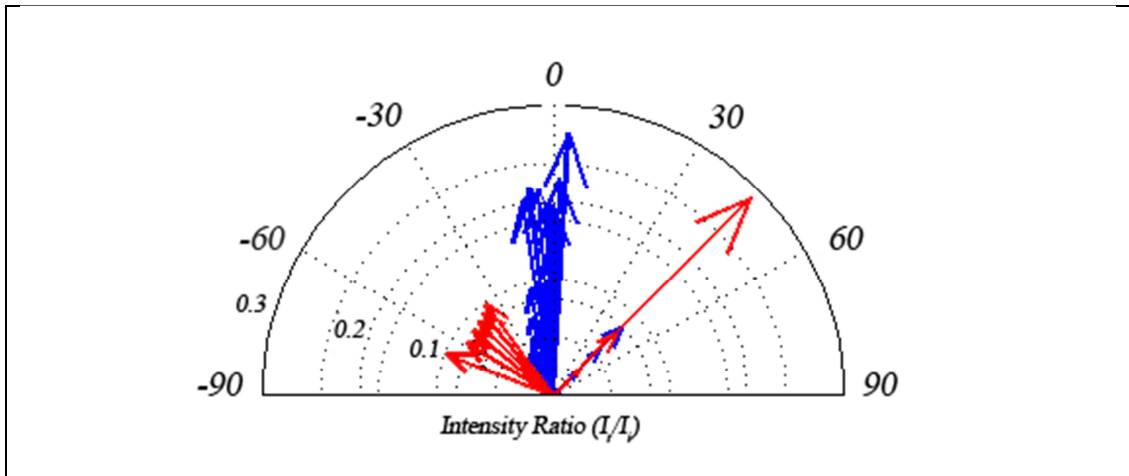


Figure 5.6 Directivity diagram of the intensity ratios for first (*blue vectors*) and second (*red vectors*) spatial harmonics with varying frequency in the reflected field.

The diagram represents the angular distribution of the first and the second spatial harmonics. The vectors are the sound intensity ratios of the reflected spatial

harmonics to the incident wave. The distribution corresponds to the scattering characteristic of the reflected field and the frequency increases along the vectors from right to left. The incidence angle for this angular distribution is set to -45° as given in the design parameters of the first scenario. The acoustic energy carried with these two spatial harmonics can be divided into two: the energy reflected with the same angle that the specular reflection occurs at 45° , and the scattered energy which is distributed from almost -70° to 5° . The distribution of scattered reflections is quite interesting. Especially for very low frequencies the angular distribution starts with an angle even larger than the incident angle which means backward scattering occurs.

This scenario does not necessarily represent the angular distribution of the higher spatial harmonics since the upper frequency limit, 1200 Hz, does not correspond to the wave length that the higher spatial harmonics can be scattered. The higher order spatial harmonics are only specularly reflected in this case.

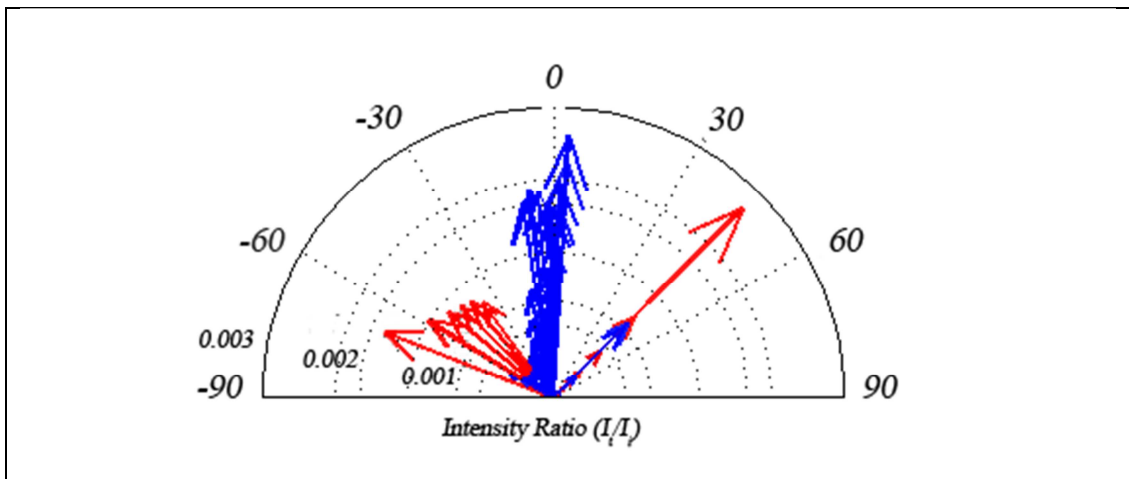


Figure 5.7 Directivity diagram of the intensity ratios for first (*blue vectors*) and second (*red vectors*) spatial harmonics with varying frequency in the transmitted field

In Figure 5.7, the angular distribution of the transmitted sound field is demonstrated with increasing frequency from left to right. Similarly; in the transmitted sound field, the same scattering distribution is obtained. Specular reflection occurs in the direction of the incident wave angle and back scattering is also present at larger angles compared to the incident angle. Although the distribution is quite similar, the energy density transmitted to the back of the diffuser is very low with a factor of almost a hundred.

The scattered energy both in reflected and transmitted sound fields is not too strong. The most of the energy is reflected or transmitted in the form of specular reflection or transmission which corresponds to the energy in the spatial harmonic of order is zero.

Similarly, the angular distribution for all spatial harmonics in the same frequency range is demonstrated in Figure 5.8, 5.9 and 5.10. Number of spatial harmonics is determined with the termination number for the limits of the summation in Equation (4.3.53). Therefore, there are $4N+1$ number of spatial harmonics to be demonstrated.

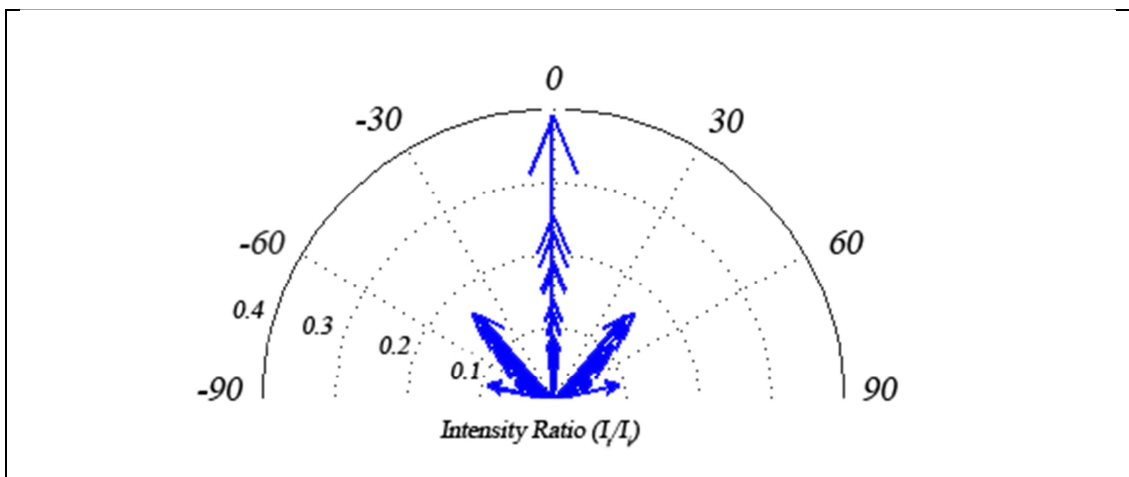


Figure 5.8 Directivity diagram of the intensity ratios considering whole spatial harmonics with varying frequency for $w = 0.06m$

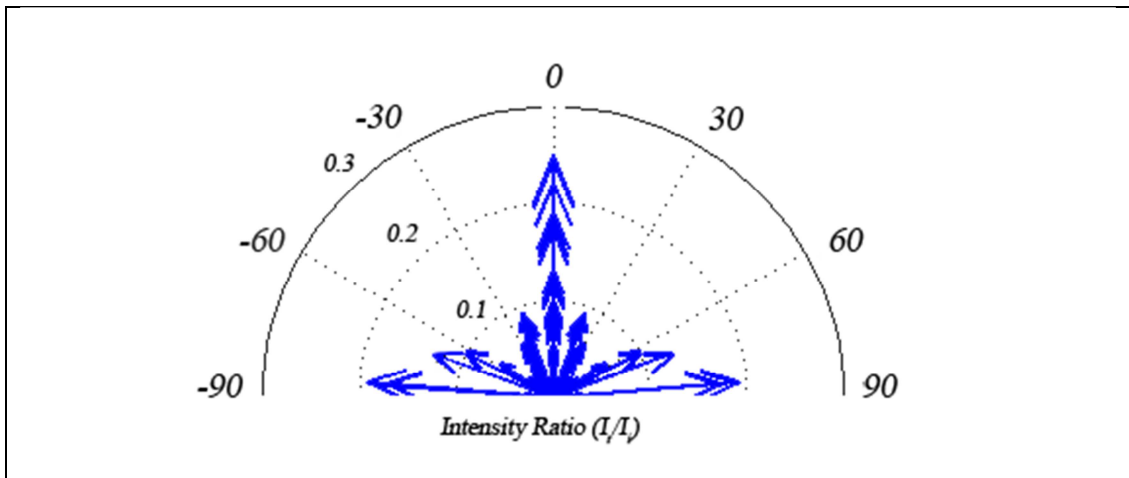


Figure 5.9 Directivity diagram of the intensity ratios considering whole spatial harmonics with varying frequency for $w = 0.12m$

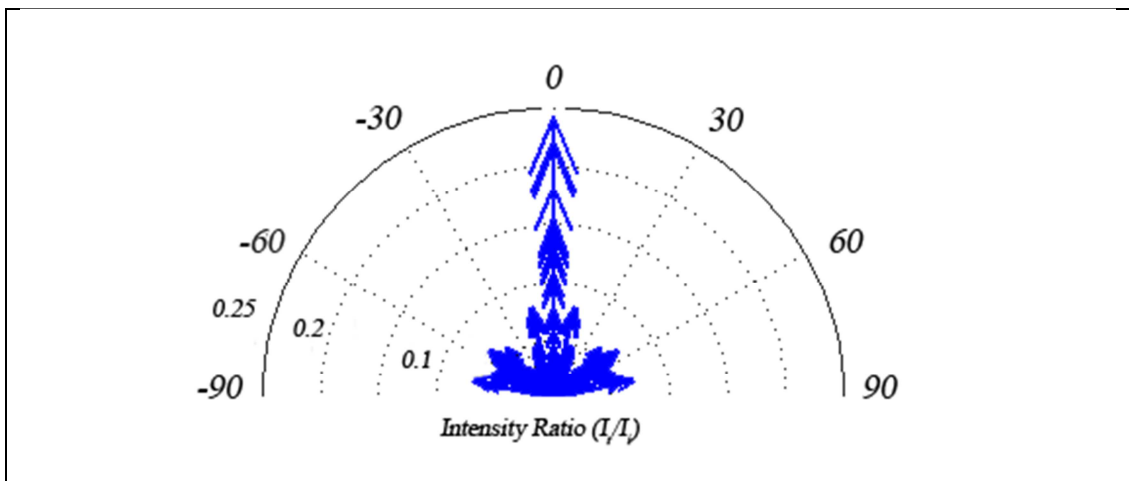


Figure 5.10 Directivity diagram of the intensity ratios considering whole spatial harmonics with varying frequency for $w = 0.18m$

The demonstrations show that, with increasing well width the domination of specular reflection becomes smaller. The energy density ratio of the specular reflection in Figure 5.8 is nearly 0.6 for $w = 0.06m$. The value of the energy density ratio becomes almost 0.25 for $w = 0.18m$ in Figure 5.16. This is due to the fact that the amount of the scattered sound energy compared with the total reflected sound energy

has increased since the number of spatial harmonics propagating to far field has increased.

5.2. Comparative Evaluation Scenarios

The basic absorption characteristic of the space diffuser is demonstrated in the previous section. Absence of a rigid backing introduced an absorption curve which starts from a moderate value and the amount of absorption maintains its presence for a wide frequency range. The absorption characteristic of the diffuser can be altered by modifying design parameters. In this section a comparative evaluation of the design parameters is going to be introduced. To fairly investigate the absorption behavior, design parameters except the one which is going to be modified are fixed and given in Table 5.4, 5.5 and 5.6.

Table 5.4 Design Parameters for the Sample Scenario-1

Design Frequency [Hz]	285
Prime Number Sequence	7
Well Width [m]	0.06
Fin Length [m]	0.003
Diffuser Depth [m]	0.667
Incidence Angle [degrees]	45
Interested Frequency Range [Hz]	1:2000

Table 5.5 Sequenced Well Depths for the Sample Scenario-1

Depth Sequence [m]						
1 st Well	2 nd Well	3 rd Well	4 th Well	5 th Well	6 th Well	7 th Well
0	0.086	0.341	0.170	0.170	0.341	0.086

Table 5.6 Micro-Perforated Panel Parameters for the Sample Scenario-1

	Front MPP	Rear MPP
Aperture Diameter [mm]	0.7	0.7
Aperture Ratio [%]	10	10
Surface Mass Density [kg/m^2]	0.1	0.1
Panel Thickness [mm]	1	1

5.2.1. Effect of Narrower Wells

In Chapter 4, the additional losses due to thermal and viscous dissipation are introduced, and the complex wave number as well as the complex effective air density is theoretically explained. In Figure 5.11 the effect of narrow well widths are demonstrated for different width values.

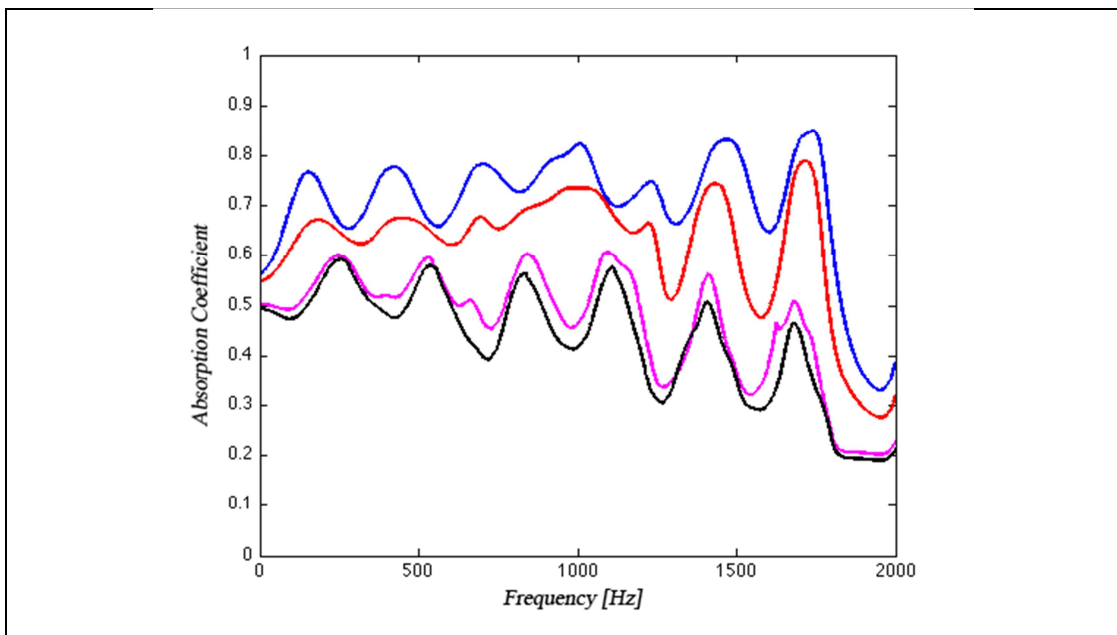


Figure 5.11 Absorption Coefficient for varying well width, $w = 0.005m$ (blue curve), $w = 0.01m$ (red curve), $w = 0.05m$ (magenta curve), $w = 0.1m$ (black curve)

It is very obvious that, while the well width decreases the amount of absorption increases. Since the depth sequence and impedance of the micro-perforated panel are preserved the resonance frequency distribution is not affected from this modification. A significant point in this analysis is that since the well widths are narrowed, the cut-off frequency for scattering also shifts to a higher frequency. This is because the period length of the diffuser has become smaller. A detailed demonstration of narrower well widths can be investigated in the results of sample scenario-2 given in Appendix B.

The 2nd scenario is a detailed demonstration of a space diffuser where the well width is fixed to 0.006m. The design parameters of this scenario are given in Table B.1, B.2 and B.3. It can easily be seen in Figure B.3 that, once the width is decreased by a factor of 10, the cut-off frequency shifts up to 3186 Hz. This condition explains the increase in the absorption at mid to high frequencies due to the absence of scattered energy. However, the absorption behavior at low frequencies is simply due to the introduced thermal and viscous losses. These dissipation mechanisms are present inside the boundary layers which are inversely proportional with the frequency. Hence, as the frequency decreases the boundary layer thicknesses becomes comparable with the width of each well and the amount of dissipation increases.

5.2.2. Effect of Number of Wells and Incidence Angle

The number of wells in each period is determined by the quadratic residue sequence for the particular modified diffuser in this study. The absorption coefficient for different sequence modifiers are demonstrated in Figure 5.12.

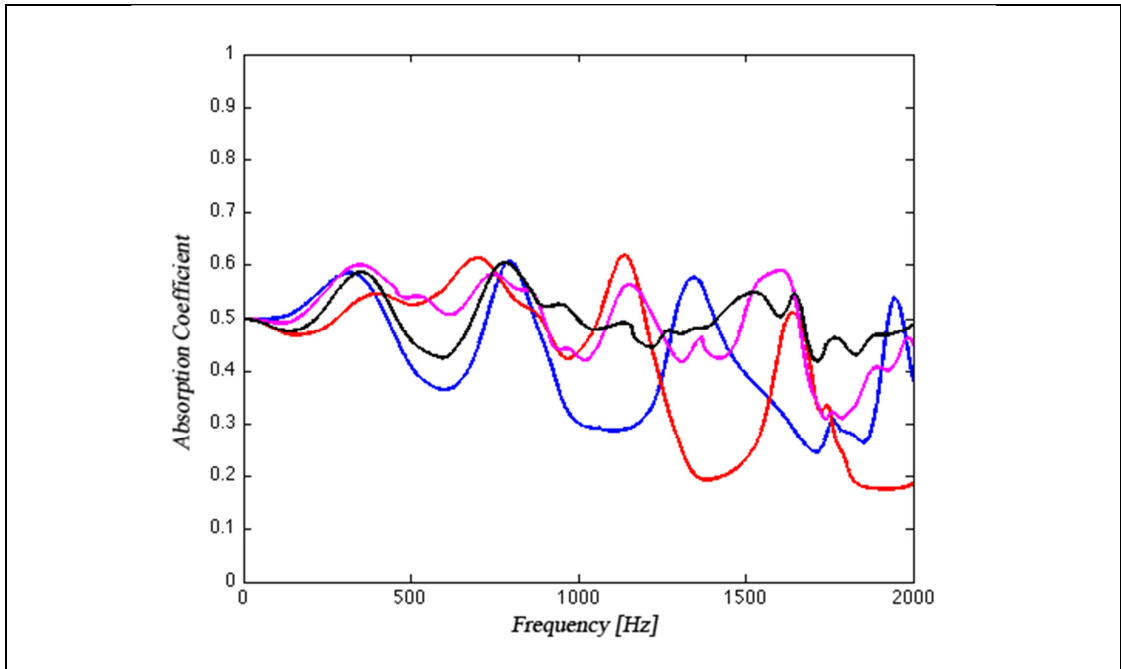


Figure 5.12 Absorption Coefficient for varying sequence modifier, $N = 3$ (blue curve), $N = 5$ (red curve), $N = 7$ (magenta curve), $N = 11$ (black curve)

The effect of sequence modifier is apparent on the distribution of the resonance frequencies. In the mathematical model the depth sequence is strictly preserved with respect to Schroeder's diffuser theory. This preservation leads to a fixed number of differently tuned wells in one period for any sequence modifier. The number of differently tuned wells is simply $N + 1/2$. The number of resonance frequencies of the diffuser is proportional with the multipliers of the number of differently tuned wells. Eventually, as the sequence modifier increases the number of resonance frequencies increases. For instance for $N = 3$, the resonance frequencies are less in number and separated from each other when compared to the other scenarios. On the other hand for $N = 11$ the number of resonance frequencies are high in number and distribution is so close such that resonances cannot be easily noticed in certain frequency ranges.

The incidence angle is another parameter that can affect the performance of absorption. Although it's not a design parameter, it has a significant role since any acoustic wave with any incidence angle can encounter a diffuser in practical applications. Figure 5.13 demonstrates the effect of incidence angle on absorption behavior of the diffuser.

The effect of the incidence angle is simply the loss in the energy absorbed by the diffuser. Since the energy transmitted with the acoustic wave in transverse direction decreases as incidence angle increases, the amount of total energy transmitted to the diffuser decreases, so as the absorbed energy.

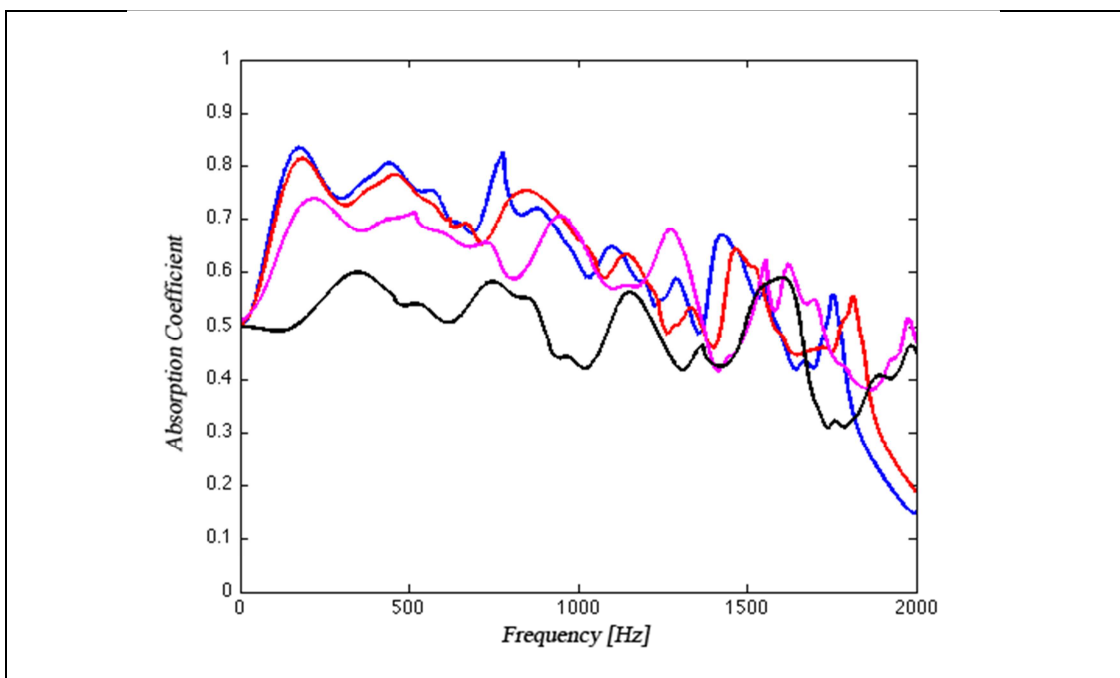


Figure 5.13 Absorption Coefficient for varying incident angle, $\theta = 0^\circ$ (blue curve), $\theta = 15^\circ$ (red curve), $\theta = 30^\circ$ (magenta curve), $\theta = 45^\circ$ (black curve)

5.2.3. Effect of Panel Impedances

Another parameter that affects the absorption characteristic of the diffuser is the impedance of the DLMPP. The impedance of a single MPP simply depends on the aperture size, aperture ratio, panel thickness and surface mass density. In general, the absorption behavior of the Schroeder Diffuser mainly depends on the mutual interaction of the acoustic waves that interferes at the surface of the diffuser in near field. Therefore, unlike MPP absorbers, the effect of aperture size, panel thickness and aperture ratio does not alter the absorption characteristic significantly. However the effect of the surface mass density has a significant effect on the absorption since this quantity dramatically changes the reactance of the MPP.

In Figure 5.14 and 5.15, the effect of mass surface density on absorption behavior is demonstrated.

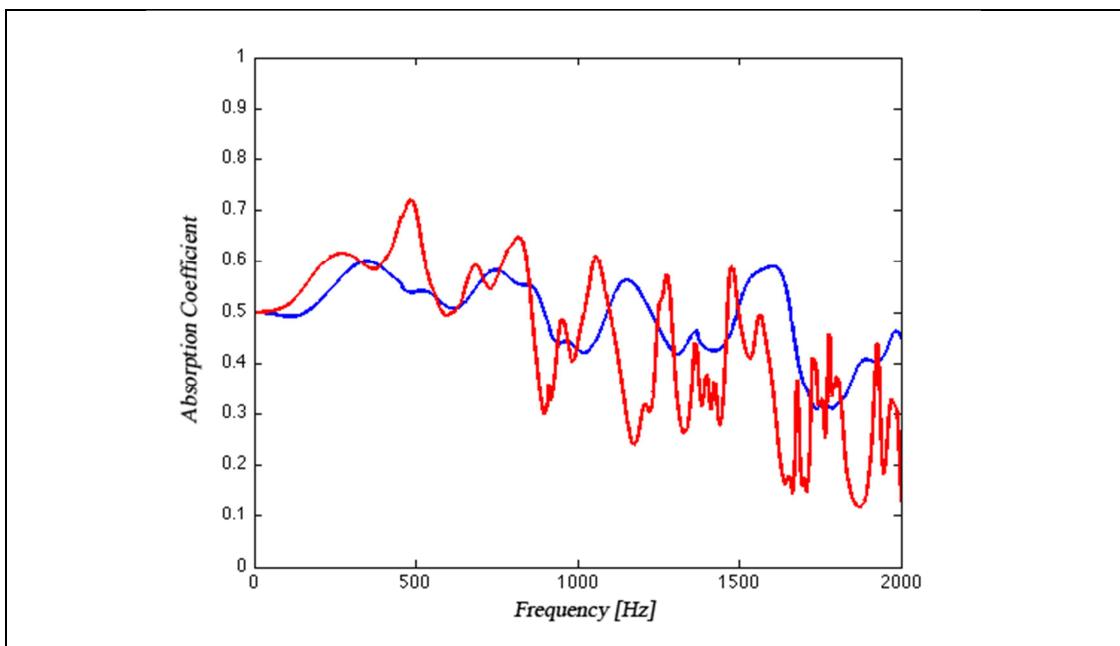


Figure 5.14 Absorption Coefficient for varying surface mass density and panel thickness, $m = 0.1 \text{ kg/m}^2$ (blue curve), $m = 0.3 \text{ kg/m}^2$ (red curve)

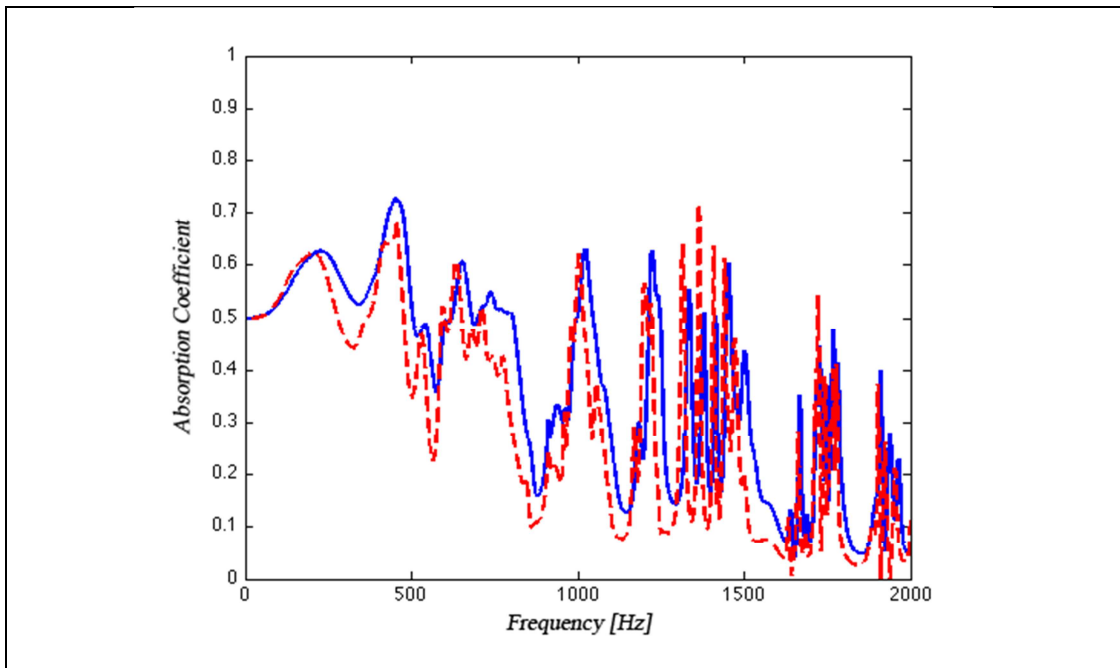


Figure 5.15 Absorption Coefficient for varying surface mass density and panel thickness, $m = 0.5 \text{ kg/m}^2$ (blue curve), $m = 0.7 \text{ kg/m}^2$ (red curve)

It can easily be seen that a change in MPP reactance dramatically changes the absorption curve behavior. As the panel surface mass density increases the number of resonance frequencies increases. The effect is directly related with the stiffness of the panel since the panel thickness is preserved while the density of the panel is increased. The effect is even larger in Figure 5.15. The number of resonance frequencies is even more increased in high frequency range.

CHAPTER 6

CONCLUSIONS

6.1. Introduction

This study is conducted to investigate absorption and scattering characteristics of a Schroeder Diffuser modified by incorporation of micro-perforated panels and removing the rigid backing in order to increase low frequency absorption. Modifications regarding perforated panel implementation into the diffuser were investigated both mathematically and experimentally in previous studies. Removing rigid backing and replacing it with another micro-perforated panel to construct a double-leaf micro-perforated panel system where the front and rear surfaces of the diffuser are exposed to air are newly released modification ideas which are introduced in this thesis.

So far in Chapter 4, a mathematical analysis is conducted to model the absorption mechanism of the modified Schroeder Diffuser. This model is simply constructed on well-known Mechel's model by modifying and improving it in order to simulate the effect of non-rigid backing in the theoretical analysis. Mechel's method is only for conventional configurations of Schroeder Diffusers where a rigid backing is employed at the rear surface of the diffuser. Eventually, the model only evaluates and determines the reflected and scattered sound field in front of the diffuser. Hence, the absorption coefficient of the diffuser can simply be obtained, once the reflected field and reflection coefficient are evaluated.

Unlike the original model, some modifications are implemented to analytically express the sound field behind the diffuser, namely the transmitted sound field. As a result, a relation can be constructed between the transmitted wave pressures and incident wave pressure to obtain the transmission coefficient of the diffuser. Eventually, the absorption coefficient can be obtained by employing both reflection and transmission coefficients.

The mathematical model which is introduced in this study is decomposed into two approaches to evaluate the transmitted sound field behind. The first approach constructs comparably a simple model where the mutual interactions between diffuser wells are partially ignored. This assumption leads to a simplified calculation process since the pressures of the reflected and transmitted sound waves can be obtained distinctly. However, in the second approach this assumption is removed to obtain both pressure waves at one single calculation process. The mutual interaction between each well is included when reflected and transmitted sound fields are modeled. In addition to the structural modification applied to the diffuser, the effect of narrow diffuser wells is also implemented into the model to investigate further increase in the amount of absorption.

The reflected and transmitted fields obtained with the mathematical model are used not only for the absorption mechanism; but also used to determine specularly reflected and scattered energy distributions for both sound fields surrounding the diffuser. Besides the energy distribution, the angle of reflection and transmission for both reflected and transmitted spatial harmonic components are derived and an angular distribution in front of the diffuser as well as at the back are obtained.

In this chapter, analytical results of absorption and scattering introduced with the modified Schroeder diffuser are going to be discussed. The results for absorption coefficients are compared with the absorption coefficients investigated within previous studies.

6.2. Comparative Evaluations and Conclusions

The main motivation in this thesis is to implement the idea of double-leaf micro-perforated panel configuration into a Schroeder Diffuser and removing the rigid backing behind the diffuser to enable a new application area. It has been expected that the removal of the rigid backing is going to introduce an enhanced absorption characteristic at low frequencies while preserving the scattering characteristics at mid to high frequencies.

The modification is implemented into the Schroeder Diffuser from the study of Sagakami, M. and Morimoto, M. [14] which is on double-leaf micro-perforated panels. In Figure 6.1, the absorption characteristics of a DMPP absorber in Sagakami's study and the modified Schroeder Diffuser in this study are compared under normal incidence condition. Both configurations are not terminated with a rigid backing. The air cavity depth of the panel absorber and diffuser depth are set to 0.227m in order to correspond to the design frequency of the diffuser which is 750 Hz.

The double-leaf micro-perforated panel absorber is a typical resonant absorber in which the absorption can be maximized at resonance frequencies. Due to non-rigid backing the absorption curve starts from a moderate value. However, due to the distribution of resonance frequencies which mainly depends on the depth of the air cavity between micro-perforated panels, the amount of absorption is not very strong at a wide frequency range. On the other hand, the well depths of the space diffuser are differently tuned. This feature of the diffuser introduces more resonance frequencies with an even distribution in a wider frequency range.

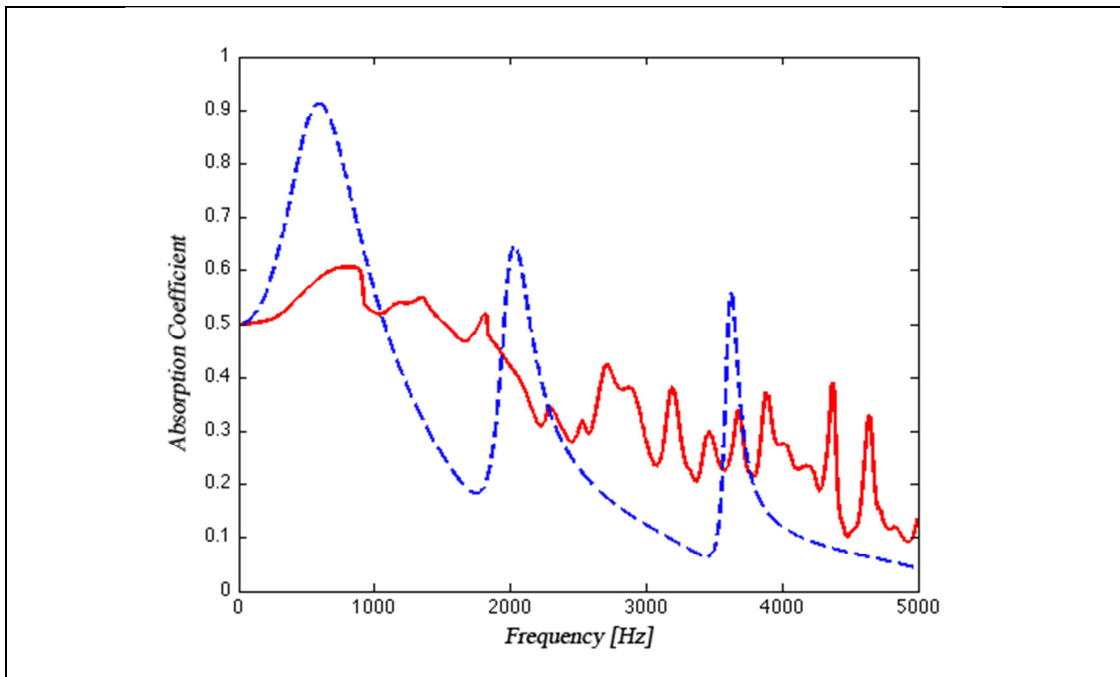


Figure 6.1 Normal incidence absorption coefficient of Double-leaf micro-perforated panel absorber (*blue curve*) and Modified Schroeder Diffuser (*red curve*)

The advantageous property of the panel absorber can only be at the first resonance frequency. It can easily be seen that the panel absorber has more potential to absorb sound energy at the first resonance frequency when compared to the space diffuser. However, the close distribution of resonance frequencies in the space diffuser introduces more potential to absorb sound energy at mid to high frequency range.

Since the space diffuser is a modified version of a regular Schroeder Diffuser, it is reasonable to compare the absorption performance with a regular Schroeder Diffuser and previous modifications applied on it. In Figure 6.2 the absorption curves of the space diffuser and regular Schroeder Diffuser are demonstrated. It is obvious that a regular Schroeder Diffuser is not capable of absorbing sound energy since it is not designed for it. On the other hand, the amount of absorption harnessed had been increased in the previous studies by adding perforated panels into the diffuser again in a regular construction. The perforation involved is not a micro-perforation but a

regular size perforation. A micro-perforation is incorporated into the diffuser in Huneke's work [22], which is a regular single-leaf micro-perforated with an air space behind. This configuration can also be applicable with Mechel's theory to investigate the reflected spatial harmonics in front of the diffuser. In Figure 6.3, the absorption curves of a QRD with regular single-leaf micro-perforated panel configuration and space diffuser are demonstrated.

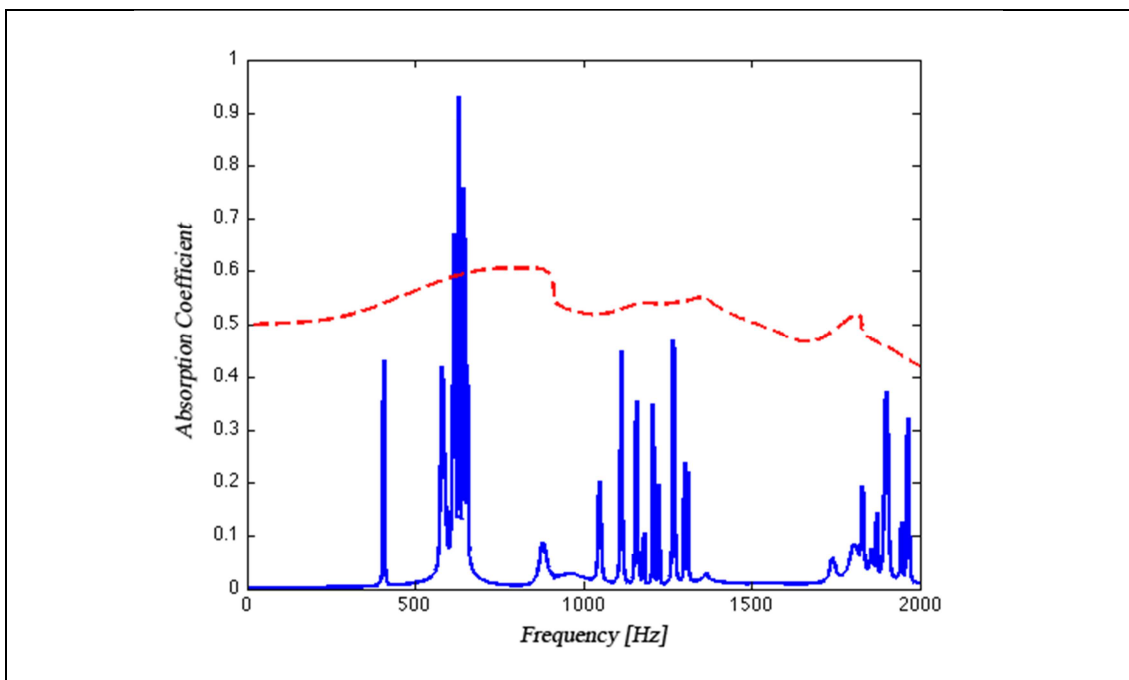


Figure 6.2 Absorption Coefficient, Space Diffuser (*red curve*), Regular Schroeder Diffuser (*blue curve*)

When the absorption curves in Figure 6.3 are compared, the only advantage that the space diffuser enables in this study is that very low frequency absorption is enhanced compared to a regular Schroeder diffuser modified with single-leaf micro-perforated panels. In general the behavior of both configurations is almost the same, regarding absorption performance. Furthermore, the comparison can be carried to a further extent where a double-leaf micro-perforated panel configuration can be incorporated with the Schroeder Diffuser with rigid backing. In Figure 6.4, the absorption curve of

this configuration is also introduced with a comparison with space diffuser. The incorporation of the DLMPP into the diffuser has changed the distribution of resonance frequencies. This is due to the addition of a second panel and an air space when compared to the configuration with single-leaf MPP. Additional resonance frequency results in a wider frequency range for absorption. Hence the amount of absorption in that frequency range is much more than the space diffuser introduces.

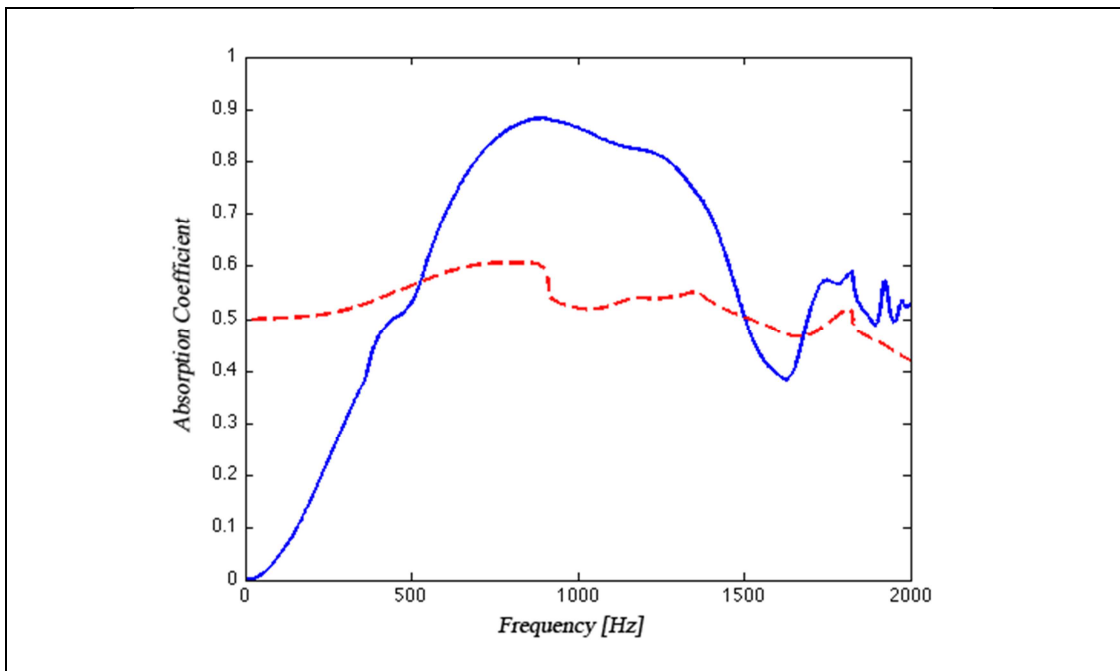


Figure 6.3 Absorption coefficient, space diffuser (*red curve*), regular Schroeder diffuser with single-leaf micro-perforated panel and with rigid backing (*blue curve*)

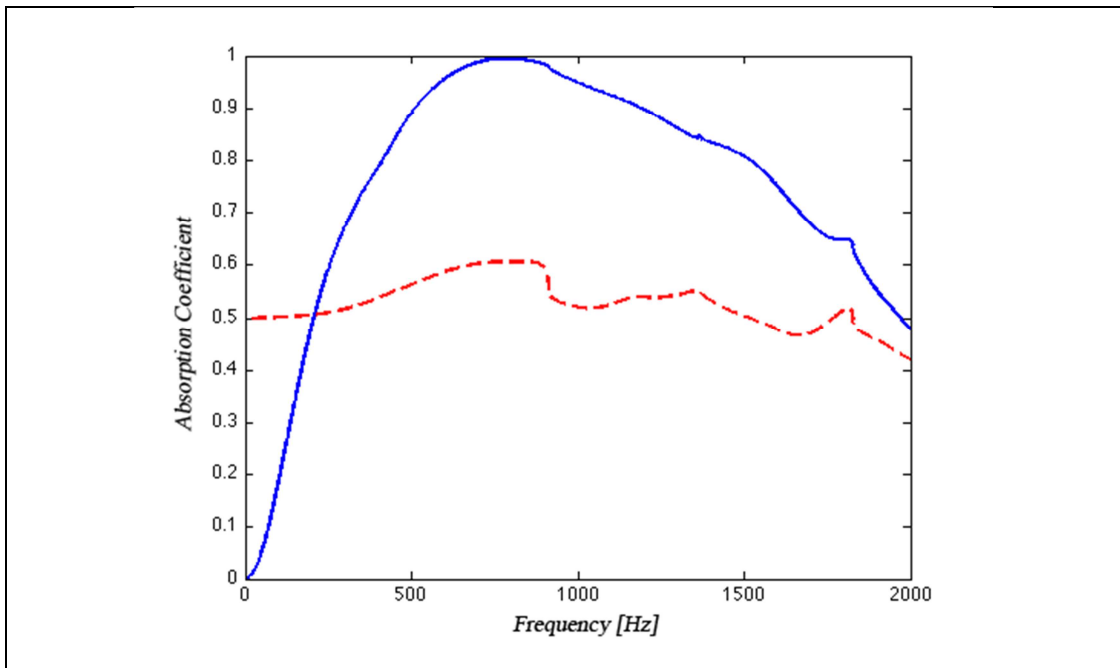


Figure 6.4 Absorption coefficient, space diffuser (*red curve*), regular Schroeder diffuser with double-leaf micro-perforated panels and with rigid backing (*blue curve*)

Furthermore, the reliability of the developed MATLAB code should be checked. The code is developed to investigate both reflected and transmitted fields; however, it is also possible to analyze the behavior of a regular diffuser with rigid backing in several ways. The impedance of the rigid backing is simply infinite where a pressure wave cannot penetrate through. The code on the other hand is developed to model the double leaf panel behavior. Eventually; the impedance of the front panel can be set to a very large value to simulate the existence of a rigid backing. In Figure 6.5, the absorption coefficient results predicted with the software is demonstrated with respect to increasing rear panel impedance. The impedance increased by modifying the surface mass density of the panel. Hence, the absorption coefficient results of the software code with increasing surface mass density can be approximated to the results of regular Schroeder diffuser.

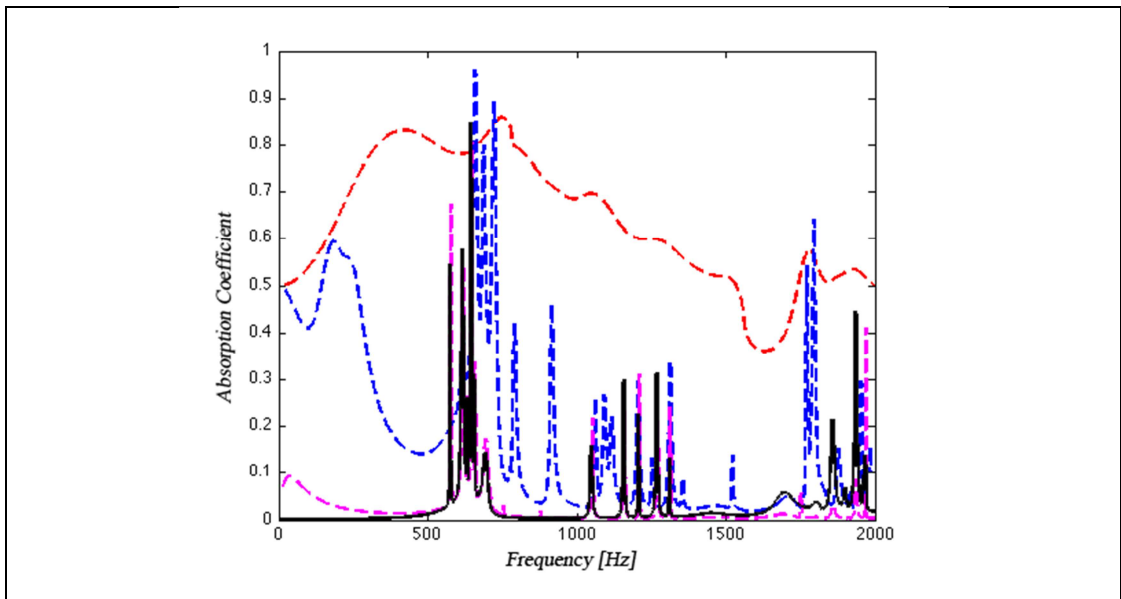


Figure 6.5 Normal incidence absorption coefficient with respect to varying front panel surface mass density, $m = 0.1 \text{ kg/m}^3$ (red curve), $m = 1 \text{ kg/m}^3$ (blue curve), $m = 1000 \text{ kg/m}^3$ (magenta curve), $m = \infty \text{ kg/m}^3$ (black curve)

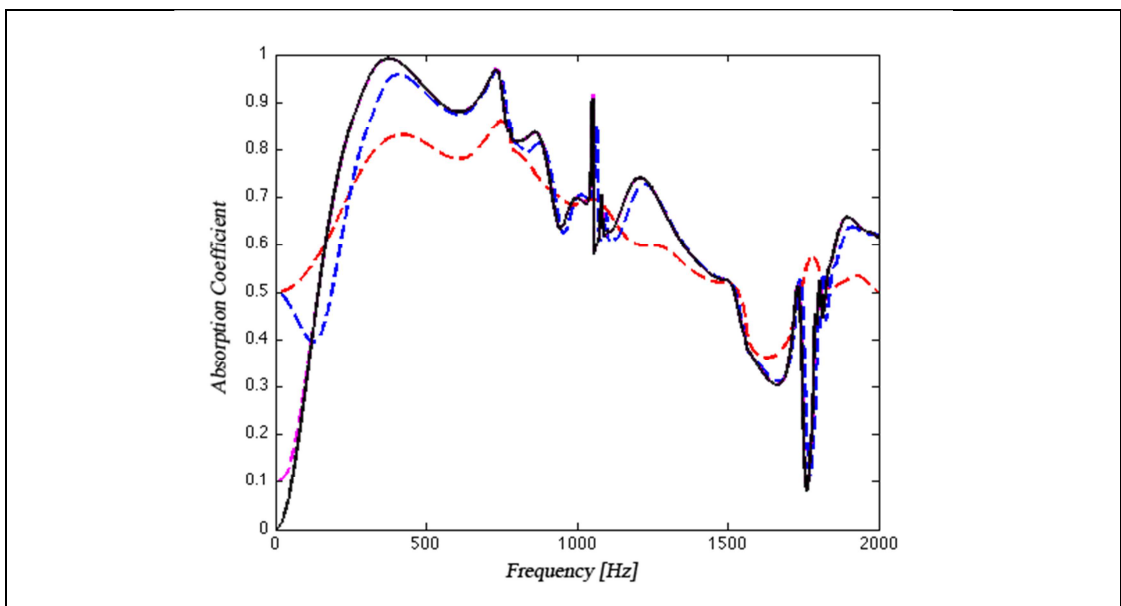


Figure 6.6 Normal incidence absorption coefficient with respect to varying rear panel surface mass density, $m = 0.1 \text{ kg/m}^3$ (red curve), $m = 1 \text{ kg/m}^3$ (blue curve), $m = 1000 \text{ kg/m}^3$ (magenta curve), $m = \infty \text{ kg/m}^3$ (black curve)

Similarly, the impedance of the rear panel can be increased gradually to demonstrate the absorption behavior of a Schroeder diffuser modified with a single-leaf micro-perforated panel where rigid backing exists. The absorption coefficient result of such configuration is demonstrated in Figure 6.6.

The red curve in Figure 6.5 and Figure 6.6 represents the absorption coefficient of a space diffuser with the design parameters given in Table 5.4, 5.6 and 5.7. On the other hand black curve represents the absorption coefficient of a regular Schroeder diffuser and a Schroeder diffuser incorporated with single-leaf micro-perforated panel with a rigid backing, respectively. It can be easily noticed that with increasing front and rear panel impedance, the software results of both cases gradually approach to the results of the regular diffuser. With both modifications in the panel parameters, the existence of the rigid backing can be simulated by disregarding the transmitted sound field behind the diffuser.

To conclude the study on absorption and scattering characteristics of the space diffuser, the author would like to express some important aspects of the study. The mathematical model constructed to identify the behavior of the sound field surrounding the diffuser, is based on Mechel's Fourier Decomposition Method. The method requires periodicity to employ the use of spatial harmonics that build up to form the specularly reflected and scattered sound fields. Since the system size is infinite in theory, the diffraction that occurs at the geometrical boundaries of the system is ignored. This feature actually enables the mathematical model to investigate only the scattering phenomenon introduced by the diffuser. However, in practical applications the diffraction also takes place in the scattering phenomenon since the diffuser cannot be constructed as an infinite object. The diffracted sound field is inevitable at the geometrical boundaries of a finite size diffuser.

However, this study gives a reasonable insight about the absorption characteristics of the space diffuser in a theoretical sense. The previously introduced studies on a

regular Schroeder diffuser show that the absorption performance can be increased with various modifications. This study shows that a new configuration beside the conventional use of the diffuser can be employed by locating it on space where the back of the diffuser is also exposed to a sound field. Since this sound field can also be manipulated with the design parameters, there is an advantage to control the sound field in an enclosed space before the generated sound waves reach to the room boundaries. The transmitted sound waves from the diffuser can be thought as a sound source with a newly introduced directivity pattern radiating to far field. Besides the directivity control, the diffuser has the potential to absorb sound energy in a significant amount at very low frequencies.

At the end, the space diffuser can be a useful device to control scattering and directivity characteristics at mid to high frequencies while a great amount of sound energy at low frequencies is absorbed. This feature enables the diffuser to have a full control on the sound field in an enclosed space. Low frequency sound, which is hard to be manageable, is absorbed and the mid and high frequency sound is both absorbed and highly scattered to the far field which enables the control of energy distribution within the room.

REFERENCES

- [1] T. J. Cox, P. D'Antonio, *Acoustic Absorbers and Diffusers* (270 Madison Avenue, New York, NY, 2009), Chapter 9
- [2] K. Fujiwara, T. Miyajima, "Absorption Characteristics of a Practically Constructed Schroeder Diffuser of Quadratic-Residue Type", *Appl. Acoust.* 35, 149 – 152, 1991
- [3] H. Kuttruff, "Sound Absorption by Pseudo stochastic Diffusers (Schroeder Diffusers)", *Appl. Acoust.* 42, 215 -231, 1994
- [4] K. Fujiwara, K. Nakai, H. Torihara, "Visualization of The Sound Field Around The Schroeder Diffuser", *Appl. Acoust.* 60, 225 – 235, 2000
- [5] F. P. Mechel, "The wide-angle Diffuser – A wide-angle Absorber?", *Acustica* 81, 379 – 401, 1995
- [6] F. P. Mechel, *Schallabsorber*(S. HirzelVerlag, Stuttgart, 1998), Vol III, Chapter 5
- [7] T. Wu, T. J. Cox, Y. W. Lam, "From a Profiled Diffuser to a Practical Absorber", *J. Acoust. Soc. Am.* 108, 643 -650, 2000
- [8] T. Wu, T. J. Cox, Y. W. Lam, "A Profiled Structure with Improved Low Frequency Absorption", *J. Acoust. Soc. Am.* 110, 3064 - 3070, 2001
- [10] L. L. Beranek, Ed., *Noise and Vibration Control* (McGraw Hill, New York, 1961), Chapter 8
- [11] P. M. Morse and K. Ingard, *Theoretical Acoustics* (McGraw-Hill, New York, 1968, Chapter 9

- [12] K. Sagakami, M. Morimoto, M. Yairi, “A note on the effect of vibration of a microperforated panel on its sound absorption characteristics”, *Acoust.Sci& Tech.* 26, 2, 2005
- [13] K. Sagakami, M. Morimoto, W. Koike, “A Numerical Study of Double-leaf Microperforated Panel Absorbers”, *Appl. Acoust.* 67, 609 – 619, 2006
- [14] K. Sagakami, M. Morimoto, M. Yairi, “Double-leaf microperforated panel space absorbers: A revised theory and detailed analysis”, *Appl. Acoust.* 70, 703 – 709, 2009
- [15] J. Kang, H. V. Fuchs, “Predicting the absorption of open weave textiles and microperforated membranes backed by an airspace”, *J. Acoust. Soc. Am.* 220, 905 - 920, 1999
- [16] D. -Y. Maa, “Microperforated Panel wide-band Absorber”, *Noise Control Eng. J.* 29, 77 – 84, 1987
- [17] L. E. Kinsler, A. R. Frey, A.B. Coppens, J. V. Sanders, *Fundamentals of Acoustics* (John Wiley & Sons, Inc., USA, 2000), Chapter 5
- [18] L. Marshall, *Architectural Acoustics*, (Elsevier Academic Press, 30 Corporate Drive, Suite 400, Burlington, MA 01803, USA, 2006), Chapter 7
- [19] P. D’Antonio, T. J. Cox, “Two decades of room diffusers. Part 1: Applications and design,” *J. Audio. Eng. Soc.* 46, 955–976, 1998
- [20] P. D’Antonio, T. J. Cox, “Two decades of room diffusers. Part 2: Measurement, prediction and characterisation,” *J. Audio. Eng. Soc.* 46, 1075–1091, 1998
- [21] M. R. Schroeder, “Binaural dissimilarity and optimum ceilings for concert halls: More lateral sound diffusion,” *J. Acoust. Soc. Am.* 65, 958– 963, 1979

[22] J. Hunecke, “*Schallstreuung und Schallabsorption von Oberflächen aus Mikroperforierten Streifen*”, PhD thesis, University of Stuttgart, 1997

APPENDIX A

Derivation of Equation (4.34) from Equation (4.32)

$$\cos \theta \cdot P_i - \sum_{n=-\infty}^{\infty} A_n \frac{\gamma_n}{k} e^{-jn\frac{2\pi}{L}x} = G(x) \left[P_i + \sum_{n=-\infty}^{\infty} A_n e^{-jn\frac{2\pi}{L}x} \right]$$

$G(x)$ is replaced with its Fourier expansion representation in Equation (4.33).

Afterwards, each term in the above equation is first multiplied with $e^{+jm\frac{2\pi}{L}x}$, then integrated over the diffuser period, L .

$$\left[\int_0^L \left(\cos \theta \cdot P_i \cdot e^{+jm\frac{2\pi}{L}x} \right) dx \right] - \left[\int_0^L \left(\sum_{n=-\infty}^{\infty} A_n \frac{\gamma_n}{k} e^{-jn\frac{2\pi}{L}x} \cdot e^{+jm\frac{2\pi}{L}x} \right) dx \right] =$$

$$\left[\int_0^L \left(P_i \sum_{n=-\infty}^{\infty} g_n e^{-jn\frac{2\pi}{L}x} \cdot e^{+jm\frac{2\pi}{L}x} \right) dx \right] + \left[\int_0^L \left(\sum_{n=-\infty}^{\infty} A_n \frac{\gamma_n}{k} e^{-jn\frac{2\pi}{L}x} \sum_{n=-\infty}^{\infty} g_n e^{-jn\frac{2\pi}{L}x} \cdot e^{+jm\frac{2\pi}{L}x} \right) dx \right]$$

$$m = -\infty, \dots, \infty$$

The first and the second integrals are solved utilizing the orthogonality principle of cosine and sine functions. Remaining terms are solved by modifying the running indices n and m . Hence the transformation results in Equation (4.34) as given below.

$$\sum_{n=-\infty}^{\infty} A_n \left[g_{m-n} + \delta_{m,n} \left(\frac{\gamma_n}{k} \right) \right] = P_i (\delta_{m,0} \cos \theta - g_m)$$

$$m = -\infty, \dots, +\infty$$

Derivation of Equation (4.54) and Equation (4.64) is similar as explained above.

APPENDIX B

Sample Case-2 Design Parameters and Software Results

Table B.1 Design Parameters for the Sample Case-2

Design Frequency [Hz]	750
Prime Number Sequence	7
Well Width [m]	0.006
Fin Length [m]	0.001
Diffuser Depth [m]	0.662
Incidence Angle [degrees]	45
Interested Frequency Range [Hz]	1:8000

Table B.2 Sequenced Well Depths for the Sample Case-2

Depth Sequence [m]						
1 st Well	2 nd Well	3 rd Well	4 th Well	5 th Well	6 th Well	7 th Well
0	0.086	0.341	0.170	0.170	0.341	0.086

Table B.3 Micro-Perforated Panel Parameters for the Sample Case-2

	Front MPP	Rear MPP
Aperture Diameter [mm]	0.7	0.7
Aperture Ratio [%]	10	10
Surface Mass Density [kg/m ²]	0.1	0.1
Panel Thickness [mm]	1	1

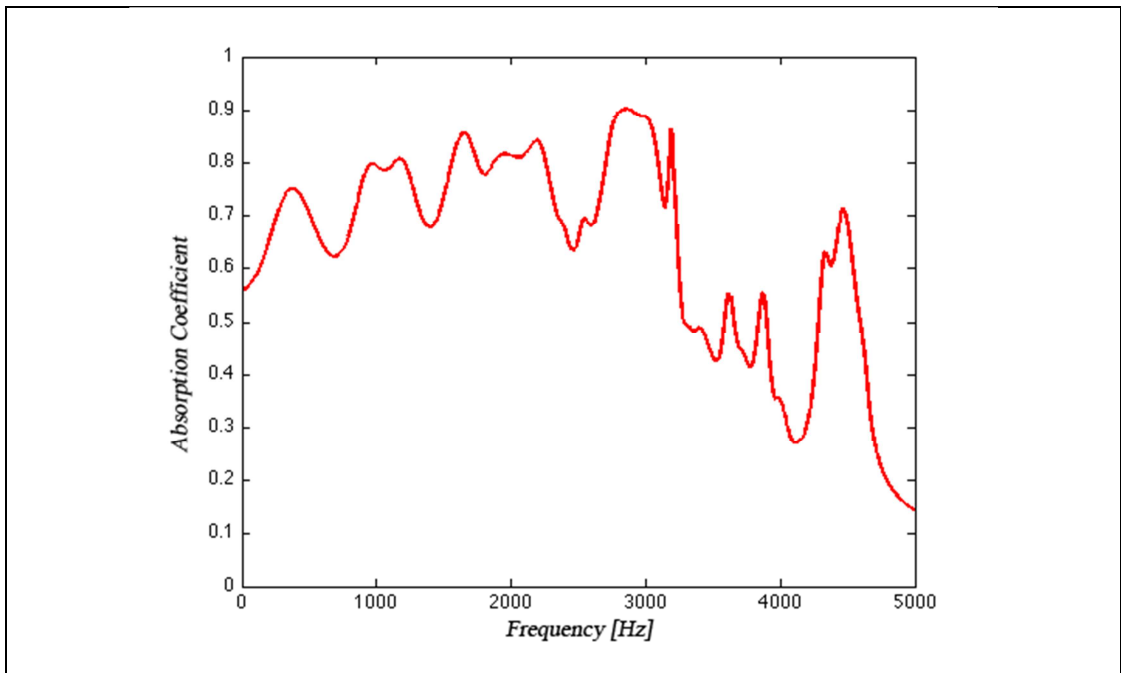


Figure B.1 Absorption Coefficient (2nd Scenario)

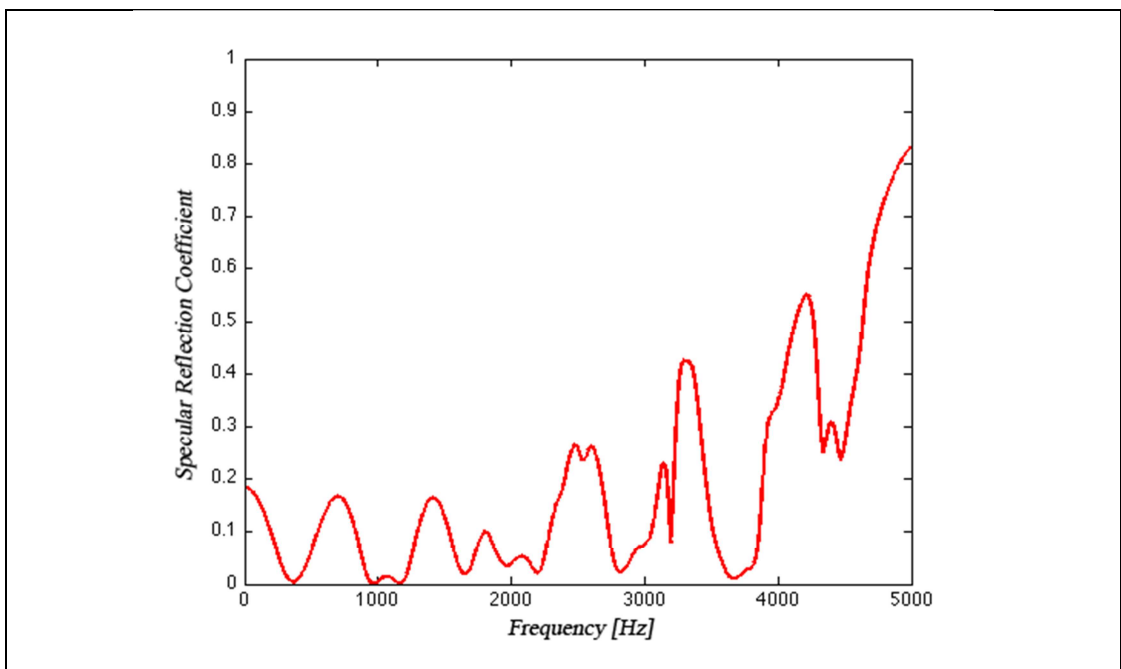


Figure B.2 Specular reflection coefficient (2nd Scenario)

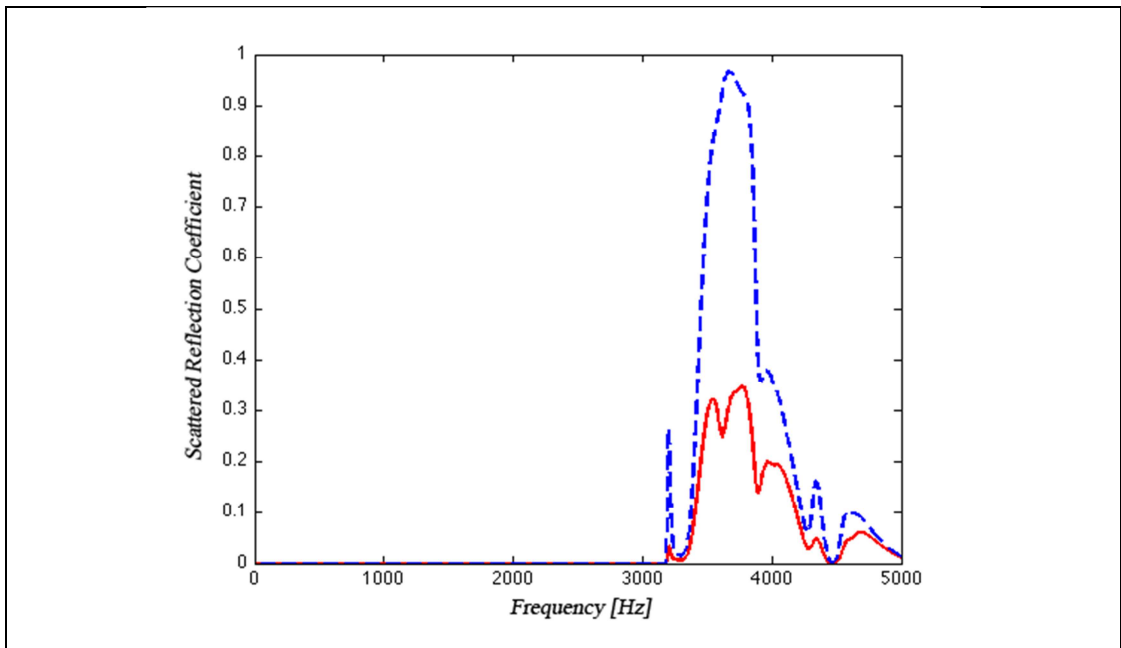


Figure B.3 Scattered reflection coefficient (*red curve*), Coefficient of redistribution (*blue curve*) (2nd Scenario)

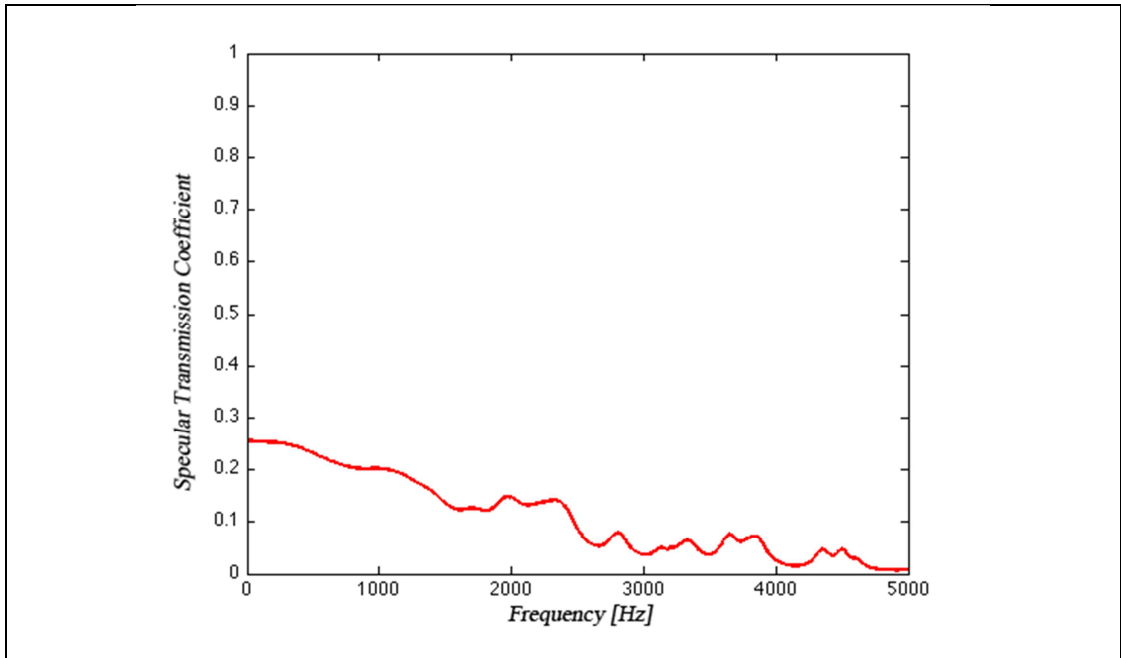


Figure B.4 Specular transmission coefficient (2nd Scenario)

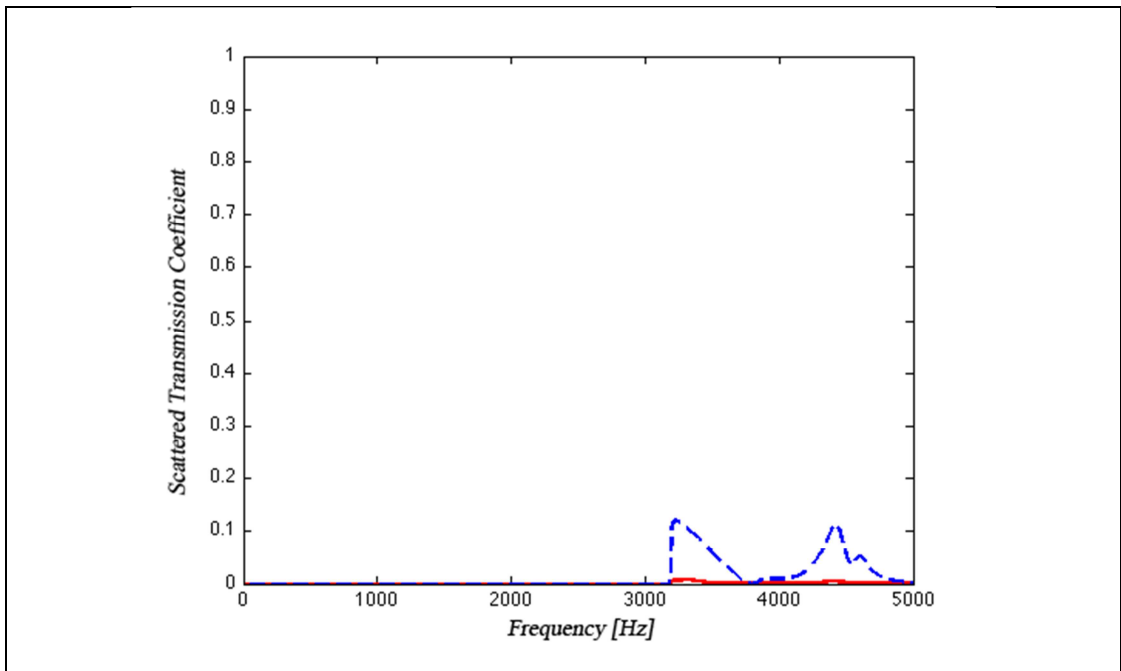


Figure B.5 Scattered transmission coefficient (*red curve*), Coefficient of redistribution (*blue curve*) (2nd Scenario)